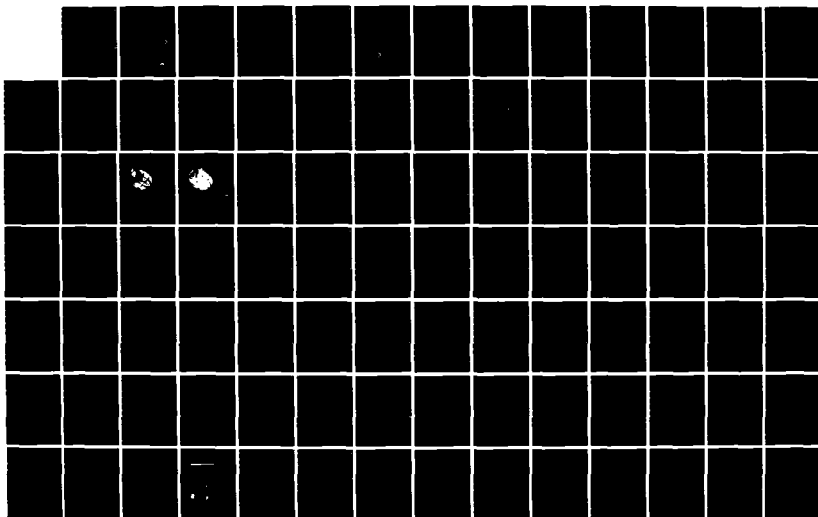
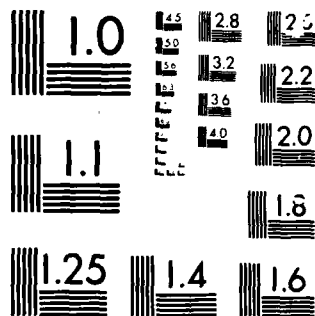


AD-A166 951 OPTIMAL ECG ELECTRODE SITES AND CRITERIA FOR DETECTION 1/2  
OF ASYMPTOMATIC CO. (U) UNIVERSITY OF SOUTHERN  
CALIFORNIA DOWNEY R H SELVESTER ET AL. DEC 85  
UNCLASSIFIED F33615-83-D-0603 F/G 14/2 NL





MICROCOPY

CHART

12

USAFSAM-TR-85-47

AD-A166 951

# OPTIMAL ECG ELECTRODE SITES AND CRITERIA FOR DETECTION OF ASYMPTOMATIC CORONARY ARTERY DISEASE AT REST AND WITH EXERCISE

Ronald H. Selvester, M.D.  
Joseph C. Solomon, M.S.

University of Southern California  
7413 Golondrinas Street  
Downey, CA 90242

DTIC  
ELECTE  
APR 15 1986  
S B D

December 1985

Final Report for Period 4 April 1984 - 25 November 1984

DTIC FILE COPY

Approved for public release; distribution is unlimited.

Prepared for  
USAF SCHOOL OF AEROSPACE MEDICINE  
Aerospace Medical Division (AFSC)  
Brooks Air Force Base, TX 78235-5301



## NOTICES

This final report was submitted by the University of Southern California, and Rancho Los Amigos Medical Center, Downey, CA 90242, under contract F33615-83-D-0603, job order 7755-27-11, with the USAF School of Aerospace Medicine, Aerospace Medical Division, AFSC, Brooks Air Force Base, Texas. Colonel Gil D. Tolan (USAFSAM/NGF) was the Laboratory Project Scientist-in-Charge.

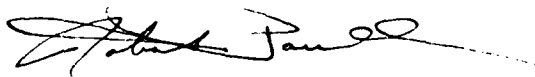
When Government drawings, specifications, or other data are used for any purpose other than in connection with a definitely Government-related procurement, the United States Government incurs no responsibility or any obligation whatsoever. The fact that the Government may have formulated or in any way supplied the said drawings, specifications, or other data, is not to be regarded by implication, or otherwise in any manner construed, as licensing the holder, or any other person or corporation; or as conveying any rights or permission to manufacture, use, or sell any patented invention that may in any way be related thereto.

The Office of Public Affairs has reviewed this report, and it is releasable to the National Technical Information Service, where it will be available to the general public, including foreign nationals.

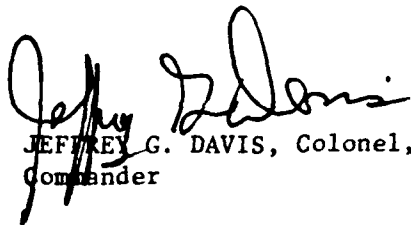
This report has been reviewed and is approved for publication.



GIL D. TOLAN, Colonel, USAF, MC  
Project Scientist



ROBERT M. PAULL, Colonel, USAF, MC  
Supervisor



JEFFREY G. DAVIS, Colonel, USAF, MC  
Commander

UNCLASSIFIED

SECURITY CLASSIFICATION OF THIS PAGE

AD-A166951

## REPORT DOCUMENTATION PAGE

1a. REPORT SECURITY CLASSIFICATION <b>Unclassified</b>			1b. RESTRICTIVE MARKINGS	
2a. SECURITY CLASSIFICATION AUTHORITY			3. DISTRIBUTION/AVAILABILITY OF REPORT Approved for public release; distribution is unlimited.	
2b. DECLASSIFICATION/DOWNGRADING SCHEDULE				
4. PERFORMING ORGANIZATION REPORT NUMBER(S)			5. MONITORING ORGANIZATION REPORT NUMBER(S)  USAFSAM-TR-85-47	
6a. NAME OF PERFORMING ORGANIZATION University of Southern California	6b. OFFICE SYMBOL (If applicable)	7a. NAME OF MONITORING ORGANIZATION  USAF School of Aerospace Medicine (NGF)		
6c. ADDRESS (City, State and ZIP Code) 7413 Golondrinas Street Downey, CA 90242		7b. ADDRESS (City, State and ZIP Code) Aerospace Medical Division Brooks Air Force Base, TX 78235-5301		
8a. NAME OF FUNDING/SPONSORING ORGANIZATION	8b. OFFICE SYMBOL (If applicable)	9. PROCUREMENT INSTRUMENT IDENTIFICATION NUMBER  F33615-83-D-0603		
8c. ADDRESS (City, State and ZIP Code)		10. SOURCE OF FUNDING NOS.		
		PROGRAM ELEMENT NO. 61101F	PROJECT NO. 7755	TASK NO. 27
				WORK UNIT NO. 11
11. TITLE (Include Security Classification) Optimal ECG Electrode Sites and Criteria for Detection of Asymptomatic Coronary Artery Disease at Rest and with Exercise				
12. PERSONAL AUTHOR(S) Selvester, Ronald H.; and Solomon, Joseph C.				
13a. TYPE OF REPORT Final	13b. TIME COVERED FROM 4/4/84 to 11/25/84	14. DATE OF REPORT (Yr., Mo., Day) 1985 December	15. PAGE COUNT 131	
16. SUPPLEMENTARY NOTATION				
17. COSATI CODES			18. SUBJECT TERMS (Continue on reverse if necessary and identify by block number)	
FIELD	GROUP	SUB GR.	Electrocardiography, Computer Forward Model, Heart Model, Body Surface Map, Exercise Tolerance Test, Coronary Artery Disease, Myocardial Infarction, Myocardial Ischemia, Dysrhythmia	
06	05			
06	16			
19. ABSTRACT (Continue on reverse if necessary and identify by block number) Depending on age, sudden death is the first symptom in 15-30% of all new coronary events in persons with previously unsuspected coronary disease. The prevalence of unrecognized but severe coronary artery disease in an apparently healthy population age 35-55 is con- servatively estimated at 1000 to 2000 per 10,000. The annual incidence of new documented first infarcts in this age group ranges from 50-100 per 10,000. The incidence of sudden death without prior suspicion of heart disease ranges from 20-50 per 10,000, and 35-50% of these subjects at autopsy will have prior (clinically unrecognized) healed myocardial infarction. Based on the fundamental work done in evaluating asymptomatic aircrewmembers by a number of workers at USAFSAM (1-4), it seems prudent to assume these statistics also apply to the pilot population. It follows from these statistics that sudden death in pilots at the controls of high-performance aircraft can be expected at the rate of at least 1 per year for every 10,000 pilots over age 35 who fly on the average of 300 hours per year. By using published figures for the cost of such high-performance aircraft, the annual cost to the Air Force for lost aircraft from this cause alone is considered to be in the millions of				
20. DISTRIBUTION AVAILABILITY OF ABSTRACT  UNCLASSIFIED UNLIMITED <input checked="" type="checkbox"/> SAME AS RPT <input type="checkbox"/> DTIC USERS <input type="checkbox"/>			21. ABSTRACT SECURITY CLASSIFICATION  Unclassified	
22a. NAME OF RESPONSIBLE INDIVIDUAL  Gil D. Tolan, Colonel, USAF, MC, SFS			22b. TELEPHONE NUMBER (Include Area Code) (512) 536-3646	22c. OFFICE SYMBOL  USAFSAM/NGF

DD FORM 1473, 83 APR

EDITION OF 1 JAN 73 IS OBSOLETE

UNCLASSIFIED

SECURITY CLASSIFICATION OF THIS PAGE

dollars, possibly 20 million to as much as 50 million or more dollars per year. If most of the 1000 to 2000 per 10,000 pilots over the age of 35 with severe coronary artery disease can be identified, the smaller subset (perhaps 200-500 per 10,000) at high risk of sudden death can then be removed from flying status. The potential savings would clearly justify a systematic exploration of the possibility that a cost-effective system for routine electrocardiographic (ECG) mapping at rest and with exercise can be developed that would identify 95% or more of these pilots. Recent findings from a number of centers and analysis of available data suggest that an overall sensitivity for detecting ischemic coronary disease of 95%-98% may be possible along with a specificity in the same range.

This technical report details previous work by us and a number of investigators defining the anatomic and physiologic basis for the simulation of depolarization/repolarization of the heart, i.e., QRS-T changes on the electrocardiogram (ECG). A detailed design of new programs to expand our fine grid (1 mm<sup>3</sup>) propagation simulation of depolarization (QRS) to include repolarization (ST-T) is presented. This forward computer model will include a family of inhomogeneous torsos representative of Air Force pilots at rest and at exercise. Using Bayesian Statistics and this model, we expect to develop criteria for local, body surface ECG changes that are specific for each of 3 (or 4) main coronary arteries and quantitative for the degree of ischemia or infarction or both in each of these coronary distributions. An optimal subset (8-32 leads) of a 176-lead rest and exercise ECG map will be chosen that gives the greatest sensitivity, specificity, and diagnostic accuracy in the detection of myocardial infarcts and significant ischemia from coronary artery disease. When validated, this database will be used to develop a portable, multi-lead ECG Mapping System. This high-fidelity, automated, digital system can be used in flight surgeon's offices worldwide for resting ECGs and exercise testing to improve significantly the detection of regional coronary ischemia and quantitate infarct size in the asymptomatic pilot. We expect to achieve a predictive accuracy of 95% or greater.

## EXECUTIVE SUMMARY

Ten to 20% of all apparently healthy people over 35 have significant but undiagnosed coronary artery disease. For 15 to 30% of these people, sudden death is the first symptom of heart disease and as many as half of those who die have had a prior unrecognized infarct (heart attack). Applying these statistics to pilots, at least 1 pilot per 10,000 over the age of 35 who fly an annual average of 300 hours in high-performance aircraft will die each year at the controls resulting in loss of the aircraft. Based on published reports, the Air Force loses from 20 million to as much as 50 million dollars per year from aircraft lost this way. Furthermore, it follows that there are 10-15 unrecognized new infarcts per year per 10,000 of these same flyers. Improving the identification of coronary disease in these pilots would lower the number flying with unrecognized heart disease. This would decrease the chances of sudden death of pilots at the controls and reduce the number of aircraft lost.

This report describes proposed enhancement of an existing computer model to improve ECG criteria and to define an optimal set of ECG electrodes for the identification of significant coronary artery disease with and without myocardial infarction. The ultimate goal is the development of a portable ECG Mapping Cart that can be used in flight surgeon's offices worldwide for resting and exercise ECGs to improve coronary artery disease detection and quantitation of infarct size in the asymptomatic pilot. *Keywords:*

**DTIC**  
**SELECTED**  
**APR 15 1986**  
**B**

"Original contains color plates: All DTIC reproductions will be in black and white"

Accession For	
NTIS GRA&I	<input checked="" type="checkbox"/>
DTIC TAB	<input type="checkbox"/>
Unannounced	<input type="checkbox"/>
Justification	
By	
Distribution	
Availability Codes	
Distribution	
<b>A-1</b>	



## TABLE OF CONTENTS

	<u>page</u>
OVERVIEW AND OBJECTIVES	
(University of Southern California Perspective) . . . . .	1
Role of Model Building . . . . .	1
Models of Ventricular Depolarization . . . . .	1
Models of Ventricular Repolarization . . . . .	2
The Role of the Computer Simulation of QRS-T in the	
Development of Quantitative Criteria and	
Optimal Lead Sets . . . . .	2
Simulation Model of QRS-T in Preliminary	
Hypothesis Testing . . . . .	4
OVERVIEW AND OBJECTIVES (U.S. Air Force Perspective) . . . . .	5
NOMENCLATURE OF REGIONAL LEFT VENTRICULAR SEGMENTS . . . . .	9
SOME WORKING DEFINITIONS . . . . .	10
TASK 1: BACKGROUND AND PREVIOUS WORK . . . . .	11
Ventricular Depolarization . . . . .	11
Clinically "Silent" Infarcts in the	
Air Force Pilot . . . . .	17
Cardiac Intracellular Action Potentials . . . . .	20
Modelling of Ventricular Repolarization . . . . .	21
Torso Transfer Impedance Changes at Rest	
and Exercise . . . . .	26
Optimal Electrode Number and Location . . . . .	29
Bibliography . . . . .	33
TASK 2: FORWARD MODEL DESIGN AND DEVELOPMENT . . . . .	47
Detailed Description of the Forward Computer	
Model Development . . . . .	49
Studies with the Forward Computer Model . . . . .	50
Validation . . . . .	52
Flow Chart of the Forward Model Program . . . . .	53
Input Data Modification Programs and Enhancements . . . . .	61
Numerical Experiments with the Model and Sequence	
of Its Development . . . . .	69



ENGINEERING CONSIDERATIONS: PORTABLE MULTILEAD DIGITAL ECG CART . . . . .	72
Present Major Commercial Vendors . . . . .	72
EDL Laboratories . . . . .	73
University-Affiliated Multilead ECG Systems Development . . . . .	73
APPENDIX: ECG Forward Model Treatise, Physiologic Research and Mathematical Theory . . . . .	75

OPTIMAL ECG ELECTRODE SITES AND CRITERIA FOR DETECTION  
OF ASYMPTOMATIC CORONARY ARTERY DISEASE  
AT REST AND WITH EXERCISE

OVERVIEW AND OBJECTIVES  
(University of Southern California Perspective)

Role of Model Building

Historically, scientific models have been used to explain inherently complex natural systems. In biology, specifically in electrocardiography and electrophysiology, Einthoven, the father of electrocardiography, viewed the heart as a single fixed locus dipole. This simple model of a complex system of cellular electrical generators still explains many aspects of the heart as an electric current source. Einthoven and associates used an equilateral triangle as a model of the human torso to relate the electrocardiographic signals from the three standard limb leads (1). This model explains so many aspects of the complex, inhomogeneous, irregularly shaped human torso that it forms a common basis for all clinical electrocardiographers to define specific changes seen on ECGs. The concept of a mean electrical axis for the ECG depends on both the equivalent dipole model of the heart as a current source and the equilateral triangle, or hexagonal reference system, as a model of the complex, inhomogeneous volume conductor through which these currents travel.

Models of Ventricular Depolarization

Sir Thomas Lewis, across the English Channel from Einthoven, went to the source and made elegant measurements on the heart itself using Einthoven's string galvanometer (2-4). From these measurements, he developed the dipole layer model to explain the propagating wave of electrical excitation he found on the epicardium. For years, his model of intramural excitation was used to explain the complex waveforms of conventional ECGs and of the ECGs of patients with myocardial infarction, bundle branch blocks, and hypertrophy of either ventricle. This early model of excitation of the ventricles was revised considerably, particularly the activation of the septum, after Allan Scher made his classic studies on intramural excitation using small, intramural plunge electrodes (5-8). Durrer and associates reported similar findings (9-13). However, the uniform propagating dipole layer was retained as the model of the excitation wave fronts moving through the heart.

When we developed the computer simulation of excitation of the human ventricle, we decided to build the simulation using measured anatomy, resistivities, and electrophysiology. From the intramural electrograms we sought data to define the dipole layer separation and the source strength of the positive and negative poles of the uniform dipole layer. We discovered that the dipole layer model of the active electromotive surface was inconsistent with measured data (14), and a new model of the propagating wave front needed

to be developed from the measured intramural data. Using a fine grid ( $1 \text{ mm}^3$ ) digital computer simulation of the propagating wave of depolarization (QRS changes) of the human heart we found that small myocardial infarcts no larger than 1-1.5 cm in diameter and 0.4-0.5 cm thick routinely produced detectable changes in the simulated ECGs (15,16). In clinical studies, we confirmed that small, clinically "silent" infarcts can be routinely detected from QRS changes in good quality resting electrocardiograms and vectorcardiograms (VCGs) when prior tracings are available for comparison. We found that serial change, or lack of it, in high-gain, high-fidelity ECG/VCG is predictive of serial ventriculographic change, or lack of it, with 98% accuracy (17).

We expect this to have particular relevance to the pilot population in whom, for reasons discussed in the Air Force perspective, it can be assumed that more than half of the myocardial infarcts suffered will have been clinically unrecognized, or "silent". Our model incorporated measured anatomy and physiology of ventricular excitation that allowed us to develop and validate new QRS criteria for quantitating myocardial infarct size (18-23). This success has given us confidence that the same strategy extended to include repolarization in the fine grid model is likely to produce more sensitive and specific ST-T criteria for detecting ischemia due to coronary disease.

#### Models of Ventricular Repolarization

Most, if not all, models of ventricular repolarization are indebted to some extent to the ventricular gradient model of Wilson (24,25) and the many studies refining it (26-49). Harumi, Burgess, and Abildskov were the first to develop a model of the T wave (50). Thiry and Rosenberg later developed a simulation of repolarization in 3 dimensions (51). Miller and Geselowitz developed a  $4 \text{ mm}^3$  grid heart model in a homogeneous torso in which they manually entered changes in excitation and recovery parameters (52-53). Essentially, we will be automating the grid heart model of Miller and Geselowitz in a  $1 \text{ mm}^3$  grid heart in an inhomogeneous torso. The success of these models in simulating typical 12-lead ECG changes of ischemia, injury, and infarction by incorporating action potential waveshapes and distributions typical of those measured in the laboratory makes the likelihood of success with the fine grid version quite high.

#### The Role of the Computer Simulation of QRS-T in the Development of Quantitative Criteria and Optimal Lead Sets

#### Simulation of Body Surface Maps at Rest

Briefly, the effort is to develop a mathematical generator for repolarization and simulate the myocardial depolarization/recovery process. Our method of constructing the repolarization generator makes use of an equation containing three arbitrary parameters that assume values which permit the time course of the EMF (electromotive force or electromotive surface in the heart) across the cell membrane to be approximated. The three parameters characterizing the action potential are the recovery potential, rate of

repolarization, and the functional refractory period. With these 3 parameters and 4 constants (initial resting potential, time to depolarize, peak depolarization potential, and a time constant which represents the time for the local region to reach equilibrium), each discrete point within the myocardium can have a unique waveform that represents it.

This equivalent generator is then combined with a Gelernter-Swihart (GS) solution for the heart-to-chest transfer impedances. Combining the generator and transfer impedances yields a mathematical-physical simulation containing arbitrary parameters that can be adjusted such that numerically computed body surface T-wave distributions can be made to agree with those measured on human subjects. Once a verified model is developed and fitted to resting and exercise normal map data, then a minimum set of chest electrodes can be selected which optimizes specificity and sensitivity of the model to ischemia with respect to ECG waveform changes.

### Simulation of Exercise Maps

It is anticipated that the coefficients and constants in the model for simulating ECGs will have to be altered to account for changes that occur with exercise. Subjects during stress testing usually exercise in an upright position; their torso geometry and resistivities change as they increase their tidal volumes and blood flow above resting; their heart position changes as does the distance between their surface ECG leads and local cardiac generators. It follows that transfer impedances from local cardiac generators to body surface leads may be significantly changed between quiet resting and exercise since they vary inversely as the square of the distance between generator and surface electrode. Trans-thoracic resistivity measurements, measured thoracic geometry, and heart location by 2-D echocardiograms during quiet supine rest and various levels of upright exercise will be used to adjust the torso simulation with the Gelernter-Swihart program to compute a series of transfer impedances between heart and surface ECG leads for these various intensities of exercise.

Additional changes in the repolarization generator parameters, such as recovery rate and functional refractory period, will be introduced. Increased heart rate and heart muscle temperature are known to change the shape of the monophasic action potential during recovery. A set of normal human subjects will be employed to adjust the G-S transfer impedances at exercise to bring simulated QRS-T wave potential distributions at exercise into agreement with observed data.

Our methods of cycle selecting and averaging exercise body surface ECGs will be the same as at rest since the principles are invariant with respect to differences between rest and exercise. Adjusting the simulation to account for exercise QRS-T wave potential distributions will be accomplished by the method of residuals. Our aim will be to reduce the residuals at exercise to a level commensurate with those attained from resting QRS-T wave distribution. This aim comes out of the desire to maintain the same level of certainty in the simulation of rest and exercise ECGs. When similar confidence limits exist on both sets of data, this simplifies the interpretation of the repolarization generator differences between rest and exercise.

### Simulation Model of QRS-T in Preliminary Hypothesis Testing

A computerized body surface ECG map simulation will provide an alternative method of studying pathophysiological mechanisms and generating less commonly observed body surface maps. A matrix transformation between difference properties (the difference between multilead ECG maps at rest and exercise) and the severity of coronary occlusion will form the basis for the analysis of regional ischemia in a selected patient population. This matrix transformation takes the form:

$$\Delta E = T \cdot C + \epsilon$$

where the elements of the vector  $\Delta E$  are the changes in ECG voltages between rest and exercise. The vector  $C$  is composed of elements whose values are the regional degree of coronary occlusion from patients with single vessel disease documented by coronary angiograms. The unknown  $T$  matrix of weighting factors will be formed from this data. The validated ECG simulation will provide data for  $C$  and  $\Delta E$  vectors not available in the learning set and will be used to fill out the unavailable elements in the  $T$  array of weighting factors. The specific hypothesis of this simulation effort is that exercise-induced ischemia and QRS-T changes in body surface maps can be transformed into degrees of regional coronary artery disease. This hypothesis is cast as mathematical transformations between exercise-induced QRS-T changes in specific regions of the torso and the ischemia produced in regional myocardium by specific coronary disease.

OVERVIEW AND OBJECTIVES  
(U.S. Air Force Perspective)  
by  
Gil D. Tolan, Colonel, USAF, MC

(Author's note: this summary from an earlier statement of work is presented here because it gives those from outside the Air Force, including our consultants, a perspective from "inside" that would not otherwise be available.)

Although coronary artery disease mortality in the United States decreased 22.6% between 1969 and 1977, at 670 deaths per 100,000 men per year, coronary artery disease still remains the number one cause of death in this country. Coronary artery disease is the cause of 70% of the nontraumatic deaths in the active duty U.S. Air Force. Rated flying personnel are not immune to developing coronary artery disease. Each year approximately 50 rated pilots and navigators on flying status are admitted to USAF hospitals where the discharge diagnosis is coronary artery disease (ICDA codes 410 through 414). Each year approximately 8 rated personnel on flying status suffer fatal myocardial infarctions. It is hard to say how many USAF aircraft accidents per year are due to coronary artery disease because frequently there is no heart found to autopsy after the crash, and because the on-board recorder does not record the ECG. Even if a pilot suffered an acute myocardial infarction in flight, there would not be sufficient time between that event and when the rest of the heart died in the crash to distinguish the acute infarction. It takes hours to days for the necrosis of an infarction to become evident at autopsy. The Armed Forces Institute of Pathology has a policy of not attributing an aircraft crash to coronary artery disease merely because an old myocardial infarction scar is found or because coronary atherosclerosis is present. Today 44% of the rated force is over 35, the age susceptible for coronary artery disease. Coronary artery disease is not confined to just older pilots. Autopsy studies on military men killed in combat in both Viet Nam and Korea found coronary artery disease in many young troops. Although we do not know how many aircraft accidents per year are due to coronary artery disease, we do know that approximately six times per year a USAF aircraft for no apparent reason impacts the ground with no prior communication from the pilot and no attempt to eject. Some suspect that the pilot was trying to recover an out-of-control aircraft right up to the end, but others believe the lack of any communication of trouble implies sudden human incapacitation. Although there are many causes of sudden incapacitation, common things occur commonly, and coronary artery disease is the most common cause of sudden incapacitation in American males.

Today the screening for coronary artery disease in the USAF rated force relies solely on the standard 12-lead ECG. The Framingham 14-year follow-up of 5000 men and women considered free of heart disease at onset found that the standard 12-lead ECG was normal in 2 out of every 3 cases which suffered a myocardial infarction in the subsequent 2 years. This number represents a 33% sensitivity for the standard 12-lead ECG as a predictor of a myocardial infarction in the next 2 years. The Framingham study also found that in those cases with scars from old myocardial infarctions found at autopsy, 36%

of these were unrecognized during life by both the patient and his doctor. In 16% of all coronary cases, the first symptom was sudden death.

Most USAF flyers enjoy flying; they get paid extra to be on flying status, and often their career progression requires that they be fit to fly. Although most flyers have IQ's three standard deviations above the mean, they nearly all score three standard deviations above the mean on the MMPI denial scale. Their ability to deny risk is a life-preserving attribute that prevents them from panicking when exposed to enemy fire. These same factors, however, decrease a flyer's propensity to report his chest pain to his flight surgeon.

In the new generation high-performance aircraft, flyers are frequently exposed to greater than 7 +G forces. By the end of this decade, two-thirds of USAF active-duty pilots will be flying high-performance aircraft. These aircraft place unprecedented demands on the heart to keep the brain perfused. Within 30 seconds of pulling 7 +G's, the pooling of blood in the lower lobes of the lungs causes the alveolae to collapse, creating a ventilation perfusion abnormality such that in healthy nonsmokers their mean arterial oxygen tension drops from 91 to 46 mmHg. At the very time the demand for cardiac output is maximum, the oxygen supply to the heart is being decreased by both this ventilation perfusion abnormality and by the shortening of diastolic filling time from the faster heart rate. Since flow of a liquid through a tube is inversely proportional to the fourth power of the radius, a slight decrease in a coronary artery's diameter can have a big effect on the amount of blood that gets by that obstruction should the flow remain laminar. Because a slight obstruction can cause turbulence, a slight coronary obstruction can be more hemodynamically significant than implied by the percent diameter narrowing. Furthermore, a healthy coronary artery can increase flow ninefold by dilating during peak workloads. By preventing dilation, circumferential atherosclerosis, even if minimal on angiography, can profoundly reduce myocardial oxygen supply during peak loads. Even without causing a myocardial infarction, an asymptomatic coronary narrowing can decrease maximum cardiac output during sustained high +G maneuvers. If during a high +G maneuver the pilot's brain is not perfused, then under the best of circumstances, it will take him on the average 15 seconds to recover from his loss of consciousness. By then it may be too late to recover his supersonic aircraft. Thus, a slight coronary artery narrowing which might never cause an infarction on the ground could prove fatal under the sustained high +G profiles of the new-generation aircraft.

For all the reasons cited above, flying safety requires that we not wait for the flyers to come to their flight surgeon with complaints of chest pain before we begin worrying whether they have coronary artery disease. We need to be able to detect coronary artery disease while it is still asymptomatic. At this time the National Institutes of Health have no plans to fund research into detecting asymptomatic coronary artery disease because "the only treatment for it is advice to modify risk factors and that advice should be given regardless of whether coronary artery obstructions already exist." If medical technology is to keep pace with the demands of new aircraft technology, then it is up to the U.S. Air Force to develop a better system to detect coronary artery disease.

The goal of this contract is to develop a system which is better than the existing method at distinguishing rated flyers with aeromedically disqualifying coronary artery disease from healthy flyers. This system includes detecting both coronary artery obstructions (ischemia) and myocardial infarctions (scars). Correctly localizing infarctions and coronary obstructions with a screening test in the field is not a requirement of this contract.

Good skin-to-electrode contact is essential to accurate electrocardiography, but good contact during stress testing is difficult to maintain because the adhesive may loosen as the patient moves and perspires. The more electrodes one adds, the greater this problem. Furthermore, additional electrodes require additional time to apply, more channels for recording and more complex analysis, all of which increase the cost. For these reasons, the U.S. Air Force needs to use enough electrodes in both resting and stress electrocardiography to ensure flying safety without adding any extra electrodes merely to determine some day if they might be useful. Any addition of electrodes will incur a considerable expense not only to acquire new ECG carts for the field, but also to train USAF physicians to interpret the new leads. For this reason, any new lead must be based upon strong scientific evidence that it adds important information not currently available. Because the expense and risks of both false positive and false negative errors are considerable, the process in developing such scientific evidence must be meticulous in every detail. Because current policy requires that rated flyers with abnormal stress tests be grounded until proven healthy by cardiac catheterization, it is essential that any new screening system maintain a specificity of 95% or better.

In 1974, Victor Froelicher, Jr., Maj, USAF, MC, reported in the American Journal of Cardiology on a group of 1,390 asymptomatic men screened at the USAF School of Aerospace Medicine for latent coronary artery disease with a double Master's two-step test followed by a symptom-limited treadmill exercise tolerance test. The follow-up period ranged from 4.1 to 8.4 years (mean 6.3). End points for coronary artery disease were angina pectoris, acute myocardial infarction, and sudden death. Only lead X (CC5) was always recorded during exercise. Leads II, III, aVF, V2, and V5 were recorded before exercise and during recovery. In this follow-up study, the Master's test had a sensitivity of 61% and a specificity of 92%. Subsequently, this institution has recorded four leads (X, Yh, Z, and CM5) during all phases of the treadmill test. No follow-up study of this lead system has been done, but we know that 60% of the asymptomatic flyers with abnormal ST segment depression on symptom-limited stress testing have no coronary artery disease found on cardiac catheterization with left ventriculography and selective coronary angiography. We have also found advanced coronary artery disease in three dozen asymptomatic flyers with normal or only borderline abnormal ST depression on their treadmill test.

In a series of four articles published in Circulation in 1973 and 1974, Fred Kornreich, M.D., of the Free University of Brussels, pointed out that neither the Frank lead vectorcardiogram nor the standard 12-lead electrocardiogram contain all the information projected by the heart to the body surface. Dr. Kornreich found that with 24 leads and a single transformation formula for all body types, one could closely reconstruct a complete body surface map. Subsequently, Robert Lux, Ph.D., at the University of Utah, Roger Barr, Ph.D., at Duke University, and others have shown that at least 24



electrodes are needed to capture all the information projected by the heart to the body surface. What remains to be determined is whether 24 electrodes are necessary to detect all disqualifying asymptomatic coronary artery disease in the USAF rated force. In 1980, Dr. Kornreich reported at the Engineering Foundation Conference on Computerized Interpretations of the ECG that adding just four electrodes to the standard 12-lead ECG for a total of 14 electrodes significantly improved the sensitivity and specificity of bonafide myocardial infarctions over just the standard 12-lead ECG or just the Frank lead VCG. At the same meeting, Frank Yanowitz, M.D., of the University of Utah, reported that using 32 leads doubled the sensitivity of stress tests for cardiac catheterization-proven significant coronary artery disease compared to using the standard 12-lead system for stress testing. He also suggested that not all 32 leads were necessary, but needed more data to prove this. In 1980, at the Computers in Cardiology Conference, R. von Essen of the Helmholtz Institute for Biomedical Engineering in West Germany, reported that a 48-precordial-lead stress test had a 96% sensitivity and 95% specificity compared with 56% sensitivity and 95% specificity of the 12-lead system for stress testing. Other investigators have reported similar improvements in sensitivity while maintaining 95% specificity by doing surface potential mapping with stress testing.

## NOMENCLATURE OF REGIONAL LEFT VENTRICULAR SEGMENTS

Considerable ambiguity exists in the current literature about the nomenclature and definition of the regional or segmental anatomy of the heart. Throughout this document we will be using the left ventricular (LV) segmental subdivision nomenclature shown in Figure 1. This subdivision is a modification of the Ideker subdivision reported in a number of recent papers (18-23), in which the octant circumferential subdivisions of the left ventricle along its long axis are combined by twos into quadrants. The LV is further subdivided from apex to base by passing two planes through it at right angles to the long axis of the LV in such a way as to divide the internal long axis into equal thirds. This system produces a 12-segment subdivision of 4 walls (anterior, superior, posterior, and inferior) with 3 subdivisions each (apical, mesial, and basal) as shown in Figure 1.

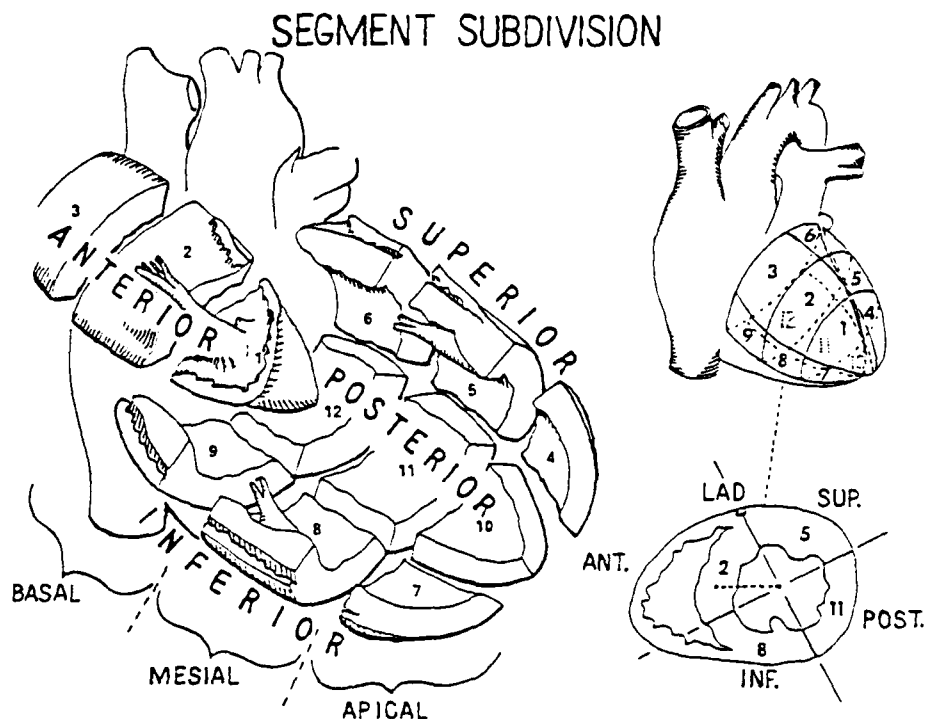


Figure 1. Twelve-segment LV subdivision and nomenclature used in this report. The advantage of using this specific subdivision is that it divides the left ventricle into segments that are in close approximation to the usual blood supply to each of the regions, i.e., segments 1-7, and 10 by the left anterior descending coronary, 8 and 9 by the right, and 11 and 12 by the circumflex.

## SOME WORKING DEFINITIONS

Activation, excitation, and depolarization of the ventricle (which produces the QRS of the ECG) will be used, throughout this report, interchangeably. The same applies to recovery and repolarization, the ST-T portion of the ECG. End diastole will be used for that time in the cardiac cycle when maximal diastolic relaxation has occurred just prior to the onset of ventricular contraction. The QRS of the ECG is recorded at this time. End systole will be taken to mean that time when the ventricular contraction has reached its maximum, the slope of the ventricular pressure curve is 0, and ventricular relaxation will soon commence, followed by aortic and pulmonic valve closure, and the return of the ventricular pressure curve to diastolic levels. Mid systole is that time midway between end diastole and end systole.

## BACKGROUND AND PREVIOUS WORK

### Ventricular Depolarization

Extensive work has been done in observing and measuring the complex bioelectric phenomenon of depolarization of myocardial cells. Over a century ago, Burdon-Sanderson and Page used mercury capillary electrometers to measure in some detail the electric current generated by both auricles and ventricles (54,55). Giving credit to previous work in the mid 1800's by Kolliker and Muller (56), Cyon (57), Donders (58), Engelman (59), and Marchand (60), they observed that the positivity of the electrical deflection that preceded contraction of the frog (and turtle) heart was related to the location of the applied electrodes as related to the long axis of the ventricles. They recorded a terminal wave, later labeled the T wave by Einthoven, and noted that it coincided with ventricular relaxation. They found that warming or cooling changed the timing and the configuration of this wave and that an electrical stimulus delivered before the terminal wave did not produce a second primary electrical wave and contraction, whereas a stimulus delivered after the terminal wave, but before the next primary wave, did.

The invention of the string galvanometer at the turn of the century and its development by Einthoven into a routine experimental tool (1,61,62) led to a great deal of experimental work in animal models. Notable was the careful work in the dog by Lewis (2-4) who described normal and abnormal activation sequences based on epicardial measurements with the string galvanometer. Lewis' version of the sequence of normal ventricular depolarization and its extrapolation to man was the basic model used to interpret clinical ECGs for the next 30 years. A number of workers explored the role of the Purkinje conduction system in controlling the activation sequence (63-69). Conflicting data was generated which led to a misnaming of right and left bundle branch block until a review paper by Wilson (70) that included convincing new work clarified the confusion. The development of the precordial leads, first the CF leads, and later the V leads using the central terminal of Wilson (71-73) added a much needed horizontal plane dimension to the ECG. This development helped clarify the localization of bundle branch blocks and local infarction as well. The development of various vectorcardiographic lead systems soon followed, which further refined the early Einthoven hypothesis that the heart could be well represented by a single fixed-locus equivalent dipole (74-78).

Papers by Prinzmetal and coworkers (79,80) and Sodi-Pallares and coworkers (81-84) recording with intracavitary and plunge electrodes in the dog heart added information about the electrical behavior of the heart with ischemia and infarction. However, the sequence of intramural excitation in the presence of infarction, or even in normal activation, remained sketchy due to the limited number of electrode sites on these electrodes. The detailed intramural mapping of the wave of excitation of the mammalian heart using small diameter, multi-point needle electrodes was reported in a number of papers by Durrer and coworkers (9-13) and in the classic papers by Scher and his coworkers (5-8). Soon thereafter, Durrer, Van Dam, and associates

presented the details of human activation sequence using revitalized human hearts of accident victims (85). These latter papers have become the basis of a number of simulations of ventricular depolarization in man, including those of Okajima (86,87), Horachek et al. (88), and Arntzenius (89), as well as our own.

In the early 1960's, we began to explore the possible role of computer simulations of the electric field of the heart in man. Our first effort was to simulate the human vectorcardiogram (90). We assumed the heart to be an equivalent dipole current source and the human activation sequence to be similar to that demonstrated by Scher in dogs. We also assumed a uniform current generator surface in the local region of a multiple segment heart. We gave each segment a dipole moment time history based on these assumptions and the Scher activation data, and a direction normal to the average wave fronts in the local region. When normal activation was simulated, normal vectorcardiograms resulted. When dipoles representing the left or right ventricle were increased in dipole moment, as would be expected with hypertrophy of either ventricle, VCGs typical of these abnormalities were produced, and when one dipole or more were removed to simulate the loss of 8% or more of the left ventricle, VCG loops (and simulated 12-lead ECGs) were produced that were quite typical of the focal infarct simulated. Moreover, the larger the infarct simulated, the greater the VCG/ECG change. When Durrer's human activation data became available at about this time, we found it very similar to our simulation. We upgraded our model with this measured data, and with distance and boundary effects (15,16). A year later, we added the Gelernter-Swihart simulation of the inhomogeneous human male torso including intracavitary blood mass (91). Finally, we added a  $1\text{ mm}^3$  grid

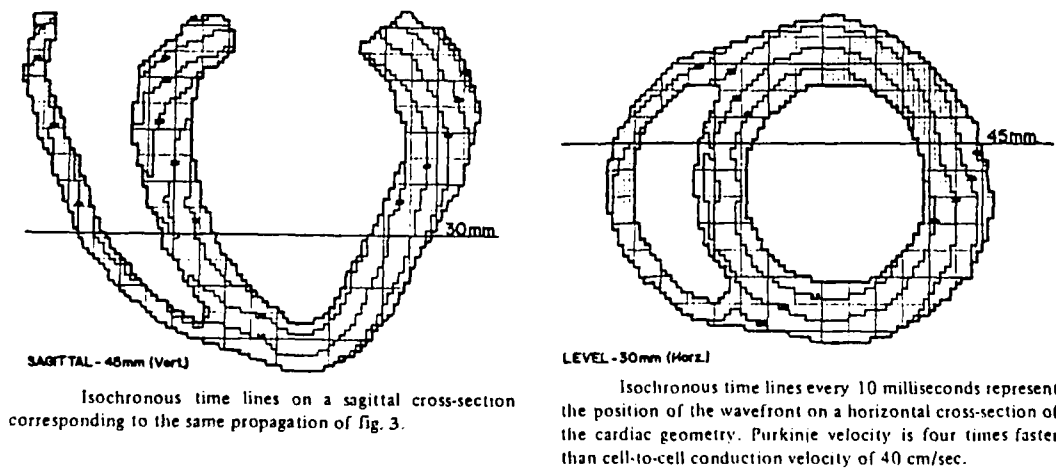


Figure 2. A transverse view along the long axis of the left ventricle is shown to the left, and a short axis view, corresponding to the 30-mm cross section identified on the long axis view, is shown to the right. Isochronous time lines every 10 milliseconds are shown on both views.

propagation model of excitation (Figure 2) which used the actual digitized geometry of a normal male human heart and included a simulation of Purkinje conduction (92,93). We now had in the simulation all the first-order variables known to influence the human ECG, and for all intents and purposes, the computer simulation behaved like the electric field of a normal human male subject. The parameters that influence wave shape, such as torso geometry, resistivities, heart location, and activation sequence of normal (Figure 3) or abnormal (Figure 4) conduction with or without hypertrophy or infarction, could be varied at will within physiologically and anatomically reasonable limits. The complex interactions of these variables could be examined in a situation where all the parameters used and the assumptions made are precisely known.

In the early stages of the experimentation with the simulations that could mimic all the classic infarcts, it became clear why conventional ECG criteria are insensitive to many infarcts. In a number of autopsy series (94-96), the ECG was found predictive of the infarcts found in only about 55% to 60% of those confluent scars that were 2 cm or greater in size at post mortem examination. Conventional ECG criteria for infarction involve the finding of abnormal Q waves or abnormal loss of initial R waves especially in precordial leads. In the simulation, small infarcts in the typical locations produced definite changes when compared to pre-infarct ECG/VCGs, but often failed to produce the classical changes. Larger infarcts in these same locations generally did produce typical changes. On the other hand, about 25% of infarcts found at autopsy involve the base of the left ventricle which is depolarized after 40 msec. Simulated infarction of these regions produced mid to late QRS changes and no initial changes at all that would be the typical or classic ECG changes of infarct. We designed one of our early experiments (97) to explore the contention by Sodi-Pallares (84,98) and others (79) that large portions of the basal septum and free wall, as well as most of the subendocardium, is electrically silent. We found that neither extensive experimental work with the dog (99) and the baboon, nor extensive work with the model that contained the details of electrophysiology and anatomy (14-16) supported this notion. In fact, while some regions deep in the chest showed an expected lower amplitude of change in surface ECG/VCGs and surface ECG maps, no region was electrically silent. To the contrary, simulated infarcts in all regions of the heart produced clear-cut changes when compared to prior ECG data. Moreover, the degree of change was proportional to the extent of infarct put into the model.

We next explored the question of what size of infarct in any of the various regions of the heart would produce detectable changes in optimally recorded 12-lead ECGs and VCGs by both a corrected [McFee-Parungao (100)] and an uncorrected [modified Grishman Cube (77)] lead system. When incorporated into the propagation simulation and the full torso model (101), lesions 7 mm to 10 mm in diameter and 3 mm thick produced serial notches and deformities in the QRS well above the noise in well-recorded, signal-processed ECG data (15). Lesions 15-20 mm in diameter and 4-5 mm thick produced quite unequivocal changes (16). Examples of these changes are shown in Figures 5 and 6 and are shown in more detail in refs. 15, 16, 22, and 101.

# VENTRICULAR PROPAGATION MODEL WITH NORMAL CONDUCTION

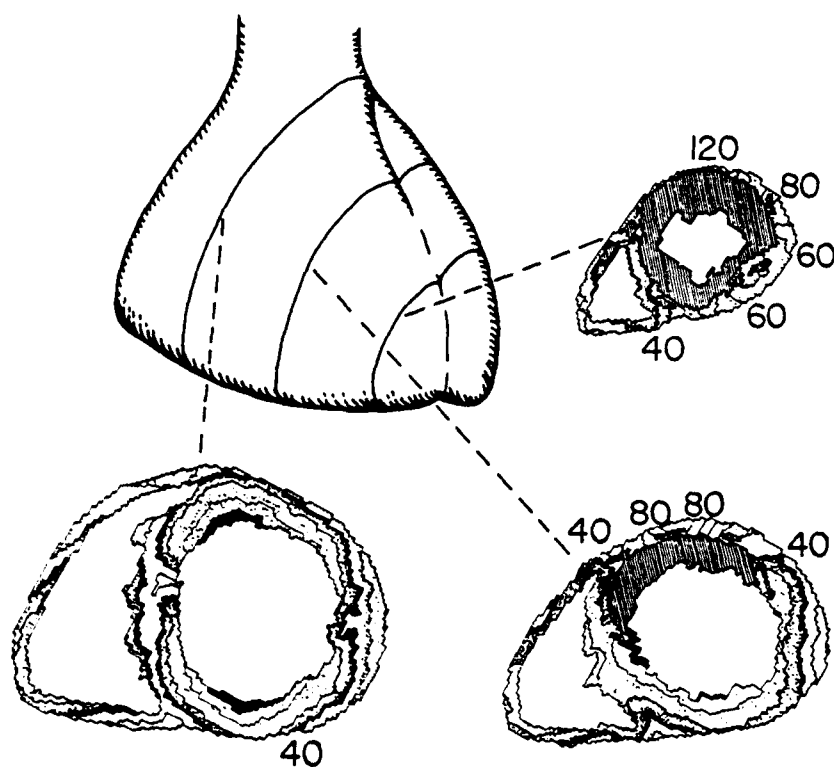


Figure 3. A moderate to large anterioapical infarct that involves 24% of the left ventricle is shown in the diagonal lined shaded areas in the apical and mid-ventricular cross sections. It is incorporated into the model along with the normal activation as shown in Fig. 2. The early activation on the mid left septal surface and up onto the endocardial surface of the superior and inferior walls is shown in solid black in this diagram. Isochronous time lines at 10-msec intervals are shown as the excitation wave propagates outward from the normal early start points on the endocardium. The 40-msec isochrone is shown in darker shaded line labeled 40 and best seen in the uninfarcted basal section. As shown here it is common for infarcts in the human heart to involve the endocardium more extensively than the epicardium and to leave a thin "peel" of relatively normal myocardium in the epicardium over the infarct. When this happens, the excitation reaches the epicardium, as in this case, from the endocardium around the infarct. Except for this small area of "peri-infarction" delay, the latest area activated was the posterior wall up near the AV groove, and the outflow tract of the right ventricle, not shown in any of these three cross sections. For more specific details about how various sized infarcts that were simulated in each coronary artery distribution affected the 12-lead ECG and the McFee VCGs on an inhomogeneous male torso, see the text, and particularly ref. 22.

# SUPERIOR AND INFERIOR FASCICULAR BLOCK IN THE PROPAGATION MODEL

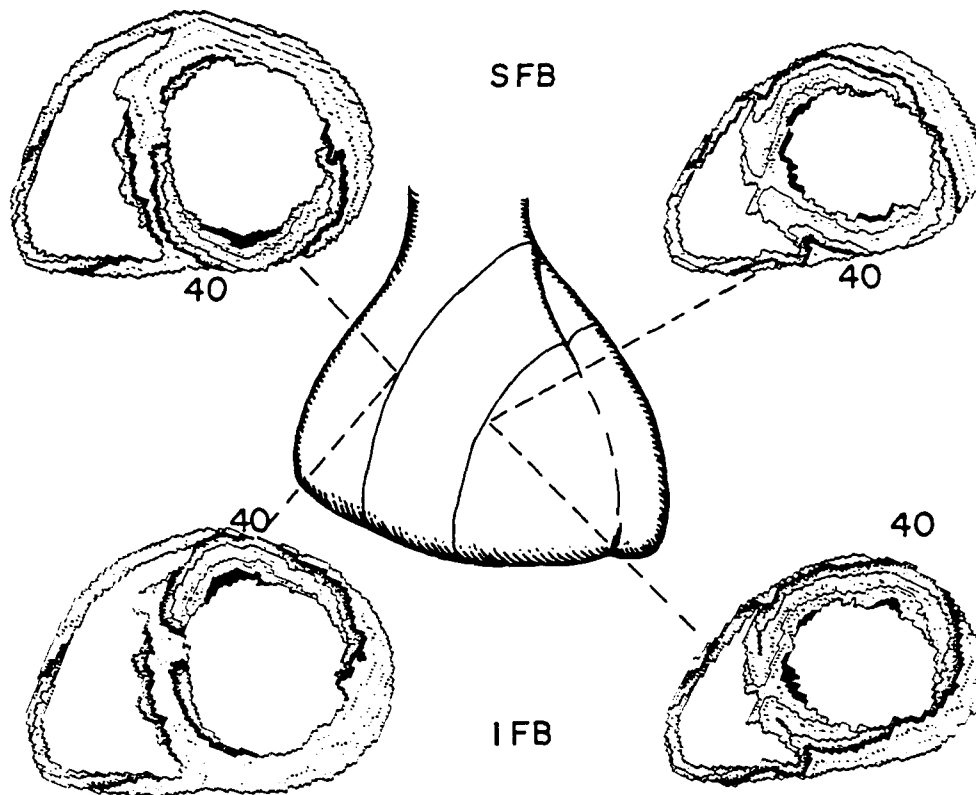


Figure 4. Superior fascicular block was simulated in this experiment by omitting the start points in the superior wall of this heart. Activation reached this region as shown here after about a 20 msec delay, arriving there via an intact peripheral endocardial Purkinje network. Such an excitation produces 20-30 msec increase in total QRS duration, a shift in early forces inferior (producing significant Q's in I and AVL), and late forces superior. Because of major unopposed late activation fronts superior (and posterior), there is a shift of the frontal mean axis superior to above  $-40$  degrees. Inferior fascicular block in this experiment produced similar degree of total QRS prolongation, initial vectors superior for 30 msec and a prominent unopposed late front inferior and posterior. The net effect of these changes was to shift mean frontal axis inferior to  $+70$  degrees. It took an unusual variant of normal excitation to produce "right axis" (i.e., beyond  $90$  to  $100$  degrees in the frontal plane with a block in the inferior fascicle). We believe that this accounts for the relative rarity of this diagnosis using conventional criteria for its diagnosis by ECG/VCG. Specifically, the criteria for the diagnosis of inferior fascicular block appear to be too stringent. In a critical review of our data base, we found that this conduction abnormality is about as common as superior fascicular block (22) and is seen most commonly in association with inferior infarction from right coronary occlusion.



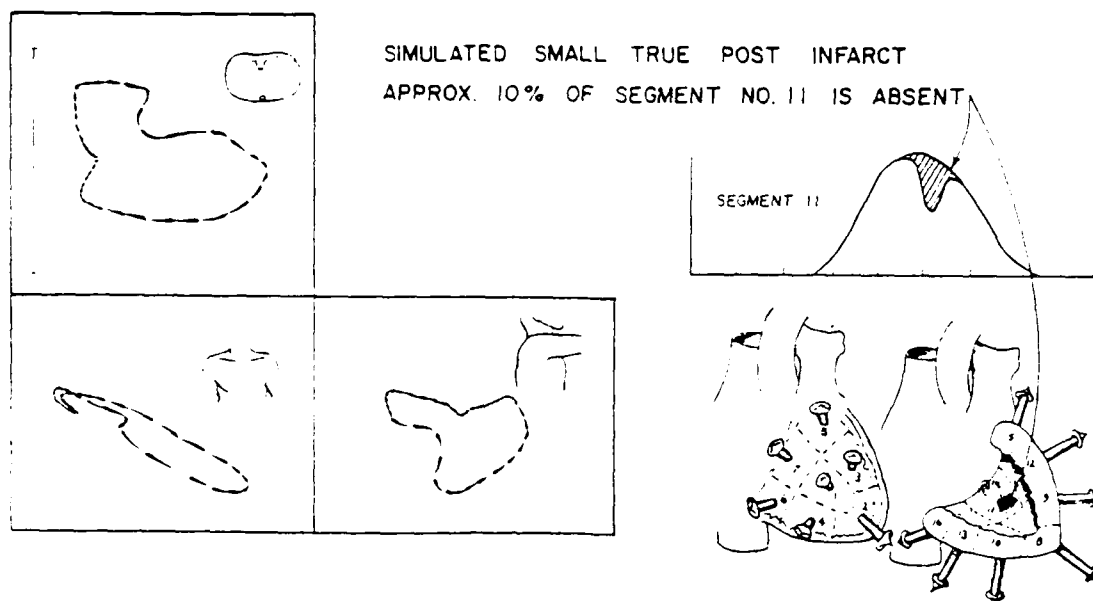


Figure 5. A small area of infarction in the outer half of segment 11 is simulated here. This simulation was done by placing a dipole with a negative directed function, represented by the shaded area above, at the same coordinate location and given the direction cosines as segment 11. The computation then sees both dipoles as one and the resultant will be the double peaked curve shown. The infarcted area shaded above is about 10% of the area under the curve representing the dipole moment history of segment 11. Thus, this vectorcardiographic change was produced by a simulated infarct representing about 2 g of myocardium.

The validity of these findings was tested in a series of patients with known coronary artery disease in whom serial coronary and biplane ventricular angiograms were done as a part of a long-term follow-up study. All had serial 12-lead ECGs, and Cube and McFee VCGs digitized at a 1 kHz sampling rate, cycle selected in expiration time aligned, and averaged to reduce noise to the 3 microvolt peak-to-peak range. The presence or absence of significant serial change as read by two blinded readers was predictive with a 98% accuracy of the presence or absence of significant serial ventriculographic change as read by 2 different blinded readers (17). These findings along with the simulations led to the development of a 54 criteria-32 point ECG infarct scoring system where each point represents 3% infarction of the left ventricle. The point scoring system, shown in detail in Table 1, has been extensively validated in a series of autopsy studies (18-20,22), and by clinical nuclear and contrast angiography studies by Wagner, Ideker, and associates (21,102). While the usual 12-lead ECGs used for these studies were not optimal by the criteria of high-fidelity, low-noise records as defined above, the good correlations achieved (see Figure 7) indicate that even in these poor quality records, clinically relevant quantitative information about infarct size and residual ventricular function is present.

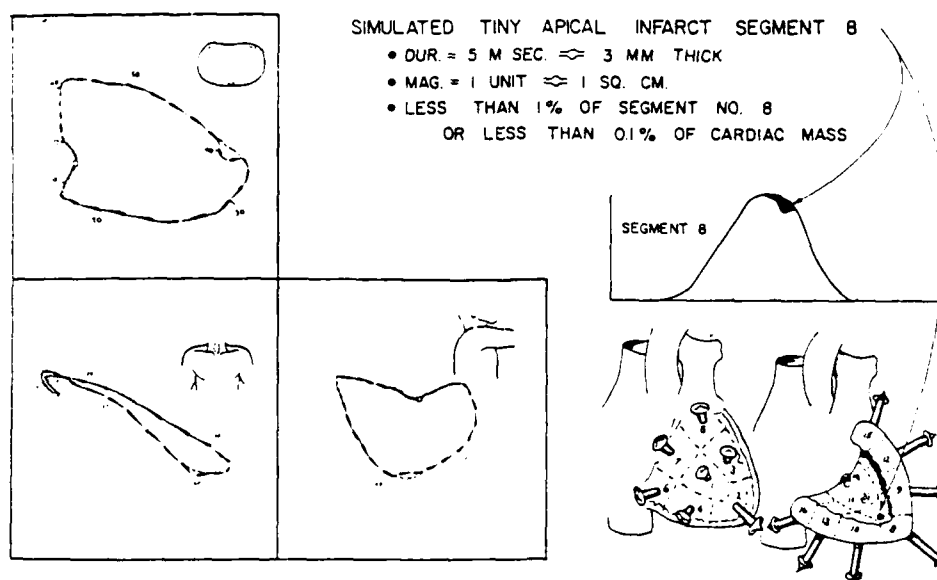


Figure 6. A tiny infarct representing less than a 6-mm lesion in segment 8 at the apex of the left ventricle is shown here. When a control record was available for comparison, a simulated small infarct of this size produced recognizable changes in any of the 20 dipole locations. These data cast doubt on the concept of electrically "silent area" of myocardium, and suggest instead that what is needed is to refine our diagnostic criteria and our measuring tools so that they are sensitive to this degree of change in the human cardiac generator.

#### Clinically "Silent" Infarcts in the Air Force Pilot

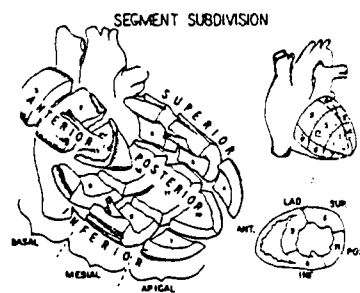
Regarding the case finding of clinically "silent" infarcts in the asymptomatic Air Force pilot population, these data indicate that in this population where serial ECGs are routine and high-fidelity VCGs are available on a large number, significant infarction (i.e., infarcts greater than 1.5 cm in diameter) should be routinely detectable. Since some 20-30% of infarcts in a civilian population are clinically silent, and since this percentage in the pilot population can be expected to be about twice as high, it follows that approximately 50 infarcts occur each year in rated pilots and navigators that are undetected clinically. Most of these infarcts are probably small to moderate in size since most infarcts are in this size range. Thus, well over half of these would not have classic ECG changes on a routine serial ECG screening. With careful attention to recording serial high-fidelity ECG/VCG data and to criteria involving the entire QRS, including significant deformities not associated with classic Q wave changes, it is to be expected that fully 90% or more of these infarcts can be found. Since a small number of false positives are inevitable from any such review of data, we propose that the serial tracings be screened for major significant non-Q wave changes, indicative of at least a moderate-sized new infarct by the ECG Point score (see Table 1) or by serial VCG change. Moderate infarcts would be 5-7 ECG

TABLE 1. COMPLETE 54-CRITERIA/32-POINT QRS SCORING SYSTEM

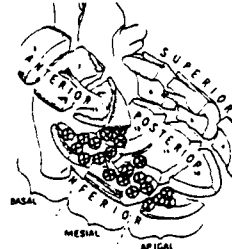
ECG POINTS (3% LV Ea)				%LV INFARCT IN 12 LV SEGMENTS											
Lead	Criteria	Pts. Ea.	Ld. Max. Pts.	L. Ant. 1	Ant. 2	Desc. 3	RCA Inf. 4	Sup. 5	6	7	8	9	Cx. Post. 10	11	12
1	Q>=30ms R/Q<1 R<=0.3Mv	1 1 1	2			1 1							1		
2	Q>=40ms Q>=30ms	2 1	2				1 2	2					1		
L	Q>=30ms R/Q<1	1 1	2			2 1									
F	Q>=50ms Q>=40ms Q>=30ms R/Q<1 R/Q<2	3 2 1 2 1	5				3 2	2					1 1		
V1	Ant Any Q S>=1.8Mv	1 1	2			1 2									
	Post R/S>=1 R>=50ms R>=1.0Mv R>=40ms R>=0.6Mv S<=0.3Mv	1 2 1 1 1 1	4				1 1						1 1 1		
V2	Ant Any Q R<=10ms R<=0.1Mv	1 1 1	1			1 1 1									
	Post R/S>=1.5 R>=60ms R>=2.0Mv R>=50ms R>=1.5Mv S<=0.4Mv	1 2 1 1 1 1	4				1 1	1					1 2 1		
V3	Any Q R<=20ms R<=0.2Mv RV3<=RV1	1 1 1 1	1			1 1		1							
V4	Q>=20ms R/Q<0.5 R/S<0.5 R/Q<1 R/S<1 R<=0.7Mv Notched R	1 2 2 1 1 1 1	3			1 1	1 1								
V5	Q>=30ms R/Q<1 R/S<1 R/Q<2 R/S<2 R<=0.7Mv Notched R	1 2 2 1 1 1 1	3			1 1	2 1								
V6	Q>=30ms R/Q<1 R/S<1 R/Q<3 R/S<3 R<=0.6Mv Notched R	1 2 2 1 1 1 1	3			1 1	1 1	2					1		

TOTAL POINTS 32 Each Point = 3% LV INFARCTED

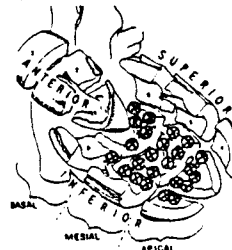
If > 1 criteria in bracket met, select 1 with most points.  
Criteria in bracket with same score are "ored" ie. even  
if 2 or more criteria met, the point is scored only once.



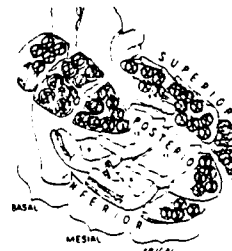
INFERIOR LEADS 2, F, 7 POINTS MAXIMUM  
(21% LV) @=1% allotted to ea. segment



POSTERIOR LEADS V1, V2, 8 POINTS MAX.  
(24% LV) @=1% allotted to each segment



ANTEROSUPERIOR LEADS 1, L, V1-V6 17 PTS. MAX.  
(51% LV) @=1% allotted to each segment



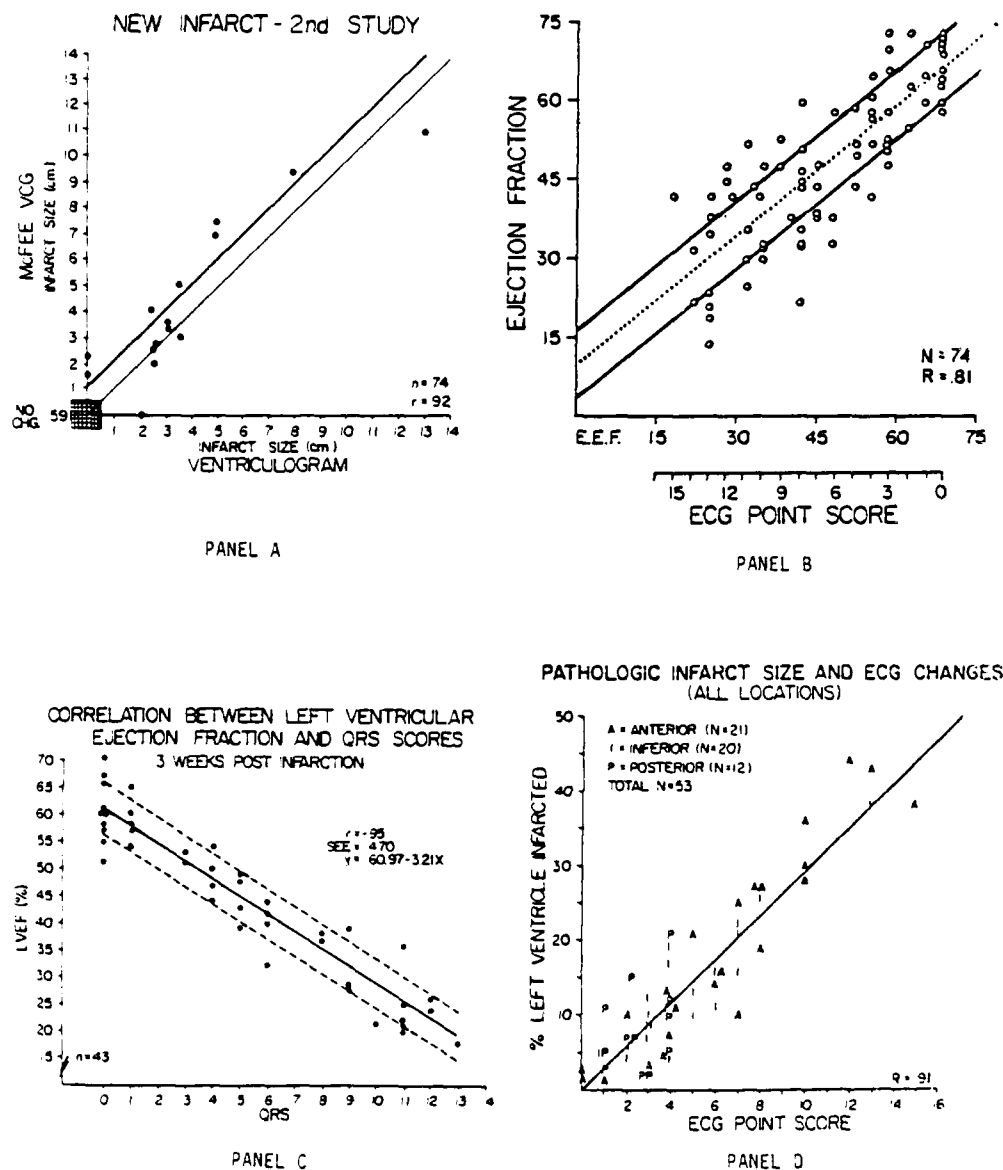


Figure 7. Panel A plots new infarct size on serial comparisons of VCG change (or lack of it) and contrast Vgrams in 77 consecutive serial coronary angiographic studies (17). The upper line is the regression line, and the lower one is line of unity. Panel B shows the correlation between our ECG point score for infarct size and ejection fraction (E.F.) in patients with chronic angina and/or infarction (22). The 2 extra lines represent 1SD on either side of the regression line. Panel C relates ECG points and nuclear E.F. in 43 patients 3 weeks after an acute infarction, the dotted lines = 2SD; Palmeri et al. (102). Panel D plots ECG point score and infarct size at quantitative planimetric pathology in the 1st 53 patients reported by Ideker et al. (19-23).

points, or 15-20% of the left ventricle. This would include a similar degree of VCG change by published criteria. The intention is to approach a 100% likelihood that pilots with these changes on their ECGs would have significant coronary artery disease on coronary angiograms.

### Cardiac Intracellular Action Potentials

The development of the fine glass capillary microelectrode by Ling and Gerard in 1949 (103) led to a new era in the exploration of intracellular action potentials from electrically active cells. The small (1  $\mu$ m or less) tip size allowed for micropuncture of a single cell without significantly changing its membrane electrophysiology. In 1951, Woodbury, Hecht and Christopherson recorded single ventricular fiber action potentials from the frog using this electrode (104); with Brady, this group examined the effects of cardiac glycosides and other interventions on this frog ventricular fiber preparation, and later measured transmembrane action potentials from the human heart (105-107). Seminal work relating the ventricular transmembrane action potential duration and wave shapes to refractory period and the T wave of the ECG was done in the 1950's by Hoffman, Kao, and Suckling (108,109). This work culminated in the publication in 1960 of the classic monograph by Hoffman and Cranefield, "Electrophysiology of the Heart" (110). This publication extensively reviewed transmembrane action potentials from various cardiac tissues and the effect of various interventions using cardioactive drugs, electrolytes, hypoxia, and injury on these cardiac cells.

The shape of the action potential, however, can be recorded relatively free of the problems of muscle movement in the intact heart if external suction electrodes are used (111). Six years before the work of Ling and Gerard with the cell puncture with microelectrodes, Schafer et al. had used the suction electrode to study the T wave (112). In 1959, Hoffman and Cranefield, working with Lepeschkin, Surawicz, and Herrlich, demonstrated that the waveform of the action potential by the two methods corresponded closely although, as might be expected, the magnitude of the potential recorded with the suction electrode was smaller (113). The main disadvantage of the suction electrode is that it must be applied to the surface of the intact heart and therefore, cannot be used to gather information about gradients of action potential durations and sequence of recovery in the intramural layers of the heart. Another limitation of the method is that it must also be used with the chest open, and repolarization is known to be quite sensitive to temperature changes. Using this method and attempting to minimize the temperature effects, Autenrieth, Surawicz, and Kuo were able to demonstrate systematic differences in the duration of action potentials on the surface of the left ventricle of the dog (114). The longest duration was at the apex, and the shortest was at the posterior base. They also noted that in most cases, the surface action potentials ended well before the end of the T wave, implying that some tissue deeper in the wall of the heart, not accessible to the electrode, repolarized later.

Based on the findings of Hoffman and Cranefield that refractory periods measured by classic methods corresponded closely to the end of the repolarization phase of the intracellular action potentials, van Dam and Durrer mapped functional refractory periods with intramural electrodes in the open-chested dog (115,116). They found that the endocardium, while depolarizing

first, recovered refractoriness latest; mid wall intramural areas recovered earliest; and the epicardium is intermediate. Burgess, Abildskov, Green, Lux, Millar, Vincent, Wyatt, Yanowitz and others of the Utah group published an important series of papers in the last 15 years repeating this work in the closed-chested dog and concluded that there is likely a linear gradient of ventricular recovery times from epicardium to endocardium with the epicardium repolarizing earliest (117-132). They found that the interventricular septum behaves like the free wall of the left ventricle. They also established that there is a gradient in functional refractory periods from apex to base with the apical regions having the longer refractory periods.

Finally, extracellular electrode recordings, both bipolar and unipolar, have been used to map excitation in detail. Their advantage over even multiple intracellular recordings is that they map the interactions of the whole system of depolarizing and repolarizing cells. Spach and his coworkers made unipolar potential maps, not only with electrodes on the torso surface, but with epicardial and intramural electrodes in animals allowed to recover for several days before the measurements were made (133-135). From some 300 electrodes implanted in each of several dogs, they were able to reconstruct detailed maps of depolarization that agreed with earlier work by them and a number of others mentioned in this report. In addition, they were able to map the recovery process in considerable detail. This preparation has the advantage that recovery is mapped in the same animal with typically normal epicardial and body surface ECG potential distributions for both depolarization and repolarization. Careful review of these papers confirms in detail the refractory period data of Burgess et al., in that the earliest recovery potentials were recorded in the right ventricular side of the interventricular septum, with epicardial basal regions beginning to show recovery potentials soon thereafter. They found that the endocardium was positive with reference to the epicardium throughout recovery with the endocardial regions at the apex being the last area to show significant recovery potentials. Spach comments that this data is consistent with the linear gradient in epicardial to endocardial recovery times postulated by Burgess, Abildskov and coworkers, and is inconsistent with the proposal by van Dam and Durrer that the mid wall of the left ventricle recovered before either the epicardium or the endocardium. These data for depolarization and repolarization are shown for our 12 segment left ventricular subdivision in Figures 8 and 9.

#### Modelling of Ventricular Repolarization

A comprehensive critical review entitled "The Origin of the T-Wave" was published in CRC Critical Reviews in Bioengineering in November 1980 by Kootsey and Johnson with M. Spach as referee (136). This monograph will be excerpted where directly applicable, but no attempt will be made to replicate the entire contents. Since this monograph was published, little new has been added to the literature that relates to the topic of simulation of recovery and the reader is urged to consider the Kootsey and Johnson paper as an integral part of this technical report.

While all models of repolarization are indebted to some extent to the notion of Ventricular Gradient summarized in the introduction and to the relating of action potential durations and functional refractory periods described in the previous section, the first attempt to describe a

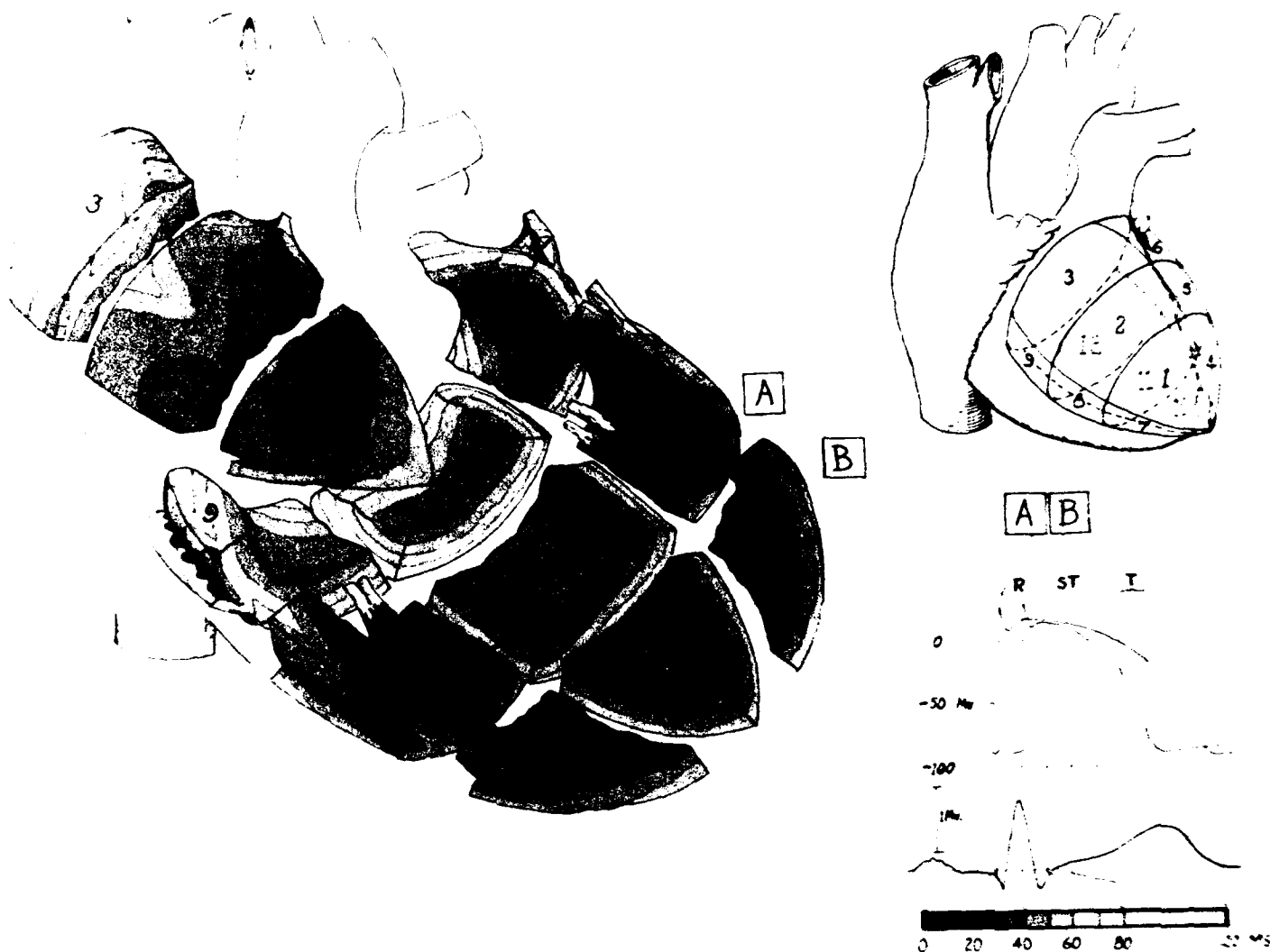


Figure 8. Activation as shown in the revitalized human hearts by Durrer and van Dam and by us in the chimpanzee and baboon with detailed intramural multipoint mapping is depicted here. Colored isochrones for each 10 msec are those defined by the expanded color code at the lower right. They depict the normal activation incorporated in our fine grid propagation model and the 12-segment subdivision used in the development of 54 criteria/32 point ECG infarct size scoring system shown in Table 1.

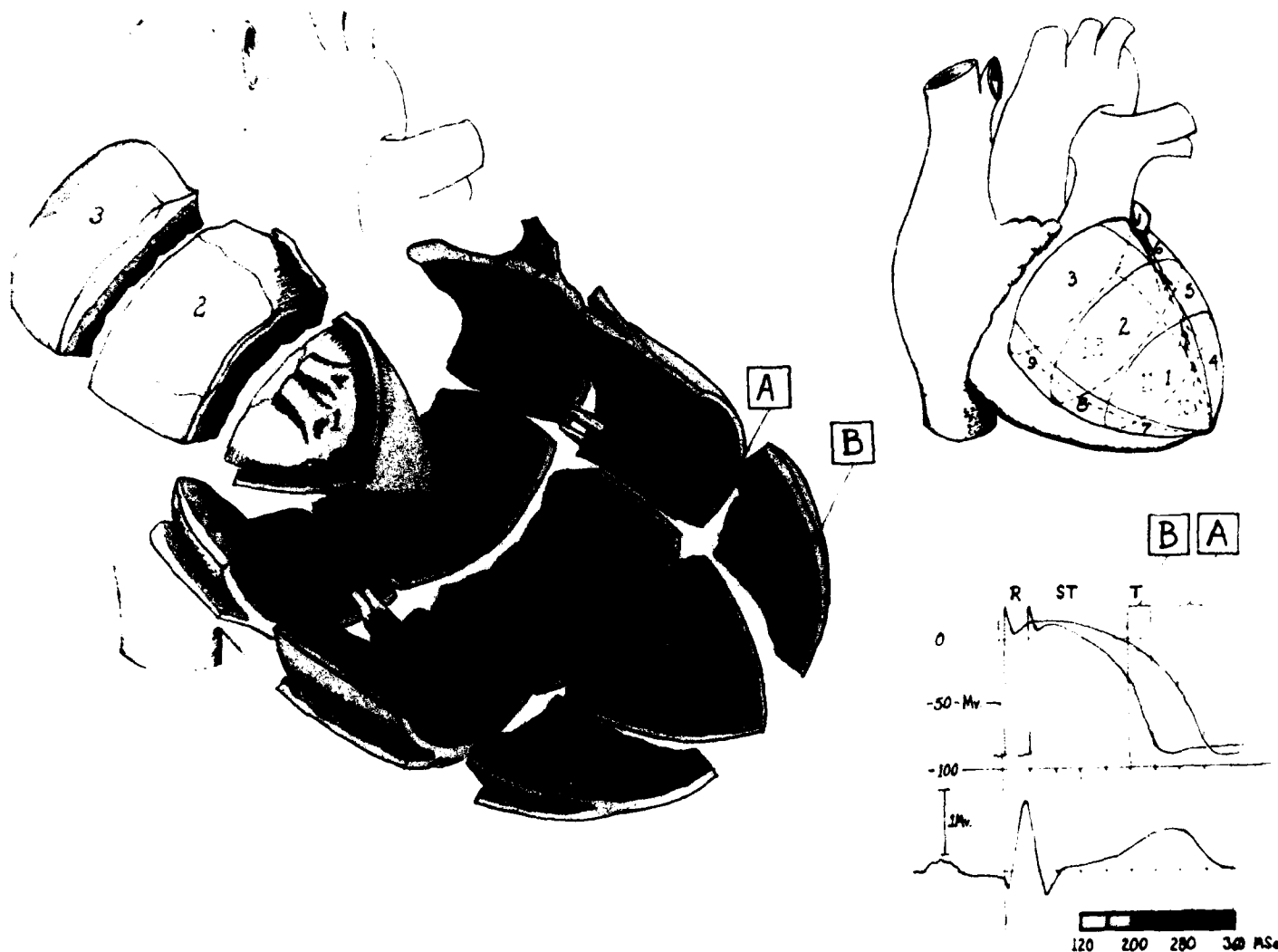


Figure 9. The sequence of ventricular recovery is depicted here adapted from the functional refractory period data of Burgess, Abildskov, and coworkers, and from the detailed intramural mapping of this phase of the cardiac cycle by Spach and coworkers in the chronic closed-chested dog described. Recovery occurs much more slowly than excitation and begins soon after depolarization, as indicated by the action potentials shown in the lower right. The color coding indicates the timing of the peak of the slope of the rapid recovery phase in each region. According to Spach, as shown here, the earliest recovery potentials appear in the right side of the septum, recovery proceeds more rapidly at the base and from epicardium to endocardium throughout. The latest recovery potentials are seen in the endocardium near the apex.



quantitative model of the T wave was in 1966 by Harumi, Burgess, and Abildskov (50). This early version was a 2-dimensional one in which the cardiac sources moved through a simple ventricular cross section. The local repolarization was assumed to be driven by the activation sequence in that cross section. A transmural gradient of action potential duration was assumed (as shown in Figure 8) with the epicardial durations being shorter than the endocardial. The magnitude of this duration gradient was adjusted so that the T vector loops computed by the solid angle theorem conformed to the experimentally recorded ones. The group at the University of Utah, including Abildskov, Burgess, Green, Lux, and others (117-132), has been active for the last several years in the investigation of the phenomenon of ventricular recovery. They have established themselves at the forefront of this activity worldwide. While they have been very active investigating regional recovery with cooling, coronary ligation, focal ischemia, and ventricular pacing, in general, they have limited their modelling efforts to the simple 2D model.

Based on the data from the University of Utah Group, Toyama, Okajima, and associates (137), and Hori, Inoue, and their coworkers (138,139,140), have reported various experimental simulations using strand, concave rectangular solids, and spherical models to explain repolarization. Little attempt to model the volume conductor was made. The numerical experiments concerned solid angle views of the surface in an infinite homogeneous medium and examined the degree of gradient in action potential durations needed to simulate a normal T vector. They established in these simulations that the gradients from epicardium to endocardium that produced upright T waves conformed to those observed in the animal laboratory by Abildskov, Burgess, and coworkers.

Thiry and Rosenberg (51,141,142) were the first to attempt a 3-dimensional model in the form of the cardiac geometry to model both excitation and the T wave. Eleven current dipoles were fixed in location and direction to represent each of 11 regions of the heart. A model of individual action potential wave shapes was developed where the duration, amplitude, and downslope could be individually varied to simulate the Burgess-Abildskov T model and their refractory period duration distributions in the wall of the left ventricle. As a matter of mathematical convenience, each local myocardial region was represented by a sphere. With this formulation, equations could be written such that different action potential waveshapes would represent endocardial, mural myocardial, and epicardial regions within this spherical "cell". In this way, regional delay in excitation, ischemia, injury, and infarction could be simulated. This model could be further refined to model subendocardial, intramural, subepicardial, or transmural ischemia, injury, or infarction in each of these regions. The volume conductor was assumed to be an infinite volume conductor of uniform resistivity. Recording sites in the medium were placed to represent the 12-lead ECG locations on an adult male torso. While the volume conductor was unrealistic in that internal torso inhomogeneities, such as intracardiac blood mass and lungs, and an external irregular torso boundary with air outside was not simulated, this was the first simulation of 3D activation and recovery from a 3D model of the actual heart geometry. This simulation produced a 12-lead ECG that mimicked regional ischemia, injury, and infarction in a way entirely consistent with clinical ECGs recorded in these situations. ECGs produced by the simulation and read by experienced electrocardiographers were interpreted as representing the process simulated.

In 1978, Horan and associates further refined the heart geometry by dividing the ventricles of a real human heart into  $3.2 \text{ mm}^3$  regions (143). The volume conductor was again assumed to be an infinite homogeneous resistive medium. They also included activation times and a base to apex and epicardial to endocardial gradient in action potential durations that matched published data. They used a simplified, trapezoidal shape of action potential waveshape. For computational simplification, the small regions were combined together in groups of 8 by first calculating the differences between the 8. The contributions of each group to the extracellular current field were estimated from the potential differences between the regions. Using dipole and quadripole contributions of the local regions, this group investigated the theoretical validity of the concept of "primary" and "secondary" T waves. They calculated an "intrinsic" T wave by simulating simultaneous excitations of all regions and compared this generator output to that calculated by the method of Abildskov et al. They found a good correlation, but not complete agreement between the two.

Miller and Geselowitz added a realistic external torso boundary simulation and more realistic action potential waveshapes to compute body surface ECG maps of the excitation-recovery process (52,53). They also produced 12-lead ECGs of simulated normals, as well as multiple combinations of regional subendocardial, subepicardial, and transmural ischemia, injury, and infarction. This is the most definitive simulation to date that incorporates measured heart geometry, activation sequences, and distributed gradients of recovery into a realistic bounded male torso. Our proposed simulation will refine the cardiac generator simulation even further (to a  $1 \text{ mm}^3$  grid) and will include internal inhomogeneities, i.e., intracardiac blood mass and lungs into the model, and will develop a library of torso shapes and internal torso geometries and properties such that when completed the simulations can be generalized to the pilot population at large, both at rest and with exercise. It will also include systolic wall motion into the simulation. When this is accomplished, we expect to have incorporated all the first-order variables into the simulation for both excitation and recovery (except ventricular ectopic beats and bundle branch blocks) that are known to effect the potential distributions on the body surface at rest and during exercise.

In its present form, the forward simulation includes the simulation of fascicular blocks in either or both the right or left bundle systems. This allows for the simulation of ischemia, injury, and infarction in the presence of left superior, middle, or inferior fascicular block. This is accomplished in the model by eliminating start points in each of these distributions where the left fascicular system inserts into the Purkinje network. At some point in the development of this forward model, it will be important to include the development of a simulation of complete left and right bundle branch block into the system. The ability to predict the presence of ischemia, injury and infarction, and/or hypertrophy in the presence of these major conduction abnormalities is of considerable interest, and the timing of its development will be dictated in this effort by the relative significance of this subset of the problem in the Air Force pilot population. Specifically at some point if the results from forward simulation effort have led us to the place where the sensitivity and specificity for the detection of asymptomatic coronary disease is such that the case finding approaches 95% in subjects without bundle branch block, then it would seem prudent to include these conduction defects in the model. At that time this group of subjects would begin to

represent a significant proportion of the residual pilot population that might have undetected asymptomatic coronary artery disease. This will be discussed in more detail along with the inclusion of regional intramural slowing of conduction and anisotropies as relates to ischemia and infarction in the section on "Numerical Experiments with the Forward Model and Sequence of Its Development".

### Torso Transfer Impedance Changes at Rest and Exercise

#### Ventricular Wall Motion with Systole

In developing the simulation of depolarization, the motion of the heart in man could be ignored since ventricular excitation occurs during the quiet end diastolic phase (or immediately presystole). In the modelling of the recovery phase or ST-T segment of the ECG, which occurs throughout systole, the motion of the heart during this time must be considered in the formulation of the transfer matrices between local heart regions and the body surface. Since potential differences between 2 points in an infinite homogeneous resistive volume conductor vary as the square of the distance between these 2 points, it follows that variations in potential at the surface of the thorax of man generated from cardiac dipole current generators are quite sensitive to changes in position of the generators with systole, especially in those generators close to the torso surface. Potential changes on the body surface produced from those regions deep in the chest will likewise be less sensitive to systolic wall motion.

Cardiac size and output measurements in man during rest and exercise have been studied using simple hemodynamic and radiographic means by Meek, McCrea, and Eyster (144,145), and by others including early work by Rushmer's group and Sarnoff and Mitchell (146-151). These data included not only the contraction and volume changes of the ventricles at rest and with exercise, but translational effects. Conflicting data with regard to a "wringing" type of rotational motion around the long axis was described in these early papers. The base of the left ventricle was generally seen to rotate clockwise around the long axis, and the apex rotated counterclockwise. The hemodynamic and volumetric effects of respiration were also delineated in these early reports.

These observations have been refined in a semiquantitative way in dogs by Hamilton and Rompf (146), and by Rushmer and collaborators (148) by suturing metal markers to the surface of the ventricles and observing them fluoroscopically. This allowed for more detailed assessment of regional wall motion, and dynamics, beat by beat in the conscious animal over extended periods of time and with various interventions. Beginning in 1963, Harrison, Goldblatt, Braunwald, Glick, and Mason (152-154) in Bethesda, McDonald (155) in Melbourne, and Ingles, Daughters, Stinson, and Alderman (156) in Palo Alto published similar studies in man with the use of small epicardial or intramural metal markers implanted at the time of open heart surgery. Cardiac dimensional studies in the intact conscious man could now be done in comparison to conventional biplane contrast ventriculograms, and once validated, using a calibrated cineradiographic system, serial measurements can be made

to determine the effects of various physiological and pharmacological interventions on epicardial dynamics.

Wildenthal in 1969 (157) demonstrated in experimental animals significant differences in beat-to-beat ventricular dynamics measured from epicardial and midwall markers. The Ingels paper (156) with tantalum markers in the midwall is the most relevant to the simulation of the ECG during the recovery phase, since the present version of the computer simulation coalesces all current generators in a given segment to a dipole at the centroid of each of the myocardial segments. Figure 10 shows the local rotational and translational effects (as demonstrated especially by Ingles et al.) in each of the 12 left ventricular segments that will be used in the simulation of systole at rest.

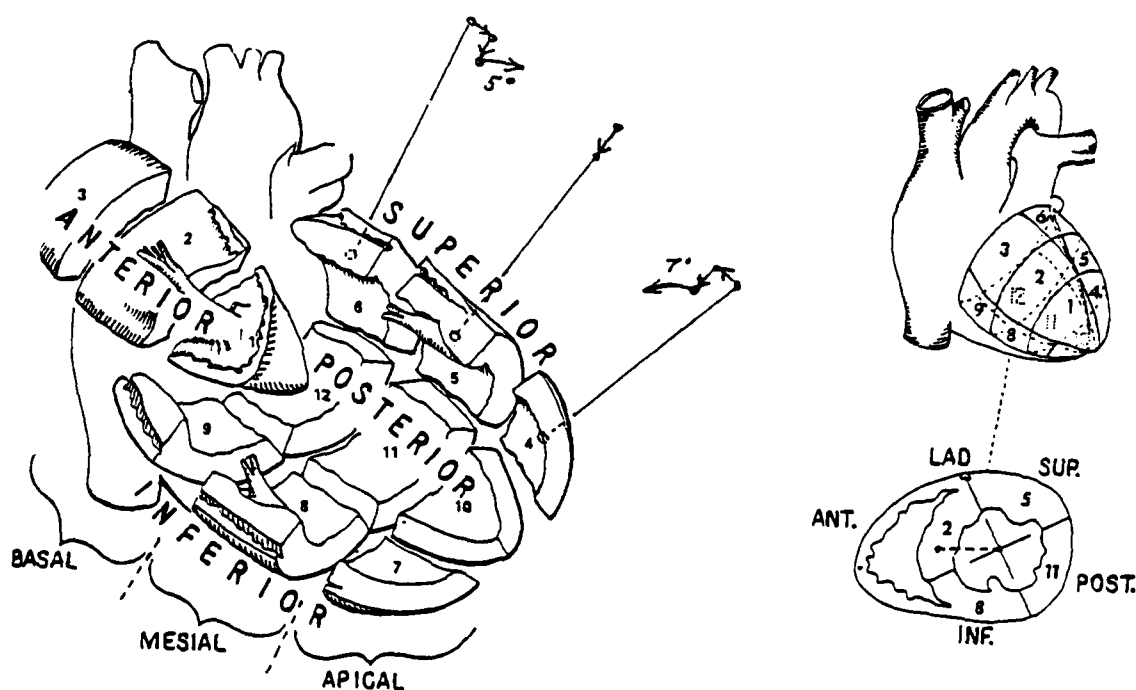


Figure 10. Examples of the complex positional changes from end diastole to peak systole are shown here for a few illustrative segments. The basal segments will move down, inward, and rotate clockwise with reference to the long axis as viewed from the apex. Apical segments will move upward, inward, and rotate counterclockwise. Mid wall segments will move mainly inward.

Coronary artery bifurcations were used by Kong, Morris and McIntosh (158) to assess regional wall function in patients with coronary artery disease. This method was checked against the method using epicardial metal markers in the experimental laboratory and it was found that for the first few beats after a coronary injection regional wall motion of the epicardial markers was not affected. This method was labor intensive but did demonstrate in this

small series that there was systolic lengthening on the distal distribution of high grade stenotic vessels, and decreased and delayed or absent regional shortening in infarcted regions distal to complete coronary obstructions. It will be important to incorporate these observations into the simulation of regional ischemia, and infarction.

The extensive recent literature in regional wall motion changes by nuclear angiographic methods and 2D Echo is pertinent in this regard. The earliest marker of regional ischemia has been shown to be thinning of the left ventricular wall, and slight outward bulging. Transmural infarction is associated with a thick collagen scar, and local akinesis. These effects, and the well-documented translocational effects of inferior infarction from right coronary occlusion, in particular, will need to be incorporated into the location changes and transfer matrix changes. Criteria for which of these variables need to be included will result from the numerical analysis studies and the numerical experiments referred to in the section "Numerical Experiments with the Model and Sequence of Its Development" (pp. 69-72).

#### Exercise-Induced Changes

A reasonable body of older literature deals with the changes in the cardiac size and output with exercise (144-149). These studies used standard biplane radiographs, and included atria and great vessels in general in the measurement of heart volumes and dimension changes with exercise. The measurement of the left ventricular wall regional changes and motion with near maximum effort is mentioned by Ingels and coworkers (156) as one of the potential uses of the midwall implanted marker technique, but no such specific data was reported. Very limited data was reported by Braunwald, Goldblatt, Harrison, and Mason (154), looking at left ventricular length by means of 2 epicardial markers (one near the apex, the other near the base) in five subjects during mild exercise. They found little change (average 6.5% decrease) in this measurement with light exercise. They concluded from review of the older data mentioned above and their own measurements that: 1) there was a modest decrease in left ventricular end diastolic and end systolic volume with exercise; 2) the main change with exercise was a significant increase in contractility, most likely due to increased sympathetic tone; and 3) the change in cardiac output was the result of an increase in systolic emptying and an increase in heart rate.

The data needed to simulate right and left ventricular dimensional changes with exercise in presumably normal adult men is likely present in the raw data of some of the 2D Echo data now being reported, but the published reports are concerned with regional and global changes in dynamics and are generally corrected for the movement of the heart downward by normalizing the systolic frames used to the aortic root. Most reports also use the subcostal long axis view where the distance to the overlying thorax is not measured. Nevertheless, in reviewing this problem with Ginston (159), who has reported on the 2D Echo changes with exercise (160), it is evident that in echogenic subjects, the nature of these local dimensional changes can be assessed, and incorporated into the model if the early numerical experiments and resolution studies indicate that this is needed. This will require fixing the relationship between the thorax of the subject and the transducer, either by

using the apical long axis views, or parasternal views at rest and during exercise.

Regarding the changes in torso resistivities with exercise, detailed data of the kind needed in the simulation is not available in the current literature, and will need to be generated as a part of the ongoing effort in later years of this project. The measurement of torso impedance changes has been done as a part of an earlier study reported by us (161) in the baboon, and preliminary studies in volunteer subjects indicate the feasibility of making these measurements in man. Transthoracic impedance measurements, as reported by Krohn (162), are done routinely as a qualitative measure of cardiac output trends, using commercially available equipment. The objective of the work being proposed by us will be to make these measurements quantitative by measuring small currents injected at one electrode site of a limited map array at all other sites, and repeating this at each electrode until an impedance map is generated.

#### Optimal Electrode Number and Location

Since the early work by Taccardi (163-166), and by Horan, Flowers, and Brody (167), on ECG body surface mapping of heart potential distribution, there has been steady progress in establishing regional ECG surface map changes that relate to regional infarct changes (168-170). Horan, Flowers, and Brody reported early work (171-173) on principal factor waveforms extraction and multipolar content of the map data. Using similar numerical (empiric) methods, Horan and coworkers (174), Lux, Burggrae and coworkers (175,176), Barr, Spach and coworkers (177-179), and Kornreich and coworkers (180,181), have shown that the total ECG surface map from 150-200 points can be reproduced to some acceptable resolution with 15 to 32 leads, depending on the diagnostic information content and the resolution desired. In some instances the resolution needed for the present effort was not attempted.

Using the total body surface map simulation, which with our adaptation of the Gerlenter Swihart inhomogeneous torso simulation generated a 1874-point ECG surface map, we looked at the map potential distribution from unit dipoles at each of the local left ventricular segments (182). Predictably some segments, like the anteroapical ones, produced large peak potentials with well localized distributions on the body surface, and others like the posterobasal segment produced a much smaller peak surface distributed over a much wider area. Generally speaking, however, there were unique surface distributions for each of the major left ventricular segments. These topographical relationships for unit dipoles are shown in Figures 11 and 12.

Using this anatomical and physiologically oriented information, we plan to use the simulation to define the expected resolution for regional ischemia in each of the 12 segments of our current version of the simulation. Specifically how much ischemia does it take in each of the local segments to produce surface ECG changes above the noise level expected in exercise ECGs? Where does this appear on the body surface? What specific criteria will be needed to detect this degree of ischemia? From the distribution of unit dipoles in Figure 11 it is clear that similar degrees of subendocardial ischemia in the apical segments will be detected with, for example, 200-300 V of ST segment change in anterior precordial leads whereas that degree of

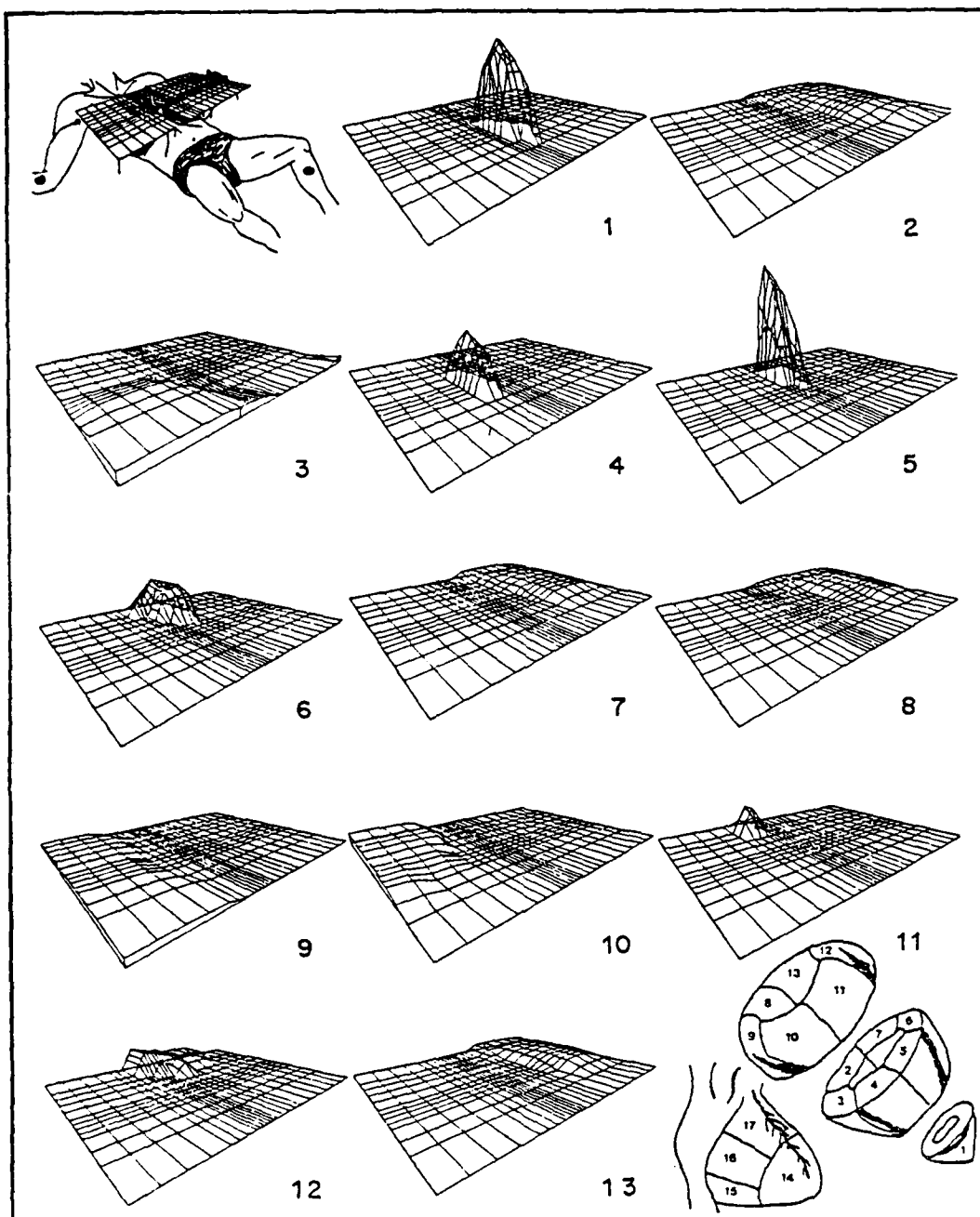


Figure 11. The flat surface represents the torso surface opened vertically at the right mid axillary line with the back unrolled to the left on the diagram. Each left ventricular unit dipole is clipped at 50% of positive potential to show the regional localization of that segment on the body surface and the strength of each local unit dipole on the surface.

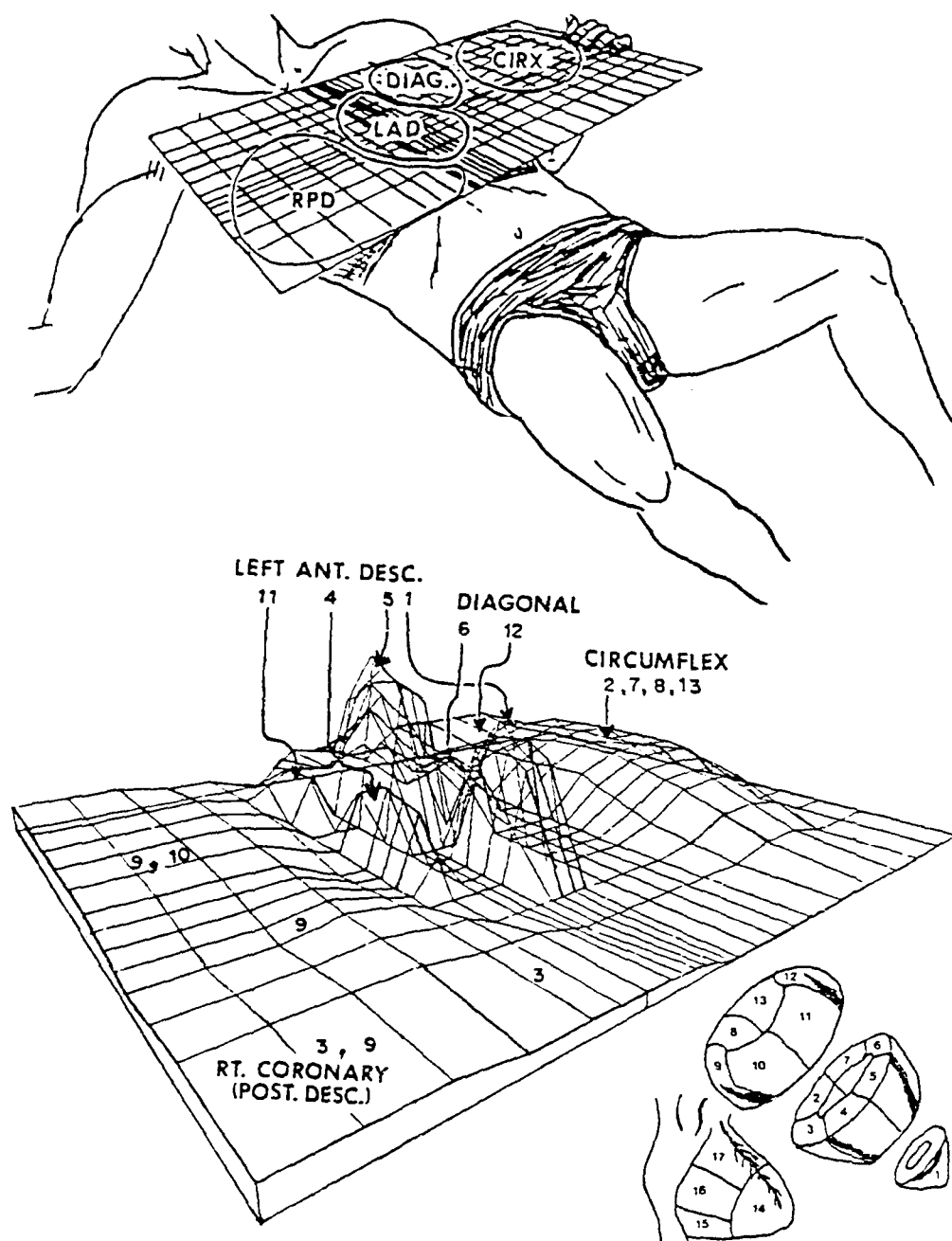


Figure 12. In this illustration the surface distribution of all the left ventricular unit dipoles shown individually in Figure 11 are projected onto the surface. The coronary artery supply to each segment is shown at the top. It will be noted in the bottom frame that the local distribution of each of the segments is well preserved. The height of each segment distribution shown is related to the sensitivity of the ECG surface map to the local left ventricular region.



ischemia in the posterobasal segment would produce only about 20-30  $\mu\text{V}$  of ST change localized preferentially to leads on the back. With existing signal processing techniques, this degree of change should be well within the limits of the technology.

The strength of this approach is that the model is put together from a  $1\text{ mm}^3$  "cell" to the body surface from anatomical and physiological information. If the simulation contains all the first-order variables that influence the output, then changes seen on the surface have a direct anatomical and physiological base. The changes so observed yield directly to anatomical and physiological diagnostic statements. On the other hand, empiric methods such as multipolar content and multipolar reductions of surface data, while computationally more efficient and mathematically more direct, do not have a direct analogy to the anatomy of the heart. For example, some quadrapole or octapole term may be quite outside two standard deviations of that seen in a significant population of normal subjects, but large clinical correlative studies will need to be done to establish the physiological or anatomical significance of the specific coefficients that were found to be abnormal.

It also follows that maps generated by the Lux leads, and Eigenvector algorithms, or by the Barr-Spach 24-lead set can be produced from the larger lead set maps that are generated by various combinations of regional ischemia and infarction using our simulation. The ability of each of these data reduction techniques to reproduce the surface ECG map to the resolution needed to detect the specific change can be directly assessed. The simulation can be used as a tool to develop a theoretical base for the interpretation of various abnormalities seen in the limited set, and to explore whether diagnostically important areas on the body surface need lower, or higher concentration of leads to achieve the needed sensitivity and specificity for either ischemia or infarction.

### Bibliography

1. Einthoven, W., Fahr, G., and De Waart, A.: Über die Richtung und die Manifeste Grosse der Potientelschwankungen im Menschlichen Herzen und über den Einfluss der Herzlage auf die Form des Elektrokardiogramms, Pflugers Arch. Ges. Physiol. 150:275, 1913.
2. Lewis, T.: The Excitatory Process in the Dog's Heart, Part I, The Auricles, Phil. Tr. Roy. Soc. Lond. 205:35, 1914.
3. Lewis, T., and Rothchild, M.A.: The Excitatory Process in the Dog's Heart, Part II, The Ventricles, Phil. Tr. Roy. Soc. Lond. 206:181, 1915.
4. Lewis, T.: The Spread of the Excitatory Process in the Vertebrate Heart, Phil. Tr. Roy. Soc. Lond. 207:221, 1916.
5. Scher, A.M., Paton, R.R., and Young, A.C.: Spread of Electrical Activity Through the Wall of the Mammalian Ventricle, Fed. Proc. 1:139, 1952.
6. Scher, A.M., Young, A.C., Malmgren, A.L., and Paton, R.R.: Spread of Electrical Activity In the Mammalian Ventricle, Circ. Res. 1:539, 1953.
7. Scher, A.M., and Young, A.C.: The Pathway of Ventricular Depolarization in the Dog, Circ. Res. 4:461, 1956.
8. Scher, A.M., and Young, A.C.: Ventricular Depolarization and the Genesis of the QRS, Ann. N.Y. Acad. Sci. 65:768, 1957.
9. Durrer, D., van der Tweel, L.H., and Blickman, J.R.: Spread of Activation in the Left Ventricular Wall of the Dog, Koninklijke Nederlandse Akademie van Wetenschappen, Proc. Series C. 56 2:288, 1953.
10. Durrer, D., and van der Tweel, L.H.: Spread of Activation in the Left Ventricular Wall of the Dog. I., Am. Heart J. 46:683, 1953.
11. Durrer, D., and van der Tweel, L.H.: Spread of Activation in the Left Ventricular Wall of the Dog. II. Activation Conditions at the Epicardial Surface, Am. Heart J. 47:192, 1954.
12. Durrer, D., van der Tweel, L.H., and Blickman, J.R.: Spread of Activation in the Left Ventricular Wall of the Dog. III. Transmural and Intramural Analysis, Am. Heart J. 48:13, 1954.
13. Durrer, D., and van der Tweel, L.H.: Excitation of the Left Ventricular Wall of the Dog and Goat, Ann. N.Y. Acad. Sci. 65:13, 1954.
14. Solomon, J.C., and Selvester, R.H.: Current Dipole Moment Density of the Heart, Am. Heart J. 81(3):351, 1971.

15. Selvester, R.H., Kalaba, R., Kagiwada, H., Collier, C.R., Bellman, R.: Simulated Myocardial Infarction with a Mathematical Model of the Heart Containing Distance and Boundary Effects. *Vectorcardiography* 1965, North Holland Publishing Co., 403, 1966.
16. Selvester, R.H., Kalaba, R., Collier, C.R., Bellman, R., Kagiwada, H.: A Digital Computer Model of the Vectorcardiogram with Distance and Boundary Effects: Simulated Myocardial Infarction. *Am. Heart J.* 74:792, 1967.
17. Selvester, R.H., Sanmarco, M.E.: Infarct Size in Hi-gain, Hi-fidelity Serial VCGs and Serial Ventriculograms in Patients with Proven Coronary Artery Disease, *Proceedings of the 4th World Congress on Electrocardiography*, 1978.
18. Wagner, G.S., Freye, C.H., Palmeri, S.T., Roark, S.F., Stack, B.A., Ideker, R.E., Harrell, F.E., Selvester, R.H.: Evaluation of a QRS Scoring System for Estimating Myocardial Infarct Size. I. Specificity and Observer Agreement. *Circ.* 65(2):342, 1982.
19. Ideker, R.E., Wagner, G.S., Ruth, W.K., Alonso, D.R., Bishop, S.P., Bloor, C.M., Fallon, J.T., Gottlieb, G.J., Hackel, D.B., Phillips, H.R., Reimer, K.A., Roark, S.F., Rogers, W.J., Savage, R.M., White, R.D., Selvester, R.H.: Evaluation of a QRS Scoring System for Estimating Myocardial Infarct Size. II. Correlation with Quantitative Anatomic Findings for Anterior Infarcts. *Am. J. Cardiol.* 49(7):1604, 1982.
20. Roark, S.F., Ideker, R.E., Wagner, G.S., Alonso, D.R., Bishop, S.P., Bloor, C.M., Bramlet, D.A., Edwards, J.E., Fallon, J.T., Gottlieb, G.J., Hackel, D.B., Phillips, H.R., Reimer, K.A., Rogers, W.J., Ruth, W.K., Savage, R.M., White, R.D., Selvester, R.H.: Evaluation of a QRS Scoring System for Estimating Myocardial Infarct Size. III. Correlation With Quantitative Anatomic Findings for Inferior Infarcts. *Am. J. Cardiol.* 51(3):382, 1983.
21. Anderson, C.I., Harrison, D.G., Stack, N.C., Ideker, R.E., Palmeri, S.T., Selvester, R.H., Wagner, G.S.: Evaluation of Serial QRS Changes During Acute Inferior Myocardial Infarction Using a QRS Scoring System. *Am. J. Cardiol.* 52(3):252, 1983.
22. Selvester, R.H., Sanmarco, M.E., Solomon, J.C., Wagner, G.S.: Methods of Determining Infarct Size, ECG: QRS Change. *Myocardial Infarction: Measurement and Intervention*. Wagner G.S., ed., Martinus Nijhoff, The Hague, Boston, London, 23, 1982.
23. Ward, R.M., White, R.D., Ideker, R.E., Hindman, N.B., Alonso, D.R., Bishop, S.P., Bloor, C.M., Fallon, J.T., Gottlieb, G.J., Hackel, D.B., Hutchins, G.M., Phillips, H.R., Reimer, K.A., Roark, S.F., Rochlani, S.P., Rogers, W.J., Ruth, W.K., Savage, R.M., Weiss, J.L., Selvester, R.H., Wagner, G.S.: Evaluation of a QRS Scoring System for Estimating Myocardial Infarct Size. IV. Correlation with Quantitative Anatomic Findings for Posterolateral Infarcts. *Am. J. Cardiol.* 53:706, 1984.

24. Wilson, F.N., Macleod, A.G., Barker, P.S., and Johnston, F.D.: The Determination and the Significance of the Areas of the Ventricular Deflections of the Electrocardiogram, *Am. Heart J.* 10:46, 1934.
25. Wilson, F.N., Macleod, A.G., and Barker, P.S.: The T Deflection of the Electrocardiogram, *Tran. Assoc. Physicians* 46:29, 1931.
26. Ashman, R., and Byer, E.: The Normal Human Ventricular Gradient. I. Factors Which Affect Its Direction and Its Relation to the Mean QRS Axis, *Am. Heart J.* 25:16, 1943.
27. Ashman, R., and Byer, E.: The Normal Human Ventricular Gradient. II. Factors Which Affect Its Manifest Area and Its Relationship to the Manifest Area of the QRS Complex, *Am. Heart J.* 25:36, 1943.
28. Ashman, R., Ferguson, F.P., Gremillion, A.I., and Byer, E.: The Normal Human Ventricular Gradient. V. The Relationship Between AQRS and G, and the Potential Variations of the Body Surface, *Am. Heart J.* 29:697, 1945.
29. Ashman, R., Gardberg, M. and Byer, E.: The Normal Human Ventricular Gradient III. The Relation Between the Anatomic and Electrical Axes, *Am. Heart J.* 26:473, 1943.
30. Berkun, M.A., Kesselman, R.H., Donoso, E., and Grishman, A.: The Spatial Ventricular Gradient: Intermittent Wolff-Parkinson-White Syndrome, Intermittent Left Bundle Branch Block and Ventricular Premature Contractions, *Circ.* 13:562, 1956.
31. Burch, G.: The Ventricular Gradient, *Med. Clin. N. Amer.* 29:464, 1945.
32. Burch, G.E., Abildskov, J.A., and Cronvich, J.A.: A Study of the Spatial Vectorcardiogram of the Ventricular Gradient, *Circ.* 9:267, 1954.
33. Burch, G.E., Abildskov, J.A., and Cronvich, J.A.: The Spatial Vectorcardiogram and Mean Spatial Ventricular Gradient in Normal Pregnant Women, *Circ.* 9:381, 1954.
34. Burch, G.E., and DePasquale, N.P.: The Electrocardiogram, Vectorcardiogram and Ventricular Gradient in Combined Pulmonary Stenosis and Interatrial Communication, *Am. J. Cardiol.* 7:646, 1961.
35. Burch, G.E., and DePasquale, N.: The Electrocardiogram, Spatial Vectorcardiogram, and Ventricular Gradient in Congenital Ventricular Septal Defect, *Am. Heart J.* 60:195, 1960.
36. Burch, G.E., and DePasquale, N.: The Electrocardiogram and Ventricular Gradient in Atrial Septal Defect, *Am. Heart J.* 58(2):190, 1959.
37. Burger, H.C.: A Theoretical Elucidation of the Notion "Ventricular Gradient," *Am. Heart J.* 53(2):240, 1957.

38. Cohn, R.L., Rush, S., and Lepeschkin, E.: Theoretical Analyses and Computer Simulation of ECG Ventricular Gradient and Recovery Waveforms, *IEEE Trans. Biomed. Eng.* BME 29(6):413, 1982.
39. Cosma, J., Levy, B., and Pipberger, H.V.: The Spatial Ventricular Gradient During Alterations in the Ventricular Activation Pathway, *Am. Heart J.* 71:84, 1966.
40. DePasquale, N.P., and Burch, G.E.: The Electrocardiogram, Vectorcardiogram, and Ventricular Gradient in the Tetralogy of Fallot, *Circ.* 24:94, 1961.
41. DePasquale, N.P., and Burch, G.E.: A Study of the Ventricular Gradient in Normal Infants and Children, *Am. J. Cardiol.* 5:464, 1960.
42. Fruehan, C.T., Crain, B., Burgess, M.J., Millar, K., and Abildskov, J.A.: Observations Concerning the Validity of the Ventricular Gradient Concept, *Am. Heart J.* 78(6):796, 1969.
43. Gardberg, M., and Rosen, I.L.: Monophasic Curve Analysis and the Ventricular Gradient in the Electrogram of Strips of Turtle Ventricle, *Circ. Res.* 8:870, 1959.
44. LaDue, J.S., and Ashman, R.: Electrocardiographic Changes in Acute Glomerulonephritis, *Am. Heart J.* 31:685, 1946.
45. Lepeschkin, E.: Role of Temperature Gradients Within Ventricular Muscle in Genesis of Normal T Wave of Electrocardiogram and Ventricular Gradient Responsible for It, *Fed. Proc.* 10:81, 1951.
46. Nims, L.F., Kartin, B., Chernoff, H.M., and Nahum, L.H.: Heart Temperature and Its Relation to the T-Wave, *Fed. Proc.* 7:86, 1948.
47. Pantridge, J.F.: Observations on the Electrocardiogram and Ventricular Gradient in Complete Left Bundle Branch Block, *Circ.* 3:589, 1951.
48. Simonson, E., Schmitt, O.H., Dahl, J., Fry, D., and Bakken, E.E.: The Theoretical and Experimental Bases of the Frontal Plane Ventricular Gradient and Its Spatial Counterpart, *Am. Heart J.* 47:122, 1954.
49. Wilson, F.N., Macleod, A.G., Barker, P.S., and Johnston, F.D.: The Determination and the Significance of the Areas of the Ventricular Deflections of the Electrocardiogram, *Am. Heart J.* 10:46, 1934.
50. Harumi, K., Burgess, M.J., and Abildskov, J.A.: A Theoretic Model of the T Wave, *Circ.* 34:657, 1966.
51. Thiry, P.S., and Rosenberg, R.M.: On Electrophysiological Activity of the Normal Heart, *J. Franklin Inst.* 297:377, 1974.
52. Miller, W.T., III, and Geselowitz, D.B.: Simulation Studies of the Electrocardiogram. I. The Normal Heart, *Circ. Res.* 43(2):301, 1978.

53. Miller, W.T., III, and Geselowitz, D.B.: Simulation Studies of the Electrocardiogram. II. Ischemia and Infarction, *Circ. Res.* 43(2):315, 1978.
54. Burdon-Sanderson, J., and Page, F.J.M.: On the Electrical Phenomena of the Excitatory Process in the Heart of the Frog and of the Tortoise, as Investigated Photographically, *J. Physiol. (Lond.)* 4:327, 1883.
55. Burdon-Sanderson, J., and Page, F.J.M.: On the Time-Relations of the Excitatory Process in the Ventricle of the Heart of the Frog, *J. Physiol. (Lond.)* 2:384, 1880.
56. Kolliker, J., and Muller, H.: Nachweis der Negativen Schwankung des Muskelstroms am Nerven sich Contrahirenden Muskel, *Verhandlungen der Physikalisch Medicinischen Gesellschaft in Wurzburg*, 6:528, 1856.
57. Cyon, von der, E.: Über den Einfluss der Temperaturänderungen auf Zahl, Dauer, und Stärke der Herzschläge, *Ludwig's Arbeiten*, 77, 1866.
58. Donders: Rustende Spierstroom en Secundaire Contractie, Nitgaande van het Hart, *Onderz. Physiol. Lab. Utrecht. Derde reeks* 1:256, 1872.
59. Engellman, G.: Über das Verhalten des Thätigen Herzens, *Pflügers Arch.* 17:68, 1874.
60. Marchand, D.: Beiträge zur Kenntniss der Reizwelle und Contractionswelle des Herzmuskels, *Pflügers Arch.* 15:511, 1872.
61. Einthoven, W.: Le Telecardiogramme, *Arch. Intern. Physiol.* 4:132, 1906.
62. Einthoven, W.: Über die Deutung des Elektrokardiograms, *Pflügers Arch.* 149:65, 1913.
63. Eppinger, H., and Rothberger, J.: Zur Analyse des Elektrokardiograms, *Wein Klin. Wchnschr.* 22:1091, 1909.
64. Eppinger, H., and Rothberger, J.: Über die Folgen der Durchschneidung der Tawaraschen Schenkel des Reizleitungsystems, *Zeitschr. Klin. Med.* 70:1, 1910.
65. Eppinger, H., and Storke, O.: Zur Klinik des Elektrokardiograms, *Zeitschr. Klin. Med.* 71:157, 1910.
66. Mathewson, G.D.: Lesions of the Branches of the Auriculo-Ventricular Bundle, *Heart* 4:385, 1913.
67. Rothberger, C.J., and Winterberg, H.: Zur Diagnose der Einseitigen Blockierung um den Tawaraschen Schenkeln, *Zentralbl. Herz U. Gefasskr.* 5:206, 1913.
68. Cohn, A., and Lewis T.: The Pathology of Bundle Branch Lesions of the Heart, *Proc. N. Y. Path. Soc.* 14:207, 1914.

69. Fahr, G.: An Analysis of the Spread of the Excitation Wave in the Human Ventricle, *Arch. Int. Med.*, 25:146, 1920.
70. Wilson, F.N., and Herrmann, G.R.: Bundle Branch Block and Arborization Block, *Arch. Intern. Med.* 26:153, 1920.
71. Wilson, F.N., Macleod, A.G., and Barker, P.S.: The Potential Variations Produced by the Heart Beat at the Apices of Einthoven's Triangle, *Am. Heart J.* 7:207, 1931.
72. Wilson, F.N., Johnston, F.D., Macleod, A.G., and Barker, P.S.: Electrocardiograms that Represent the Potential Variation of a Single Electrode, *Am. Heart J.* 9:447, 1934.
73. Wilson, F.N., Johnston, F.D., Rosenbaum, F.F., Erlanger, H., Kossman, C.E., Hecht, H.H., Cotrim, N., Menezes de Oliveira, R., Scarsi, R., and Barker, P.S.: The Precordial Electrocardiogram, *Am. Heart J.* 27:19, 1944.
74. Abildskov, J.A., Burch, G.E., and Cronvich, J.A.: Validity of Equilateral Triangle as a Spatial Reference System, *Circ.* 2:122, 1950.
75. Duchosal, P.W., and Groscurin, J.R.: The Spatial Vectorcardiogram Obtained by Use of a Trihedron and its Scalar Comparisons, *Circ.* 5:237, 1952.
76. Frank, E.: A Direct Experimental Study of Three Systems of Spatial Vectorcardiography, *Circ.* 10:101, 1954.
77. Grishman, A., Borun, E.R., and Jaffe, H.L.: Spatial Vectorcardiography: Technique for the Simultaneous Recording of the Frontal, Sagittal, and Horizontal Projections: I., *Am. Heart J.* 41:483, 1951.
78. Lamb, L.E., and Dimond, E.G.: The Spatial Vectorcardiogram During the First Decade of Life, *Am. Heart J.* 44:174, 1952.
79. Prinzmetal, M., Rexford-Kennamer, S., Shaw, C.M., Jr., Kimura, N., Lindgren, I., and Goldman, A.: Intramural Depolarization Potentials in Myocardial Infarction, *Circ.* 7:11, 1953.
80. Prinzmetal, M., Shaw, C.M., Jr., Maxwell, M.H., Flamm, E.J., Goldman, A., Kimura, N., Rakita, L., Borduas, J., Rothman, S., and Kennamer, R.: Studies on the Mechanism of Ventricular Activity: VI. The Depolarization Complex in Pure Subendocardial Infarction. Role of the Subendocardial Region in the Normal Electrocardiogram, *Am. J. Med.* 16:469, 1959.
81. Sodi-Pallares, D., Barbato, E., and Delmar, A.: Relationship Between the Intrinsic Deflection and Subendocardial Activation. An Experimental Study, *Am. Heart J.* 39:387, 1950.
82. Sodi-Pallares, D., Rodriguez, M.I., Chait, L.O., and Zuckermann, R.: The Activation of the Interventricular Septum, *Am. Heart J.* 41:569, 1951.

83. Sodi-Pallares, D., and Cisneros, F.: Ventricular Activation in the Dog's Heart, Abstracts of Papers, Second World Congress of Cardiology, 214, 1954.
84. Sodi-Pallares, D., Bisteni, A., Medrano, G.A., and Cisneros, F.: The Activation of the Free Left Ventricular Wall in the Dog's Heart. In Normal Conduction and in Left Bundle Branch Block, Am. Heart J. 49:587, 1955.
85. Durrer, D., Van Dam, R.T., Freud, G.E., Janse, M.J., Meijler, F.L., and Arzbaeher, R.C.: Total Excitation of the Isolated Human Heart, Circ. 41:899, 1970.
86. Okajima, M., Fujino, T., Kobayashi, T., and Yamada, K.: Computer Simulation of the Propagation Process in Excitation of the Ventricles, Circ. Res. 23:203, 1968.
87. Okajima, M., Doniwa, K., Ishikawa, T., Niimi, N., and Koike, Y.: On body Surface VAT "Isochrone" Maps Generated by Computer Using Simulated Excitation Sequences in Ventricular Model, Computers in Cardiology 1980, IEEE, New York, 187, 1981.
88. Horachek, B.M, Macchi, E., and Rautaharju, P.M.: Atrial Surface Excitation Wavefronts and Body Surface Potentials. A Simulation Study. Adv Cardiol 10:126-138, 1974.
89. Arntzenius, A.C.: A Geometrical Model of Successive Stages in Excitation of the Human Heart: Its Value as a Link Between Excitation and Clinical Vectorcardiography, Cardiovasc. Res. 3:198, 1969.
90. Selvester, R.H., Collier, C.R., and Pearson, R.B.: Analog Computer Model of the Vectorcardiogram, Circ. 31:45, 1965.
91. Gelernter, H.L., and Swihart, J.C.: Mathematical Physical Model of the Genesis of the Electrocardiogram, Biophys. J. 4:285, 1964.
92. Solomon, J.C., Selvester, R.H.: Myocardial Activation Sequence Simulation. Proceedings of the XIth Vectorcardiography Symposium. Vector Cardiology, North Holland Publishing Co., 175, 1973.
93. Solomon, J.C., Selvester, R.H.: Simulation of Measured Activation Sequence in the Human Heart. Am. Heart J. 85(4):518, 1973.
94. Paton, B.C.: The Accuracy of Diagnosis of Myocardial Infarction, Arch. Intern. Med. 103:253, 1959.
95. Johnson, W.J., Achor, R.W.P., Burchell, H.B., and Edwards, J.E.: Unrecognized Myocardial Infarction, Arch. Intern. Med. 103:253, 1959.
96. Zinn, W.J., and Cosby, R.S.: A Re-evaluation of the Diagnostic Accuracy of the Electrocardiogram, Am. J. Med. 8:177, 1950.



97. Selvester, R.H., Kirk, W.L., Pearson, R.B.: Propagation Velocities and Voltage Magnitudes in Local Segments of Myocardium. *Circ. Res.* 27(4):619, 1970.
98. Sodi-Pallares, D., and Calder, R.M.: Activation Process of the Human Heart, *New Bases of Electrocardiography*, St. Louis, Mosby, 369, 1956.
99. Durrer, D., Van Dam, R.T., Meijler, F.L., Arzbaecher, R.C., Muller, E.J., and Freud, G.E.: Electrical Activation and Membrane Action Potentials of the Perfused Normal Human Heart, *Circ.* 34:92, 1966.
100. McFee, R., and Parungao, A.: An Orthogonal Lead System for Clinical Electrocardiography, *Am. Heart J.* 62:93, 1961.
101. Selvester, R.H., Solomon, J.C., and Gillespie, T.L.: Digital Computer Model of a Total Body ECG Surface Map. An Adult Male Torso Simulation with Lungs. *Circ.* 38:684, 1968.
102. Palmeri, S.T., Harrison, D.G., Cobb, F.R., Morris, K.G., Harrell, F.E., Ideker, R.E., Selvester, R.H., Wagner, G.S.: A QRS Scoring System for Assessing Left Ventricular Function after Myocardial Infarction. *N. Engl. J. Med.* 306(1):4, 1982.
103. Ling, G., and Gerard, R.W.: The Normal Membrane Potential of the Frog Sartorius Fibers, *J. Cell. Comp. Physiol.* 34:383, 1949.
104. Woodbury, L.A., Hecht, H.H., and Christopherson, A.R.: Membrane Resting and Action Potentials of Single Cardiac Muscle Fibers of the Frog Ventricle, *Am. J. Physiol.* 164:307, 1952.
105. Woodbury, L.A., and Hecht, H.H.: Effects of Cardiac Glycosides upon the Electrical Activity of Single Ventricular Fibers of the Frog Heart, and Their Relation to the Digitalis Effect of the Electrocardiogram, *Circ.* 6:172, 1952.
106. Woodbury, J.W., and Brady, A.J.: Intracellular Recording from Moving Tissues with a Flexibly Mounted Ultramicroelectrode, *Science* 123:100, 1956.
107. Brady, A.J., and Woodbury, J.W.: Effects of Sodium and Potassium on Repolarization in Frog Ventricular Fibers, in H. Hecht (ed.), *The Electrophysiology of the Heart*, Ann. N.Y. Acad. Sci. 65:687, 1957.
108. Hoffman, B.F., Kao, C.Y., and Suckling, E.E.: Refractoriness in Cardiac Muscle, *Am. J. Physiol.* 190(3):473, 1957.
109. Hoffman, B.F., and Suckling, E.E.: Relationship Between Cardiac Cellular Potentials and the Deflections of the Electrogram, *Am. J. Physiol.* 171:737, 1952.
110. Hoffman, B.F., and Cranefield, P.F.: *Electrophysiology of the Heart*, McGraw-Hill, New York, 1960.

111. Sarachek, N.S., Roberts, J., and Leonard, J.J.: A New Method to Measure Non-Uniformity in the Intact Heart, *J. Electrocard.* 5(4):341, 1972.
112. Schafer, H., Pena, A., and Scholmerich, P.: Der Monophasische Aktionsstrom von Spitze und Basis des Warmbluterherzens und die Theorie der T-Welle des EKG, *Pflugers Arch.* 246:728, 1943.
113. Hoffman, B.F., Cranefield, P.F., Lepeschkin, E., Surawicz, B., and Herrlich, H.C.: Comparison of Cardiac Monophasic Action Potentials Recorded by Intracellular and Suction Electrodes, *Am. J. Physiol.* 171:737, 1952.
114. Autenrieth, G., Surawicz, B., and Kuo, C.S.: Sequence of Repolarization on the Ventricular Surface in the Dog, *Am. Heart J.* 89(4):463, 1975.
115. van Dam, R.T., and Durrer, D.: The T Wave and Ventricular Repolarization, *Am. J. Cardiol.* 14:294, 1964.
116. van Dam, R.T., and Durrer, D.: Experimental Study on the Intramural Distribution of the Excitability Cycle and on the Form of the Epicardial T Wave in the Dog Heart, *Am. Heart J.* 61(4):537, 1961.
117. Abildskov, J.A.: The Prolonged QT Interval, *Ann. Rev. Med.* 30:171, 1979.
118. Abildskov, J.A.: Effects of Activation Sequence on the Local Recovery of Ventricular Excitability in the Dog, *Circ. Res.* 38(4):240, 1976.
119. Abildskov, J.A.: The Sequence of Normal Recovery of Excitability in the Dog Heart, *Circ.* 52:442, 1975.
120. Abildskov, J.A., Burgess, M.J., Lux, R.L., Wyatt, R.F., and Vincent, G.M.: The Expression of Normal Ventricular Repolarization in the Body Surface Distribution of T Potentials, *Circ.* 54(6):901, 1976.
121. Abildskov, J.A., Burgess, M.J., Millar, K., Wyatt, R., and Baule, G.: The Primary T Wave--A New Electrocardiographic Waveform, *Am. Heart J.* 81(2):242, 1971.
122. Abildskov, J.A., Evans, A.K., Lux, R.L., and Burgess, M.J.: Ventricular Recovery Properties and QRST Deflection Area in Cardiac Electrograms, *Am. J. Physiol.* 239 (Heart Circ. Physiol. 8):H227, 1980.
123. Abildskov, J.A., Green, L.S., Evans, A.K., and Lux, R.L.: The QRST Deflection Area of Electrograms during Global Alterations of Ventricular Repolarization, *J. Electrocard.* 15(2):103, 1982.
124. Abildskov, J.A., Millar, K., Burgess, M.J., and Green, L.: Characteristics of Ventricular Recovery as Defined by the Vectorcardiographic T Loop, *Am. J. Cardiol.* 28:670, 1971.
125. Burgess, M.J.: Relation of Ventricular Repolarization to Electrocardiographic T Wave-Form and Arrhythmia Vulnerability, *Am. J. Physiol.* 236(3): H391, 1979.

126. Burgess, M.J., and Coyle, J.: Effects of Premature Depolarization on Refractoriness of Ischemic Canine Myocardium, *J. Electrocardiol.* 15(4):335, 1982.
127. Burgess, M.J., Green, L.S., Millar, K., Wyatt, R., and Abildskov, J.A.: The Sequence of Normal Ventricular Recovery, *Am. Heart J.* 84(5):660, 1972.
128. Burgess, M.J., and Haws, C.W.: Effects of Sympathetic Stimulation on Refractory Periods of Ischemic Canine Ventricular Myocardium, *J. Electrocardiol.* 15(1):1, 1982.
129. Burgess, M.J., Lux, R.L., Wyatt, R.F., and Abildskov, J.A.: The Relation of Localized Myocardial Warming to Changes in Cardiac Surface Electrograms in Dogs, *Circ. Res.* 43(6):899, 1978.
130. Burgess, M.J., Millar, K., and Abildskov, J.A.: The Geometry of Ventricular Repolarization Boundaries, *Am. Heart J.* 79(4):524, 1970.
131. Burgess, M.J., Millar, K., and Abildskov, J.A.: Cancellation of Electrocardiographic Effects During Ventricular Recovery, *J. Electrocardiol.* 2(2):101, 1969.
132. Lux, R.L., Urie, P.M., Burgess, M.J., and Abildskov, J.A.: Variability of the Body Surface Distributions of QRS, ST-T, and QRST Deflection Areas with Varied Activation Sequence in Dogs, *Cardiovascular Res.* 14:607, 1980.
133. Spach, M.S., and Barr, R.C.: Origin of Epicardial ST-T Wave Potentials in the Intact Dog, *Circ. Res.* 39(4):475, 1976.
134. Spach, M.S. and Barr, R.C.: Analysis of Ventricular Activation and Repolarization from Intramural and Epicardial Potential Distributions for Ectopic Beats in the Intact Dog, *Circ. Res.* 37:830, 1975.
135. Spach, M.S., and Barr, R.C.: Ventricular Intramural and Epicardial Potential Distributions During Ventricular Activation and Repolarization in the Intact Dog, *Circ. Res.* 37:243, 1975.
136. Kootsey, J.M., and Johnson, E.A.: The Origin of the T Wave, *CRC Crit. Rev. Bioeng.* (Nov.):233, 1980.
137. Toyama, J., Kobayashi, T., Muraki, H., Fujino, T., Hori, K., Okajima, M., and Yamada, K.: On Mathematical Reconstruction of T-Wave Patterns--Representation of Equivalent Cardiac Generator During Repolarization and Interpretation of Concordance of T Wave with QRS Complex, *Jap. Circ. J.* 31:313, 1967.
138. Hori, M.: Simulation Study of QRS-T Waves Based on an Eccentric Spherical Model of the Heart, *Jpn. Circ. J.* 42:539, 1978.
139. Inoue, M., Hori, M., Kajiwa, F., Kusuoka, H., Abe, H., Furukawa, T., and Takasugi, S.: Theoretical Analysis of T-Wave Polarity Based on a Model of Cardiac Electrical Activity, *J. Electrocardiol.* 11:171, 1978.

140. Inoue, M., Inada, H., Hoki, N., Fukushima, M., Hori, M., Kusuoka, H., Abe, H., Kajiya, F., Furukawa, T., and Takasugi, S.: A Simulation of QRS-T Wave Based on the Transmembrane Action Potential of Myocardial Cell, *Jpn. J. Med. Electron. Biol. Eng.* 15:121, 1977.
141. Rosenberg, R.M., Chao, C.H., and Abbott, J.A.: A New Mathematical Model of Electrical Cardiac Activity, *Math. Biosci.* 14:367, 1972.
142. Thiry, P.S., Rosenberg, R.M., and Abbott, J.A.: A Mechanism for the Electrocardiogram Response to Left Ventricular Hypertrophy and Acute Ischemia, *Circ. Res.* 36:92, 1975.
143. Horan, L.G., Hand, R.C., Johnson, J.C., Sridharan, M.R., Rankin, T.B., and Flowers, N.C.: A Theoretical Examination of Ventricular Repolarization and the Secondary T-Wave, *Circ. Res.* 42:750, 1978.
144. Meek, W.T., and Eyster, T.A.E.: Cardiac Size and Output in Man During Rest and Moderate Exercise, *Am. J. Physiol.* 63:400, 1923.
145. McCrea, F.D., Eyster, T.A.E., and Meek, W.T.: The Effects of Exercise upon Diastolic Heart Size, *Am. J. Physiol.* 83:678, 1928.
146. Hamilton, W.F., and Rompf, J.H.: Movements of the Base of the Ventricle and the Relative Constancy of the Cardiac Volume, *Am. J. Physiol.* 102:559, 1932.
147. Sarnoff, S.J., and Mitchell, J.H.: The Regulation of the Performance of the Heart, *Am. J. Med.* 30:747, 1961.
148. Rushmer, R.F., Crystal, D.K., and Wagner, C.: The Functional Anatomy of Ventricular Contraction, *Circ. Res.* 1:162, 1953.
149. Rusher, R.F.: Physical Characteristics of Myocardial Performance, *Am. J. Cardiol.* 18:6, 1966.
150. Shuler, R.H., Ensor, C., Gunning, R.E., Moss, W.G., and Johnson, V.: The Differential Effects of Respiration on the Left and Right Ventricles, *Am. J. Physiol.* 137:620, 1942.
151. Lauson, H.D., Bloomfield, R.A., and Cournand, A.: The Influence of Respiration on the Circulation of Man, *Am. J. Med.* 1:315, 1946.
152. Harrison, D.C., Goldblatt, A., and Braunwald, E.: Studies on Cardiac Dimensions in Intact, Unanesthetized Man. I. Description of Techniques and Their Validation, *Circ. Res.* 13:448, 1963.
153. Goldblatt, A., Harrison, D.C., Glick, G. and Braunwald, E.: Studies on Cardiac Dimensions in Intact, Unanesthetized Man. II. Effects of Respiration, *Circ. Res.* 13:455, 1963.
154. Braunwald, E., Goldblatt, A., Harrison, D.C., and Mason, D.T.: Studies on Cardiac Dimensions in Intact, Unanesthetized Man. III. Effects of Muscular Exercise, *Circ. Res.* 13:460, 1963.

155. McDonald, I.G.: The Shape and Movements of the Left Ventricle During Systole. A Study by Cineangiography and by Cineradiography of Epicardial Markers, *Am. J. Cardiol.* 26(3):221, 1970.
156. Ingels, N.B., Jr., Daughters, G.T., II., Stinson, E.B., and Alderman, E.L.: Measurement of Midwall Myocardial Dynamics in Intact Man by Radiography of Surgically Implanted Markers, *Circ.* 52:859, 1975.
157. Wildenthal, K., Mitchell, J.H.,: Dimensional Analysis of the Left Ventricle in the Unanesthetized Dog, *J. Appl. Physiol.* 27:115, 1969.
158. Kong, Y., Morris, J.J., Jr., and McIntosh, H.D.: Assessment of Regional Myocardial Performance from Biplane Coronary Cineangiograms, *Am. J. Cardiol.* 27:529, 1971.
159. Ginston, L.: Personal communication.
160. Ginston, L., Thigpen, T., Conant, R., Brizendine, M. and Lax, M.: Computer Based Quantitative Regional Wall Motion Analysis During Maximal Bicycle Exercise: Identification of Patients With Coronary Artery Disease. *Computers in Cardiology, Proc. IEEE Computer Soc.*, 1984
161. Solomon, J.C., and Selvester, R.H.: Myocardial Assessment by Inverse Electrocardiography. *Computers in Cardiology, Proc. IEEE Computer Society.* 347-50, 1980.
162. Krohn, B.G., Dunne, E., Magidson, O.: The Electric Impedance Cardiogram in Health and Disease. *Amer. Heart J.* 76:377-87, 1968.
163. Taccardi, B.: Distribution of Heart Potentials on the Thoracic Surface of Normal Human Subjects, *Circ. Res.* 12:341, 1963.
164. Taccardi, B., and Marchetti, G.: Distribution of Heart Potentials on the Body surface abd in Artificial Conducting Media, B. Taccardi and G. Marchetti, eds., *Electrophysiology of the Heart*, Pergamon Press, Oxford, 257, 1965.
165. Taccardi, B.: Body Surface Distribution of Equipotential Lines During Atrial Depolarization and Ventricular Repolarization, *Circ. Res.* 19(5):865, 1966.
166. Taccardi, B., De Ambroggi, L., and Viganotti, C.: Characteristic Features of Surface Potentials Maps During QRS and S-T Intervals, *Advances in Cardiology*, Vol. 10, Karger, New York, 248, 1974.
167. Horan, L.G., Flowers, N.C., and Brody, D.A.: Body Surface Potential Distribution, *Circ. Res.* 13:373, 1963.
168. Flowers, N.C., Horan, L.G., Sohi, G.S., Hand, R.C., and Johnson, J.C.: New Evidence for Inferoposterior Myocardial Infarction on Surface Potential Maps, *Am. J. Cardiol.* 38:576, 1976.

169. Flowers, N.C., Horan, L.G., and Johnson, J.C.: Anterior Infarctional Changes Occurring During Mid and Late Ventricular Activation Detectable by Surface Mapping Techniques, *Circ.* 54:906, 1976.
170. Flowers, N.C., Hand, R.C., Sridharan, M.R., Horan, L.G., and Sohi, G.S.: Surface Reflections of Cardiac Excitation and the Assessment of Infarct Volume, *Circ. Res.* 43:406, 1978.
171. Horan, L.G., Flowers, N.C., and Brody, D.A.: Principal Factor Waveforms of the Thoracic QRS Complex, *Circ. Res.* 15:131, 1964.
172. Horan, L.G., and Flowers, N.C.: The Principle of Waveform Correlation in Electrocardiographic Research, *J. Electrocardiol.* 1:43, 1968.
173. Horan, L.G., Hand, R.C., Flowers, N.C., Johnson, J.C., and Brody, D.A.: The Multipolar Content of the Human Electrocardiogram, *J. Ann. Biomed. Eng.* 4:280, 1976.
174. Horan, L.G., Hand, R.C., Flowers, N.C., Johnson, J.C., and Sridharan, M.R.: The Influence of Electrode Placement in the Reconstruction and Analysis of Body Surface Potential Maps from Limited Thoracic Arrays, *J. Electrocardiol.* 13(4):311, 1980.
175. Lux, R.L., Burgess, M.J., Wyatt, R.F., Evans, A.K., Vincent, G.M., and Abildskov, J.A.: A Clinically Practical Lead System for Improved Electrocardiography: Comparison with Precordial Grids and Conventional Lead Systems, *Circ.* 59(2):356, 1979.
176. Lux, R.L., Smith, C.R., Wyatt, R.F., and Abildskov, J.A.: Limited Lead Selection for Estimation of Body Surface Potential Maps in Electrocardiography, *IEEE Trans. Biomed. Eng.* BME 25(3):270, 1978.
177. Barr, R.C., Spach, M.S., Herman-Giddens, G.S.: Selection of the Number and Positions of Measuring Locations for Electrocardiography, *IEEE Trans. Biomed. Eng.* BME-18:125, 1971.
178. Warren, R.B.: Determining the Number and Positions of Measuring Locations for Body Surface Mapping, Ph.D. dissertation, Duke University, Durham, NC, 1977.
179. Miller, W.T., III, Spach, M.S., and Warren, R.B.: Total Body Surface Potential Mapping During Exercise: QRS-T-Wave Changes in Normal Young Adults, *Circ.* 62(3):632, 1980.
180. Kornreich, F., Holt, J., Rijlant, P., Barnard, A.C.L., Tiberghien, J., Kramer, J., Snoeck, J.: New ECG Techniques in the Diagnosis of Infarction and Hypertrophy, I. Hoffman and R.I. Hamby, eds., *Vectorcardiography*, 3rd ed., Elsevier-North Holland, Amsterdam, 171, 1976.

181. Kornreich, F., Rautaharju, P.M., Warren, J.W., Block, P., and Dramaix, M. The Contribution of Body Surface Potentials Maps to Optimal Lead Sets. Computerized Interpretation of the ECG IX, Proceedings of the Engineering Foundation Conference. ed., R. Selvester, Engineering Foundation, 182, 1983
182. Selvester, R.H., and Gillespie, T.L., Simulated ECG Surface Map's Sensitivity to Local Segments of Myocardium, in Body Surface Mapping of Cardiac Fields, ed., Rush S., and Lepeschkin, E., Adv. Cardiol., 10:120-125, Karger, Basel, 1974.

## FORWARD MODEL DESIGN AND DEVELOPMENT

Task 1 has been completed as of December 31, 1984. The review of the literature, and the design and upgrading of the Selvester-Solomon fine grid (1 mm<sup>3</sup>) forward propagation model of human ventricular excitation to include repolarization have been accomplished. The presentation of this document, a USAFSAM technical report, summarizes these findings and completes Task 1. The design of the upgraded model is presented as a Treatise beginning in the Appendix. Its development and implementation are described as Task 2.

Task 2: The Forward Model Development has two major subtasks (2A and 2B) that, because of limited funding, will be run serially (2-year effort). Subtask 2A (a 1-year effort) is the actual development of a working version of the model with one or more torso simulations representative of the Air Force pilot population and typical examples of local ischemia, injury, and infarct. Significant programmatic efficiencies described next would result if the funding can be upgraded at the end of 2A to allow Subtask 2B and Task 3 to develop concurrently. Subtask 2B (a 1-year effort at the current funding level) is the development of the table-driven subroutines to modify the geometry, activation, and action potentials in order to simulate at will a comprehensive catalog of regional ischemia, injury and infarction, at rest and with exercise. Upon the completion of Task 2 (in two years at current funding levels) we expect to begin Task 3 (Optimal Leads and Criteria) along with early work on the validation studies.

Subtask 2A is the actual development of a working version of the model with a typical torso and a few typical areas of ischemia, injury, and infarct (see "Flow Chart of the Forward Model Program"). In addition to the Forward Computer Model development described in detail, this includes:

- a. Torso tank verification of the Gelernter-Swihart simulation for a broad range, representative set of local dipoles and torso resistivities to include the expected extrema of locations, torso shapes, and resistivities.
- b. Torso tank studies on the potential errors in lead placement, interelectrode resistivity measurements, and methods for verifying the relationship between the leads.
- c. Measurement of torso geometry and impedance changes in man with near maximal and maximal exercise.

This effort requires 1 man year of physicist/analyst time and 1/4 man year of cardiologist-physiologist time.

Subtask 2B is a separate effort to develop the table-driven subroutines that modify the local initial conditions of size, transmural extent, and location of ischemia, injury, and infarct, and whether these are single or multiple. These modifying subroutines will be able to change heart location and long axis orientation in the chest, etc., simulate local or generalized



hypertrophy or dilatation of either or both ventricles, and simulate variations in body build and resistivities. Torso properties, heart locations, etc., may be modified from on line torso resistivity, anthropometric (skin-folds, torso geometry, etc.), and 2-D echocardiography measurements, if error analysis and analysis of the causes of variances indicate this may improve the resolution of the program. This subtask requires 1 man year of a physicist/analyst/programmer and 1/4 man year of cardiologist/physiologist time.

By running Subtasks 2B and Task 3 concurrently, significant efficiencies and facilitation of the overall objectives will be realized. The following staffing will be required: 1 man year of a physicist/analyst, 1 man year of an experienced scientific utility programmer, 1 man year of a research technician, and 1/2 man year of cardiologist/physiologist time.

IN SUMMARY: Our forward model design begins with the simulation of normal heart depolarization and repolarization in a typical inhomogeneous male torso. This model is an extension of the work we have already done on simulating the QRS activation and will include the physiology of action potentials, particularly the epicardial to endocardial and base to apex gradients of action potential duration and downslope, and the geometry of the heart at a  $1\text{ mm}^3$  grid. This normal simulation will be modified to include the geometry of infarct and ischemia as well as the motion of the walls (dipoles) with contraction. At this point, we will be able to test two hypotheses: 1) the Miller-Geselowitz model of ischemia where there is a series of border zones surrounding the dead tissue with progressively less ischemia the farther from the necrotic area one measures; and 2) that there is a sharp border separating infarcted tissue from healthy tissue and it is the complexity of the geometry of the infarct that produces the observed electrocardiographic changes.

Once this is established, we will use a  $1\text{ mm}^3$  discretization of the heart as a starting point. Since developing transfer impedances from such a large number of points is unwieldy, we will group these points into 12 subsets for the left ventricle and 8 for the right ventricle for a total of 20 dipoles. We will check the Thiry-Rosenberg method of representing the cardiac dipoles against this 1-mm grid model with 20 dipoles to see which method is operationally most tractable and computationally the most economical. After the optimal subsets have been determined, we will develop transfer impedances for a variety of normal male torsos. The next step is to generate ECG maps. We will be able to display scalars, 12-lead, VCG's, perspective plots, isopotential plots (in color or black and white) with various sized single or multiple areas of infarct, injury, and ischemia in normal hearts or associated with hypertrophy, dilatation, and/or conduction abnormalities. Isoarea QRS, ST, T, and QRST maps will also be examined.

### Detailed Description of the Forward Computer Model Development

The Task 2 model development consists of writing the source code, debugging, testing, and documenting the three programs that constitute the forward simulation.

1. The wave propagation program simulates the myocardial activation front.
2. The equivalent cardiac source program generates equivalent myocardial sources for depolarization repolarization.
3. The ECG program computes body surface ECG data from the equivalent cardiac generators and the inhomogeneous torso transfer impedances.

#### Subtask 2A-1: Propagation Model.

We will do the following:

1. Create a normal human heart and Purkinje geometry file for input.
2. Write the propagation program source code to execute on the VAX-780/VMS system
3. Generate an output file of the myocardial activation data for the normal human heart that is format compatible with the equivalent cardiac source program.
4. Run the propagation program on a spherical geometry and verify against the analytical activation.
5. Produce graphic output in CRT and hard copy of the activation in the normal heart geometry at various levels of vertical and horizontal cross section to verify that the programs' algorithms are error free.
6. Document the source code and describe the input/output data and file formats.

#### Subtask 2A-2: Equivalent Source Program.

This program includes the 1 mm<sup>3</sup> discretization and the grouping of these into 12 LV and 8 RV myocardial segments (20 dipoles). We will do the following:

1. Create a nominal value file for the action potential profiles throughout the myocardium.
2. Write the source code for the equivalent source program to run on the VAX-780/VMS system.
3. Verify that the program will read the compatible activation data from the wave propagation program under all possible variations.

4. Have the program generate an output file of the equivalent cardiac source that is compatible with the ECG program.
5. Display graphically the equivalent cardiac generators (action potential profiles) on CRT and hard copy and verify the program output by comparison with hand computed values based on the input data files.
6. Test the program with a 10 mm cube of simulated myocardium and nominal action potential profiles.
7. Display graphically (CRT and hard copy) the output of the 20 dipole myocardial segment subdivision.
8. Document the source code and describe the input/output data and formats.

#### Subtask 2A-3: ECG Data Program.

We will do the following:

1. Solve the inhomogeneous boundary value problem for a normal set of transfer impedances from heart generators to torso surface leads.
2. Write source code to compute ECG data from the input files.
3. Verify that the source code can read the equivalent cardiac source input file under all possible variations.
4. Code the ECG data program to generate an output file formatted in sections which contain contiguous blocks of data for each type of output, such as 12 lead ECG, McFee vector, Frank vector, body surface map, etc.
5. Test the boundary value solution against the electrolytic torso tank for several sources to demonstrate the agreement between the mathematical solution and physical measurements.
6. Graphically display the ECG output data file for unit transfer impedances and unit orthogonal dipole sources to verify the program algorithms.
7. Document the source code and describe the input/output data and formats.

#### Studies with the Forward Computer Model

#### Subtask 2A-4. Verification of the Transfer Impedances on the Electrolytic Tank:

Since the transfer impedances of the forward model simulation are derived from a mathematical solution to a boundary value problem using matrix and iterative methods, it becomes necessary to verify the mathematical solutions in an experimental configuration. Verification will consist of computing the transfer impedances for the electrolytic torso tank that contains a number of

dipole sources and comparing them with the actual measured values. Results of such a verification experiment determine the errors in the boundary value solution relative to the location and direction of the dipoles imbedded in the volume conductor. There is no other reliable test of the program code, convergence, and accuracy than a physical verification.

#### Subtask 2A-5. Electrode Misplacement and Reconstruction:

An experimental study will be conducted on the electrolytic tank to develop a method of identifying chest lead misplacements and reconstruct the correct ECG. This procedure will investigate the use of small sinusoidal currents impressed on the torso to detect and correct for improper transfer impedances. Safety considerations for use on humans will be identified and established.

#### Subtask 2A-6. Effects of Exercise on Torso Transfer Impedances:

A major part of the forward model application is in determining optimal leads and criteria at exercise. For this reason, the torso volume conductor changes that occur in normal adult males at exercise will be measured. Changes in volume conductor characteristics measured between rest and exercise will be computed with the boundary value solution program to estimate the properties of the torso transfer impedances at exercise. These effects will become a part of the variations included in the transfer impedance library for the forward simulation program.

#### Subtask 2B: Develop the Input/Output Data Generation Programs:

We will develop the input/output programs that produce the disk files used for input to the forward ECG simulation programs. These data generation programs interact with the operator and the simulation programs. An operator responds to this set of programs to generate various input conditions that produce a desired ECG simulation. The four programs to be developed to interface the operator with the simulation programs are as follows:

1. Heart geometry alteration routine.
2. Purkinje modification including starting points.
3. Action potential distribution program for specifying the regional distribution parameters for equivalent cardiac sources.
4. Transfer impedance selection program that retrieves a specific set of transfer impedances from a cataloged library.

#### Task 2C: Torso Transfer Impedance Library:

The Gelernter-Swihart method of computing a matrix of torso impedances requires several hours of time for each variation of heart location or geometry, torso shape, or resistivity. The development of a comprehensive library of torso transfer impedances will be a major ongoing effort requiring 1-3 years for completion depending on the availability of computer time and funds. At the start up of Task 2, we will immediately begin generation of the library of inhomogeneous torso (volume conductor) transfer impedances

from equivalent source locations in the heart to torso surface electrode sites.

Initially a 20-dipole equivalent heart source will be used to represent the electrical activity, and the transfer impedances will be determined for the three orthogonal components of each of the 20 dipoles. Transfer impedances will be computed for numerous variations about the nominal (typical) case. These variations include short, medium, and tall torso dimensions (relative to Air Force standards), as well as thin, typical, and heavy body weights.

Anterior-posterior to lateral ratios will be included. Another first-order transfer impedance variable is the position and orientation of the heart in the chest. Transfer impedances will be computed for various aortic root locations and Euler angles specifying the orientation of the heart. Initially, three sets of transfer impedances for each distinct torso condition will be computed; one each in diastole, mid systole, and end systole. Interpolation through these three cases will be utilized to obtain transfer impedances for ST-T wave computation while the heart is in motion.

Variations in lung and blood mass conductivities in the Air Force pilot population is likely to be a second-order effect and may not need to be included. However, such variations would be included if more detailed analysis of the subjects indicates that it is required.

#### Validation

Autopsy: The standard 12-lead ECG taken no more than 10 days before death will be simulated in the following 6 male patients, age 25 through 55. Two subjects will have no organic heart disease on post mortem examination by the quantitative planimetric method of Idecker and Hackel: two cases will have at least one coronary artery showing at least 50% cross-sectional luminal narrowing and no evidence of myocardial infarct, and two subjects will have had at least one old infarct. No subject will have had a recent infarct, myocarditis, cardiomyopathy, congenital or valvular heart disease, evidence for passive congestion or abnormal fluid accumulation in any body cavity, or any electrolyte abnormality at the time the ECG was taken. Cases will be selected that are of the same general height, weight, body build and torso configurations as found in typical airmen. The 12-lead ECG of all 6 subjects will be simulated and expected to pass the following performance tests: when compared to the last antemortem ECG, the simulated ECG shall have 1) less than 10 degrees difference in frontal plane mean axis of both QRS and T wave; 2) less than 10-msec difference in both the QRS interval and the interval from the onset of QRS to the peak of the T wave in those leads with unambiguous fiducial points; and 3) less than 100- $\mu$ v difference in the amplitude of the following: Q, R, S, R', S', ST 80 msec after J, and peak T.

Clinical validation: The autopsy validations above establish the physiologic and anatomic reasonableness of the simulation. The real utility of the model, however, will be in the development of optimal lead sets and criteria in those leads for detection of ischemia. The testing of these criteria in clinical populations would be the next and mandatory step in the clinical validation of the model. This is Task 3 of this overall effort, and

not dealt with directly in the present document. In Task 3, after optimal leads and criteria have been developed, specific protocols will need to be set up to test the specificity, sensitivity, and predictive value of the criteria. From a review of the literature in body surface ECG mapping with exercise, and from the data summarized in this report, it is reasonable to expect sensitivities, and specificities in the 95-98% range for the detection of unsuspected ischemia in the asymptomatic pilot population. If funding can be increased in the 02 yr to run Task 3 concurrently with Task 2B, detailed clinical validation protocols that have been previously developed will be reviewed at that time.

#### Flow Chart of the Forward Model Program

OVERVIEW: The forward simulation program of human ECG data, as flow charted here, is a structured program executed from the top down as single pass, non-recursive and non-reentrant code. Control of variation of input conditions is through question and answer dialog. Simulation programs execute using only input data contained in current data files, all ancillary or modification programs only update these current files. Hence, input data or other operator inputs never alter the manner in which any of the simulation programs execute. Special programs are invoked by operator responses that allow current input data files to be modified and in some cases require specific peripheral devices such as digitizers and plotters. The four current input data files required to execute the entire simulation process are discussed next:

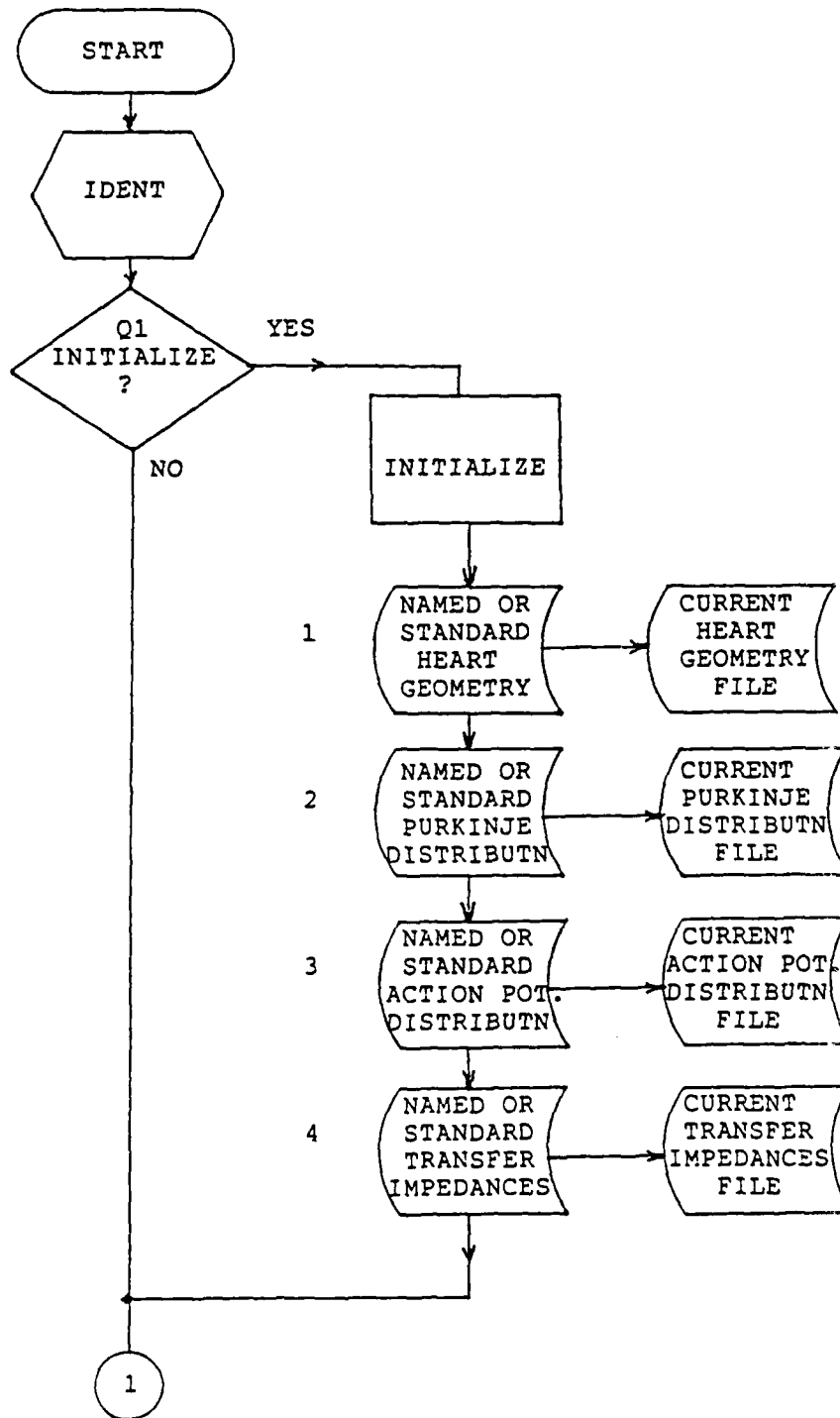
1. Current Heart Geometry File: Normal cardiac muscle and regions of infarction and/or hypertrophy are digitized from photographs, drawings, or plots with a digitizing table, raster scanner, or similar device. This file is an input data file for the Wave Propagation Program and is updated by the Geometry Alteration Program. A normal adult male heart geometry is available for normal ECG simulations and for testing purposes. This standard heart geometry can be copied to the current heart geometry file on program initialization.

2. Current Purkinje Network File: A standard set of Purkinje points distributed over the endocardium of the standard heart geometry, along with normal starting points are used to initialize the current Purkinje Network File. The Purkinje Modification Program is provided to simulate changes in the Purkinje network and different starting points.

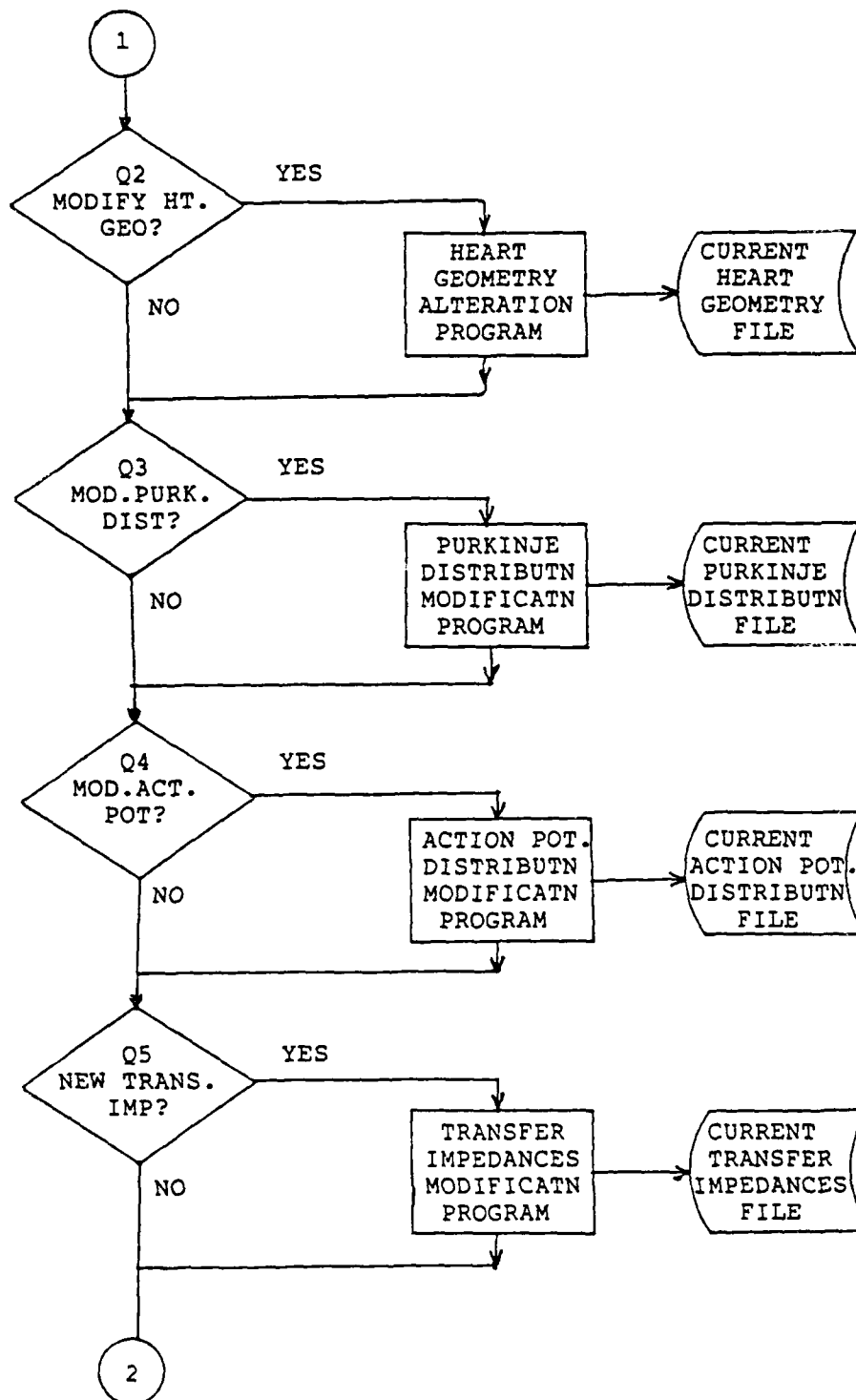
3. Current Action Potential Distribution File: A normal set of parameters characterizing the action potential profiles in each region of the cardiac subdivisions will be designated as the standard Action Potential Distribution File. Upon initialization, this file is copied to the current Action Potential Distribution File where it can be altered by the Action Potential Modification Program which provides any change in the current profiles of action potential parameters. The regional anatomy of infarct, ischemia, injury, and hypertrophy provide the basis for establishing a library of regional changes in the action potential parameters. The Current Action Potential Distribution File is updated with the changes and the program process continues.

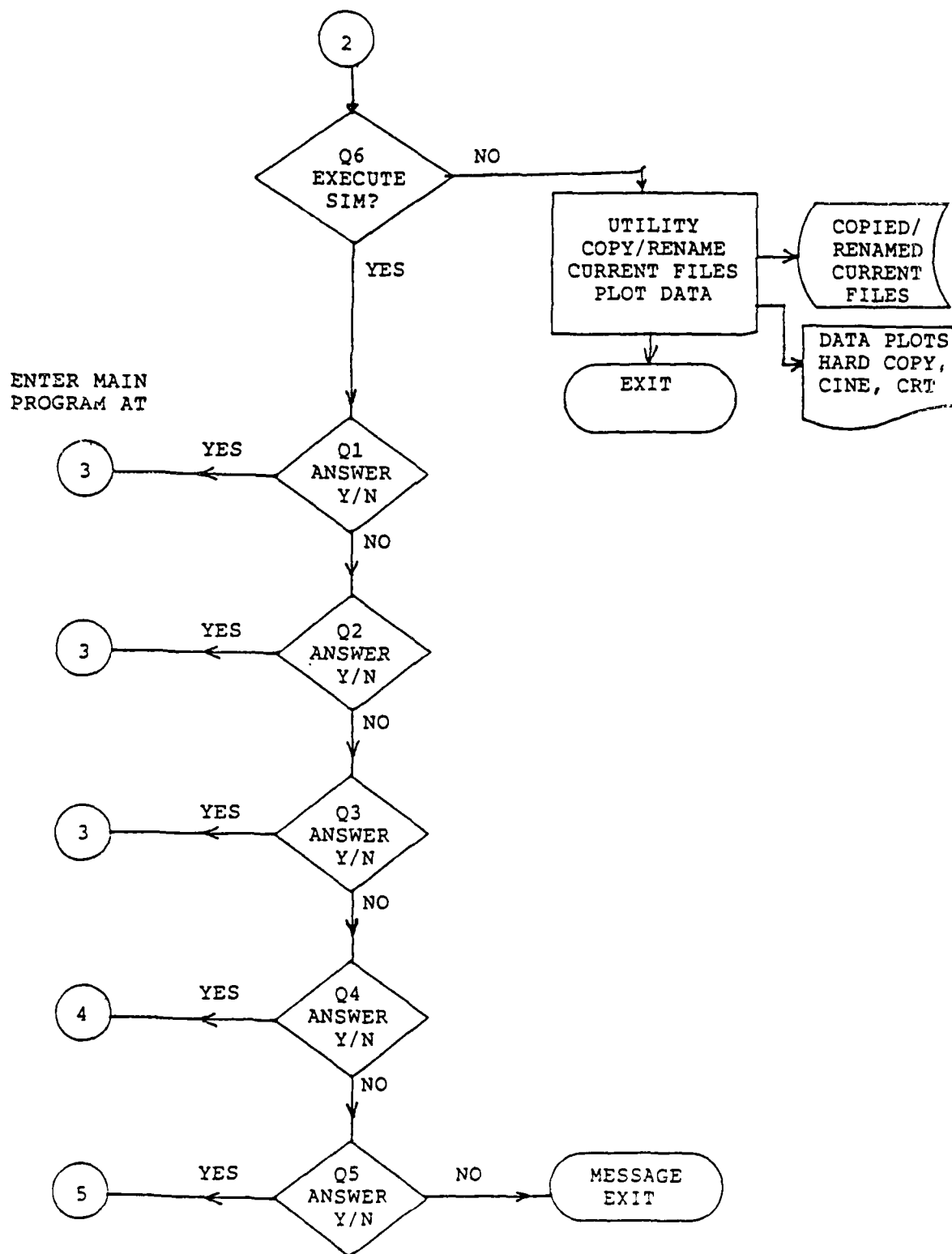
4. Current Transfer Impedance File: The current file used during any simulation procedure is a copy of a file from the library of torso transfer impedances. A catalog will be maintained for choosing a specific heart location, contractile pattern, torso shape and conductivities. This catalog will uniquely identify the specific Transfer Impedance File in the library. Provisions are made in the simulation programs to load the specific file with an entry from the catalog.

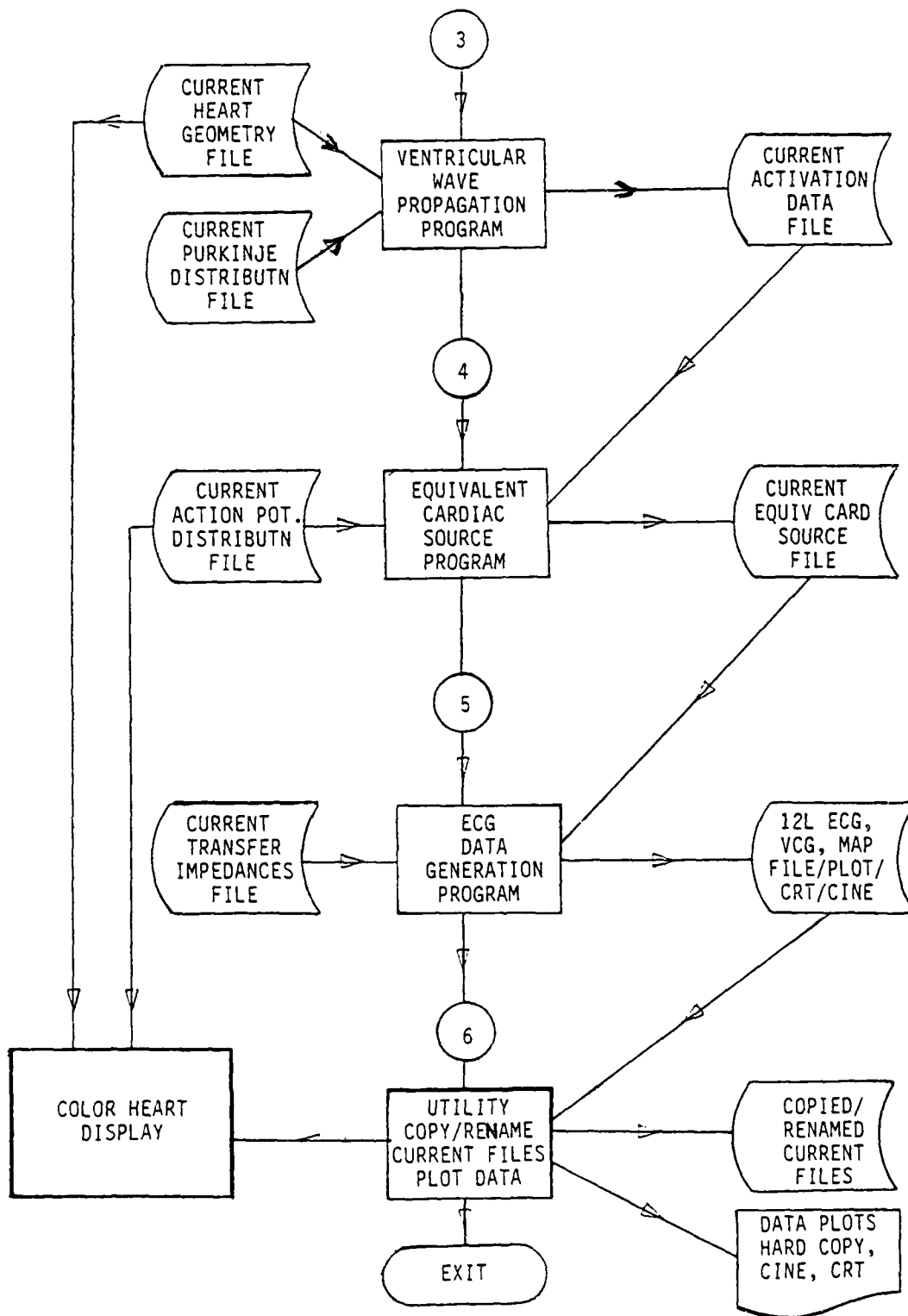
# FLOW CHART OF THE FORWARD MODEL PROGRAM











## Discussion of the Flow Chart

On start-up, the main program requests the date and time from the operating system. Both will be stamped on current files and final output data forms for identification purposes. In addition, the IDENT routine will request a unique identification number and a short sentence that will appear on the output data form. The purpose of this is to describe and identify the particular type of input conditions or modifications that were used in the simulation. For example, the operator might specify a 2-cm subendocardial infarct in segment 5 and identify the output of the simulation by the number 54321. The ECGs, vectors, body surface maps, heart and/or torso cross sections, etc., that appear in hard copy and disk or tape storage would have the name of the operator, date, time, ID number, and the descriptive sentence as a label or header. The main program consists of a series of six questions for which either yes or no answers are given by the operator at the terminal.

Question 1. If the operator wishes to perform a simulation, he answers yes to the question. In the process of initializing by responding to a series of questions in this section, the current input data files are filled with either standard or specific named data files. Named data files are those files for heart geometry, Purkinje network, action potential profiles, and torso transfer impedances that were created in previous simulation sessions and saved on mass storage devices under a specific name and file specification. In this way, a particular heart geometry with an infarct, for example, could be simulated under various other input data changes and where the entire study might extend over many sessions or days without the need to ever recreate the infarct geometry within the heart geometry. Standard and various named input data files would be useful in debugging and testing the simulation process following any program modification or upgrades.

Question 2. If an infarct, hypertrophy, or other heart geometry change is desired, a yes response to question 2 will invoke the Heart Geometry Alteration Program. This program requires the operator to identify the regions to be altered and then input the changes through the digitizing table from a drawing or photograph of the heart geometry under modification, usually the current standard heart geometry file data. This alteration program updates the current Heart Geometry File to reflect the modifications and then returns to the Main Program.

Question 3. A yes response invokes the Purkinje Distribution Modification Program. In addition to modifying the Purkinje distribution over the subendocardial surface this program is used to specify the starting points for the Purkinje activation. Such starting points correspond to the positions within the Purkinje network where the arborizations of the right and left bundles of the specialized conduction system are inserted. Hence, the simulation of certain conduction defects is accomplished by first modifying the start points with this Purkinje Modification Program.

Changing the Purkinje network is accomplished in the same way as the heart alterations, that is by digitizing the additional regions or deleting regions that are damaged. Special consideration and care must be used when modifying the Purkinje network whenever the heart geometry is altered at the endocardial surface. By definition, the Purkinje network is on the endocardial surface and must be contiguous with the subendocardial myocardium

everywhere. In addition, the network must be continuous at a 1 millimeter spacing to represent normal Purkinje and yield a normal excitation velocity in the wave propagation program. These considerations will be covered in detail in the user guide. After inputting the new starting points or modifying the Purkinje the program updates the current Purkinje Distribution File and returns to the Main Program.

Question 4. A yes response invokes the Action Potential Distribution Modification Program. This program does not alter the definition of the cardiac segments and zones. The active myocardium is subdivided into 20 segments, 12 in the left ventricle and septum and 8 in the right ventricle. Each segment is further subdivided into zones from endocardium to epicardium. Using drawings of the segments and zones within the segments the operator responds to requests for specific regions or zones where action potentials are to be altered. The operator then enters the new action potential parameters for the particular local region. Requests for additional input continue until the operator indicates the end. The Action Potential Distribution Program updates the current Action Potential Distribution Files and returns to the Main Program.

Question 5. Specifying that a new set of transfer impedances from the cardiac generator to the torso surface be introduced into the simulation is accomplished by table look-up of the desired file from the library of transfer impedances. The library is created by solving the appropriate boundary value problem for various torso shapes, lung and blood mass geometries, heart locations and rotations, regional wall motion abnormalities and internal conductivities. A large set of boundary value solutions, containing known important differences in geometry and conductivity will be computed and uniquely labeled and described. This catalog and disk library will be updated as additional sets of transfer impedances arrays are produced during the 02 (and 03) year(s).

Question 6. Under certain conditions such as debugging or testing of the program, it will be desirable to enter the utilities program without executing the simulation. A no response to question 6 would invoke the utilities program and allow the operator to rename files, print or plot data, or other utility type operations invoked through operating system requests. Otherwise, a yes response will send the simulation programs into execution at the appropriate entry points defined by the responses to the previous questions. If the operator enters the utilities program at question 6, it may be desirable to chose between exiting the program or branching back to the starting point in the main routine. This re-entry question will have to be considered in further detail at the time of the program generation because of the many ramifications of re-entry as relates to the operating system characteristics.

### Simulation Programs

Positions 3, 4, and 5 in the Main Program are entry points in the simulation determined by answers to Questions 1 - 5. The program structure minimizes the execution time by not using the entire set of programs when no changes have occurred. Entry at point 3 causes the entire set of programs to be executed starting with the wave propagation program. Current data files

shown on the left in the flow diagram, and generated output files appear on the right-hand side. As illustrated in the flow chart, the Wave Propagation Program inputs the current Heart Geometry and Purkinje Network Files and produces as output the current Cardiac Activation Data File. Cardiac Activation Data File becomes the input to the next program, the Equivalent Cardiac Sources Program which combines it with the current Action Potential Distribution Data File and generates an Equivalent Cardiac Source File representing the electrical activity of the heart being simulated during depolarization and repolarization.

The last stage of the simulation process is the ECG Program which combines the Cardiac Source and the volume conductor Transfer Impedance Data Files to produce the output ECG's, VCG's, and body surface maps. The latter may be displayed as isopotential or perspective plots for each 2.5 msec or as isoarea maps, 1 plot each for QRS, ST, T, or QRST.

The utility program is inserted at the end of the simulation program to permit the operator to exercise various options for outputting data or storing data for future reference. Some of the routines within the utility program would be system requests such as copying, renaming, or deleting files from the mass storage device. Other options would include printing ECG data, plotting ECG data, printing or plotting any of the current input data files. As the forward model programs are developed, the utilities required to test, debug, and analyze the simulation process will be added to the utility program. Various graphics aids, given appropriate hardware, could also be added.

### Color Heart Display Program

This program will be developed under Task 2A and consists of a color graphics display of the heart geometry under simulation at the time it is called into execution. Two input data files are processed into the display: the current heart geometry and the current action potential distribution files. The operator will select from a menu the slices of the heart to be displayed. From the above 2 input files, the heart geometry will be displayed on a dark green background. Healthy myocardium will be presented in red, infarcted regions in white, and ischemic zones in blue.

### Input Data Modification Programs and Enhancements

#### Initialization Program

Generally, the initialization program is the first program to be executed. Its purpose is to fill the current data files with either a standard or normal configuration. A set of standard or normal input data files is used to simulate normal ECGs or generate a standard test set of output data. These files are required for debugging the program following any modifications to the source code. In addition, after a simulation session on the computer, the current data files can be renamed and saved with the utility program. Therefore, the next simulation session could, on initialization,

specify any of the previous files to be reloaded into current data files. At the start of a simulation session, the operator should assume the current data files to be undefined and execute the initialization routine, thereby creating new current data files with standard or normal data, or by specifying some file or files that had been preserved from previous sessions.

The initialization program will be designed to solicit responses from the operator as to which files to load or default to the normal simulation data. For example, a normal set of transfer impedances from the cardiac generators to the ECG leads at the chest surface would always be loaded by default, a normal adult-male heart geometry for the wave propagation program with its normal Purkinje distribution, and a set of distributed action potential parameters. These files are required to exist at the time of execution and would be set to normal values unless decided otherwise by the operator. To accomplish this, the program will request the filespec of the desired current data files at the beginning of the program.

#### Geometry Alteration Program

Figure 13 shows the form in which the heart geometry is represented. This particular cross-section happens to be at location  $Z=51$  mm, measured from the apex towards the base of the heart. A similar cross-section exists for each 1 mm of myocardium. In the horizontal projection the heart geometry is defined by a raster scan in the Y direction; that is, for each 1-mm increment in the Y direction the values of the Y coordinates for fixed X specify the endocardial and epicardial surfaces. In Figure 13, for example, the value  $X_n$  represents a fixed value of the X coordinate and the scan in the Y direction picks up the values  $Y_1, Y_2, \dots, Y_6$ . The myocardium in which the wave of excitation will propagate is input in the following format:

```
Z=51
(Xn,Y1,Y2)
(Xn,Y3,Y4)
(Xn,Y5,Y6).
```

With this input data the wave propagation program will construct "normal myocardium" between all coordinates between  $Y_1$  and  $Y_2$  for the given value of  $X_n$  and  $Z=50$ . All other coordinates are set this same way, leaving unspecified coordinates as volume regions where the wavefront cannot propagate.

If infarction is to be simulated, then the operator must specify the infarct in the same manner through the heart geometry alteration program. For the purpose of the simulation, an infarct specification is defined as a region of the myocardial geometry where the activation front will not be allowed to propagate. This means that the activation front will propagate around the 3-dimensional infarct region and the infarct will not contribute to the equivalent cardiac generators producing the body surface ECGs.

As an example of how the first infarcts were simulated, consider the cross-section of normal heart geometry in Figure 14 taped to the digitizing table. An infarct was defined by a line circumscribing the region. The digitizing cursor was reset at position 1 to define the origin; then cursor

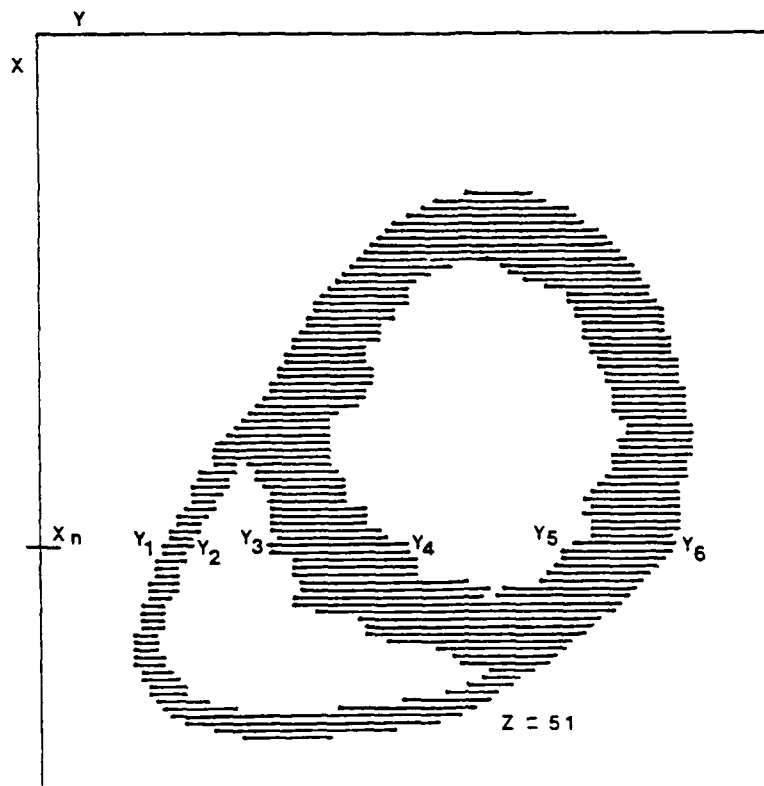


Figure 13. Example of the raster scan that defines the cross section of cardiac geometry.

position readings were taken at locations 2 and 3 to correct for possible rotation of the X and Y axes. Next the operator scanned the infarct region recording the coordinate positions  $(X_1, Y_1, Y_2)$ ,  $(X_2, Y_1, Y_2)$ , ...,  $(X_k, Y_1, Y_2)$ . A request/answer program prompted the operator for the Z level of the heart geometry or to exit. Following the last level digitized the program concatenates the infarct geometry file to the normal heart geometry file to produce an input file for the wave propagation program.

During Task 2A the simulation program will insert infarct data manually by appending the infarct coordinates to the current heart geometry file that was loaded initially with the normal geometry.

A menu-driven method of inserting infarction into the zones within each segment will be provided during Task 2B. Those combinations of infarction data the operator selects will be appended to the current heart geometry file from a library containing infarct-specification coordinates for every zone of each segment. For example, Figure 15 will be displayed when level 61 is selected by the operator at the keyboard. The operator will be requested to enter the numbers corresponding to the desired region of infarction.



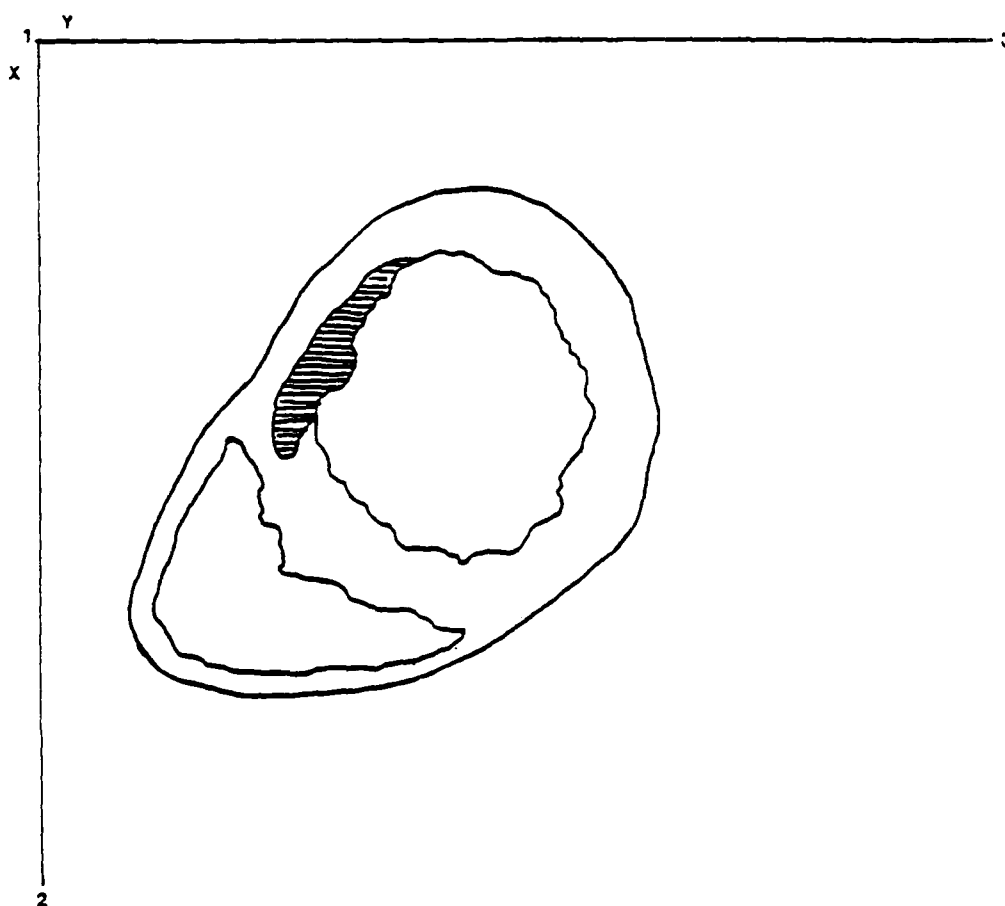


Figure 14. The geometry of a typical infarct is superimposed on the geometry of an appropriate heart cross-section.

An automatic form of interactive graphics hardware/software such as a light pen or plotter and digitizer will be developed in Task 3 to alter heart geometry. This will permit the operator to display sections of the heart on a graphics terminal, and interactively specify infarction on the displayed cross-section or modify the geometry to include dilation of the ventricles. Such a program will be designed to automatically append either infarction and/or hypertrophy to whatever data is in the current heart geometry file. Figure 16 shows the same cross-section as before; however, the operator is requested to trace out any infarcted region and trace out any hypertrophied region to be included as illustrated in the drawing. Obviously, the operator must have available in advance the information on where to draw the regions.

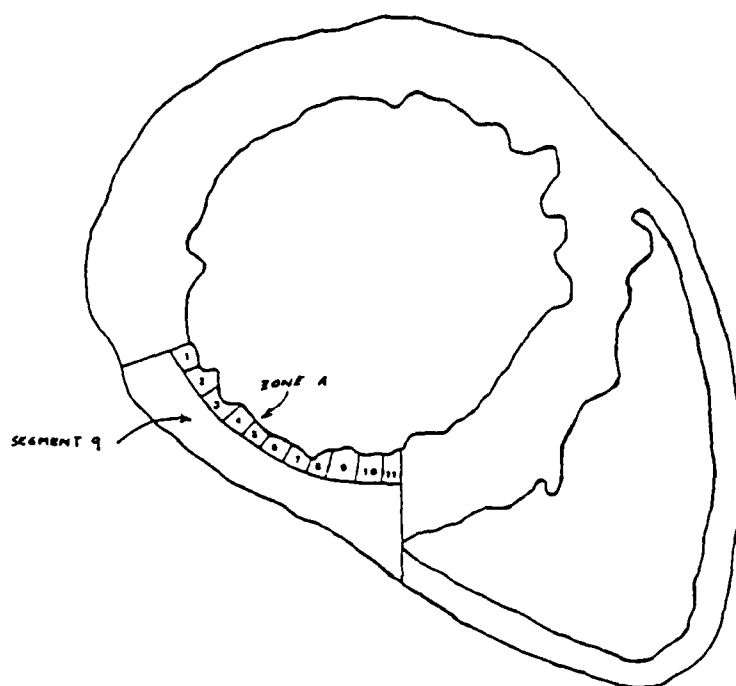


Figure 15. Typical cross-section (Level 61) displayed on a graphics terminal when requested by operator for the purpose of inserting infarction or ischemia, etc.

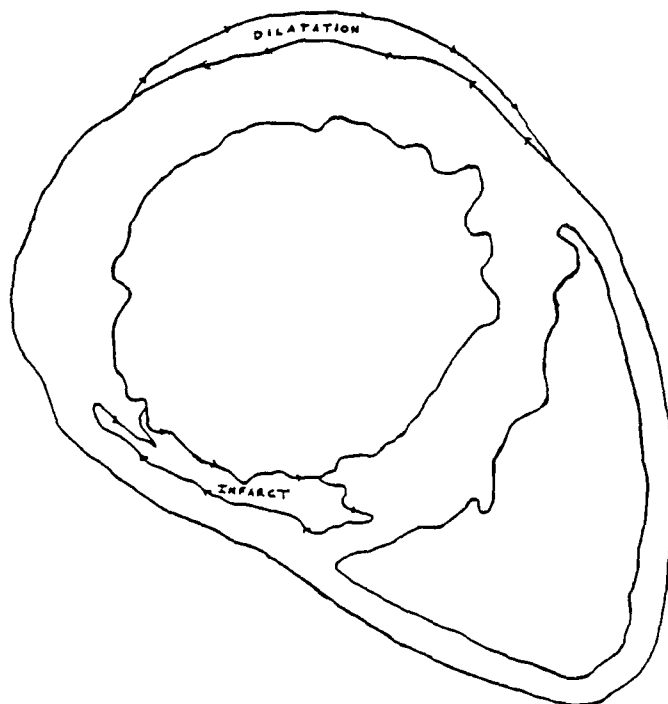


Figure 16. Same cross section as Figure 15 with an area of infarct indicated along with dilatation.

### Purkinje Modification Program

Geometry for the Purkinje distribution is taken from the endocardial surface of the normal human heart geometry. It includes all of the endocardial surface with the exception of the region near the base of the heart. There are only several limited conditions under which the Purkinje network can be altered or modified. One condition for Purkinje modification will occur if the endocardial surface of the heart geometry is altered by the geometry modification program. If such a heart geometry modification extended the endocardial surface either into cavity or decreased the wall thickness from the endocardial surface, then that portion of the Purkinje distribution effected would have to be modified by this routine. The reason for this is that the Purkinje distribution must be contiguous with the endocardial surface geometry.

A second reason for modifying the Purkinje network would be to simulate a sub-endocardial infarction for which the Purkinje network under the infarction has not survived. Therefore, the activation of the Purkinje would propagate around the infarcted region.

Purkinje input data has the same format as the raster scan of the heart geometry. Modifying the Purkinje input data follows the same procedure as for the heart geometry. A plot of the normal heart geometry is mounted on the digitizing table. Regions of the Purkinje network to be redefined are outlined and then the cursor scans in a raster mode and picks up the points. The operator must exercise care and be certain the Purkinje network is continuous everywhere at a 1 mm resolution; that is, there can be no distances between points of the Purkinje network that exceed 1 mm.

Starting points are selected from the Purkinje distribution data and inserted at the end of the current Purkinje distribution file. A set of normal starting points will be used for default values if not specifically entered by the operator.

Task 2A will include a set of starting points and a normal Purkinje distribution on the endocardial surface of the normal heart geometry, with changes made manually to the Purkinje distribution file.

A menu-driven program to specify regional Purkinje infarction is probably not justified as an interim solution for modifying the network, since little could be accomplished with the simulation program for such variations in Purkinje morphology.

During Task 3, the same interactive graphics method of modifying the heart geometry will be incorporated into the design for modifying Purkinje distribution and specifying starting points.

### Action Potential Distribution

Variations in the action potential distribution are simulated by modifying the current activation potential file containing the distributed voltage profiles. Ischemia and other action potential related anomalies are simulated by specifying the coefficients in the action potential profiles as

they apply to regions of the heart. A discussion of the coefficients and equation for the potential profile is contained in the Forward Model Treatise. All regions of the non-infarcted heart geometry require a set of coefficients before the equivalent cardiac generators can be calculated. During Task 2A of the program development, a set of normal coefficients for every zone of each segment of the heart subdivision will be established and incorporated into the model as the default values. Modification of the regional values of the coefficients will be menu-driven for the various zones of each segment as depicted in Figure 15, a cross section of the heart showing the configuration of a mid-ventricular slice. The program will prompt the operator for the segment number followed by a prompt for the zone within that segment. The operator will insert the value of the coefficient requested by the program. When no further coefficients are to be specified the operator exits the routine, which inserts the modification into the current action potential distribution file for input to the equivalent cardiac source program.

An automatic method of specifying the regions of ischemia to be simulated is scheduled for development during Task 2B. The proposed method will display/plot a cross-section of the heart geometry, contained in the current file, where the ischemic regions are to be specified. The operator will label the region uniquely, then with a light pen or cursor trace out the region. At the conclusion of tracing, the program will prompt the operator for a set of coefficients to be assigned to the action potential profile for this unique region. The program will loop in this mode until the operator has finished all modifications. Again, this data will be inserted into the current action potential distribution program. Figure 17 depicts the input design for interactive specification of ischemic geometry.

#### Transfer Impedance Modification Program

The proposed transfer impedance modification routine will be a library look-up for specific cases. A set of transfer impedances have to be computed as the solution for a boundary value problem for any change in torso geometry, cardiac source locations, and conductivities. A library of transfer impedances will be computed throughout Tasks 2A, 2B, and 3. This transfer impedance selection routine will prompt the operator for the file specification of the desired set of transfer impedances. Filespecs will be contained in a catalog of the updated library and include a unique description of the transfer impedances.

Simulation of wall motion during systole and cardiac dilatation are examples that require specification of the cardiac source locations as a function of time. A discussion of how this information must be specified is in the ECG Forward Model Treatise. Briefly, a set of cardiac generator locations must be specified at several instants of time during the systolic interval, the solution to the boundary value problem is computed for each instant, and then the remaining transfer impedances are computed by interpolating over this finite set.

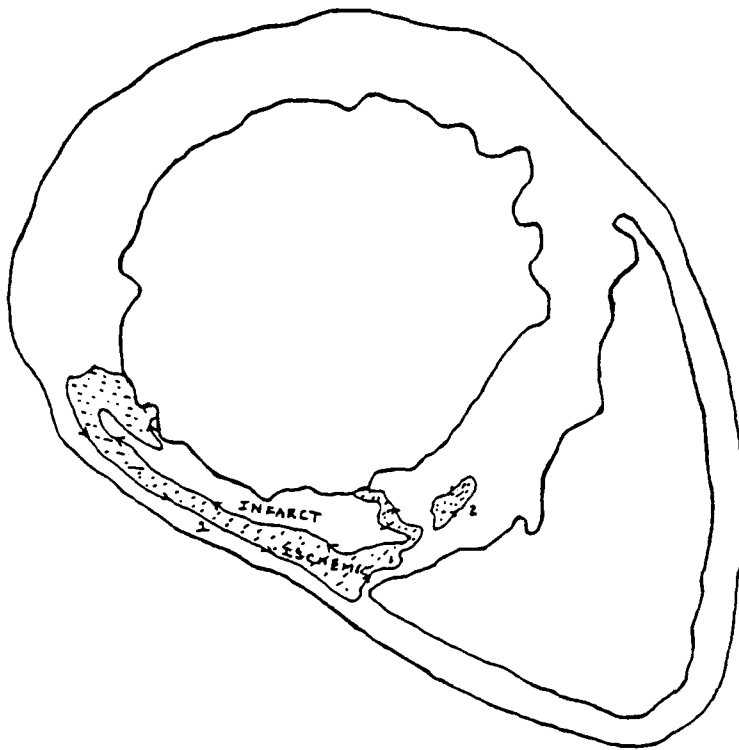


Figure 17. Same cross-section and infarct is shown as Figure 16. A border zone of ischemia is shown.

#### Enhancements to Forward Model

Several enhancements to the wave propagation simulation program are under consideration as part of Task 3:

1. Rather than execute the program in two separate phases, first the rapid Purkinje activation followed by slower cell-to-cell conduction, the program can be modified to run both Purkinje and wall activation concurrently at their respective velocities. Such an enhancement would permit the simulation of conduction system defects that result in Purkinje re-entry. This enhancement will be added to the original activation model.

2. Another enhancement to the propagation model would be to include non-uniform conduction velocity according to certain regional specifications, because ischemic regions conduct slower than normal myocardium and activation in normal tissue is asymmetric. Two concerns mediate against such an enhancement (over and above the obvious increase in computer resources): a) the information from laboratory experiments is not available to specify the magnitude and direction of the conduction velocity in the intact human heart; and b) it hasn't been ascertained whether the inclusion of non-uniform velocity is a first-order effect

that projects onto the body surface ECG leads. Experiments will be conducted to determine if the simulation of regional variations in conduction velocity produce a first-order effect in the surface ECGs. If the results demonstrate that velocity variations are first-order, then the propagation model will be enhanced to include both variations in conduction velocity and Purkinje re-entry into a single module.

3. During Task 3, an analysis should be performed to determine whether there exists a set of torso geometries, lung fields, blood masses, conductivity ratios and generator locations for which transfer impedances could be calculated and then by interpolation and/or extrapolation, all other transfer impedances could be obtained from a specification of parameters, such as A-P and lateral dimensions, height, or information from chest x-rays, echos, and ventriculograms.

### Numerical Experiments with the Model and Sequence of its Development

#### Systolic Wall Motion and Dipole Location

The most computer-intensive portion of the modelling effort is the generation of a library of transfer impedances for the various combinations of torso resistivities and heart locations. This is due to the fact that the Gelernter Swihart (G-S) simulation of the homogeneous torso volume conductor requires the solution of some 3000 simultaneous equations. It therefore becomes of primary importance to investigate the relative importance of changes in heart location that might be related to systolic wall motion and the potential significance of exercise-related changes in the volume conductor early on in the systems analysis. Given that, at the source, one would expect a 10%-20% change in ST segments opposite to the major QRS deflection as a reasonable indicator of subendocardial ischemia, a series of experiments can be performed in the first months of this effort to begin to assess if the kind of regional wall motion changes expected with systole, including the rotational effects, are first-order or lesser-order effects.

Specifically, the potential distribution on a typical adult male torso (a body surface ECG map) from the propagation model for QRS will be computed. Antero-septal, superoapical, posteroapical, inferobasal and posterobasal unit dipoles from this model will be moved 10 mm in, out, basally, apically, clockwise, and counter-clockwise from the expected median position; G-S solutions to the inhomogeneous volume conductor will be calculated for each perturbation in location; the absolute change in voltage that would be produced on a surface map by a 10%-20% change in each unit dipole will be assessed. In the analysis of the data it will be asked: Which dipoles when changed by either 10% or 20% provoked changes in surface measured voltages outside the expected noise in clinically recorded rest and exercise ECG surface maps? A relevant cardiological and clinical question is: What is the extent of regional subendocardial ischemia that would be indicative of significant coronary narrowing in each of the major coronary distributions? For this purpose, the main diagonal branch of the left anterior descending coronary artery will be considered as a separate arterial distribution since it perfuses a volume of myocardium roughly equivalent to that perfused by the

right and circumflex coronary arteries. Analysis of this data in the context of clinically relevant areas of ischemia will give a first order approximation of the potential resolution of this method. Earlier outputs from the model (see Figure 11 in the Background section) suggest that significant subendocardial ischemia involving the major portion of the inner 2-3 mm of each of the 12 LV segments will produce changes above the noise level that can be achieved in the typical exercising patient with normal torso geometry and resistivities.

A related question that might result in very major savings in computation time is: What are the potential physiological, and clinical cardiological results of considering these 12 regions as having "fuzzy borders"? What are the conceptual electrophysiological consequences of assuming the borders have that same 10-mm uncertainty by keeping the unit dipole location constant and not trying to simulate rotational and motion changes with systole, and with the dilatation of ischemia? It may be quite enough to say that there is significant ischemia somewhere in each of the 4 main coronary artery distributions. The main question now would be: When this simplifying assumption is made and a single set of transfer matrices is used, does the failure to be realistic at the source level result in interpretable body surface maps, and can the validation criteria outlined on pages 52 and 53 be met?

#### Subendocardial Ischemic Area Size: Sensitivity and Resolution Studies

When the action potential distribution profiles have been incorporated in the whole ventricular geometry, it will be possible to approach this same problem with a more rational and physiologically quantitative approach. For example, one can now ask: How would subendocardial ischemia involving the inner 2 mm of each region but only extending over an elliptical area measuring 10 x 15 mm be seen on the body surface? This could be assessed with a single typical set of transfer impedances for the mid systolic position. The size of the internal surface area of ischemia and its transmural extent could be systematically varied to assess the limits of resolution of each region on the body surface, and which local ECG leads best discriminate that change. What size or extent of typical subendocardial ischemia in each of the 4 main coronary artery distributions can be identified in the 12 lead ECG when the simulation of the non-ischemic normal is available for comparison, and what criteria in these leads would identify this regional ischemia? A typical experiment simulating subendocardial ischemia in the distribution of the distal circumflex and the marginal circumflex coronary arteries is shown in Figure 18.

#### Intramural Conduction Velocities with Ischemia

While the data is conflicting about whether during acute subendocardial ischemia the conduction velocity through the wall is slowed or accelerated, both effects can be explored systematically with the model. To be efficient about these numerical experiments, these will best be accomplished after the "Input Data Modification Programs and Enhancements" described on pages 61-69

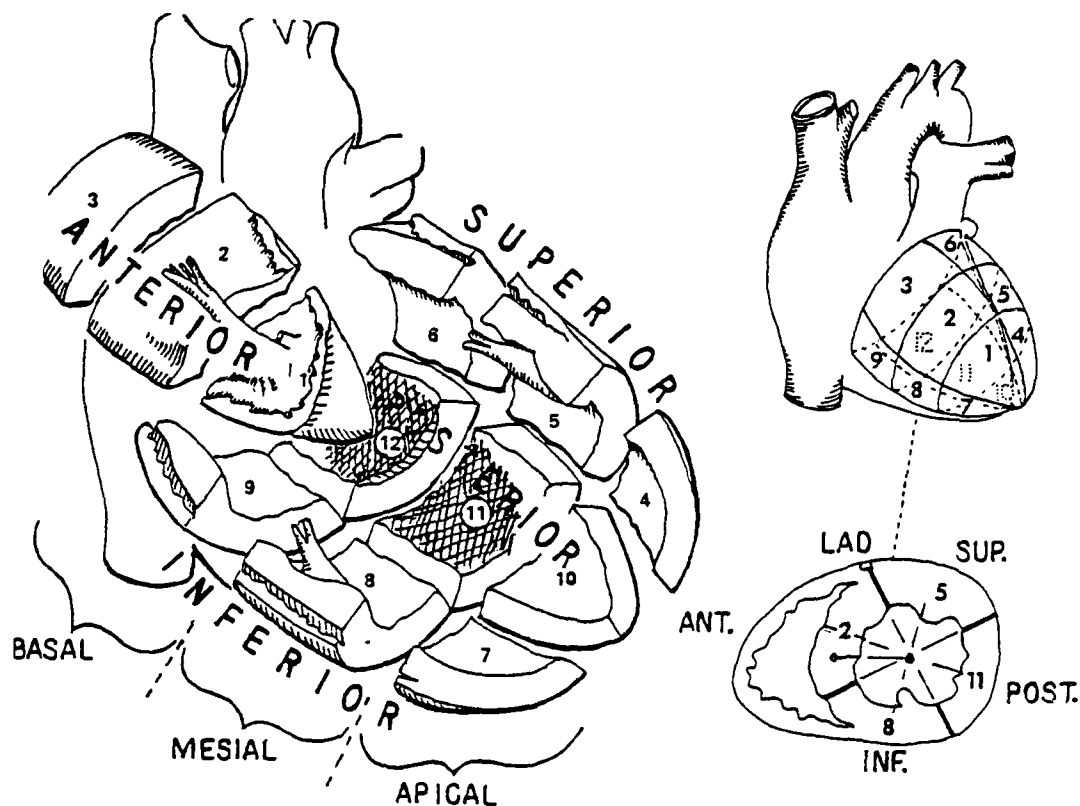


Figure 18. A typical numerical experiment evaluating the effect of local sub-endocardial ischemia in the region of the distal circumflex coronary artery (segment 12) and the marginal circumflex (segment 11) is shown in this diagram. The effects of either alone on the body surface potential distribution as compared to normal (ECG surface map changes) can be assessed. The effect of proximal circumflex coronary narrowing can be simulated by combining the effects of both of these two segments. Regional wall motion abnormalities in these same regions can be simulated by using appropriate transfer matrices from the Transfer Matrix Library that emulate dilatation and regional thinning in the local segment.

have been accomplished. To aid in the planning and priority setting of the development of the model, preliminary assessment of the effect of varying local intramural conduction velocities will be done late in the 1st year of this development effort.

#### Combined Effects of Wall Motion Abnormalities and Ischemia

When the studies described above have been completed, including simulating large multi-segment areas of subendocardial ischemia, the next phase will be to combine location changes with regional ischemic changes. The plan is to change each variable systematically. We will first assess the role of regional thinning and dilatation with ischemia, which has been shown to be



one of the earliest changes. We will then compare what this change does to the ECG surface map with that produced by action potential changes in sub-endocardial regions, as separate effects and as combined effects (for small, medium, large, and very large areas of regional ischemia). Most of these systematic studies done by varying generator locations will depend on having appropriate sets of transfer impedances in the library. These will take time to accumulate. To make the systematic modifications in the heart geometry files, and the action potential distribution files in an efficient manner will require that the input data modification programs be available. These studies will therefore be done in the main after the development of the computer routines to modify the input data to each of the stages of the program. This is Subtask 2B, page 51 (discussed in more detail on pages 61-69) and is projected to be done in the 2nd year of this development effort.

#### Combined Infarction, Injury, and Ischemia

With the comprehensive set of programs for easily modifying the input data files we will also be in a position to systematically vary the heart geometry to simulate all sizes of infarction in any distribution from sub-endocardium to intramural, to subepicardial and transmural in any region of the heart including the right ventricle, with or without hypertrophy and/or dilatation. All variations of subendocardial, intramural, subepicardial, and transmural injury and ischemia in the various coronary artery distributions can be simulated by using the Action Potential Distribution Modification Program. Changes that occur in any or all of the above in the presence of interventricular conduction defects can be simulated with the Purkinje Modification Program. With time, when a comprehensive library of Torso Impedance Files is generated, the simulation can be made to deal with all combinations of body builds, internal changes in resistivity as might occur with +G loading, exercise, and in chronic emphysema.

### ENGINEERING CONSIDERATIONS: PORTABLE MULTILEAD DIGITAL ECG CART

#### Present Major Commercial Vendors

Both vendor representatives, Steve Koerper (and now Francis Charbonnier) for Hewlett Packard, and Timothy Mickelsen for Marquette Electronics indicate a continued interest by their companies in maintaining close contact with the development of any new ECG Cart System that might result from the current effort. Both have indicated that they would give serious consideration to a request for bid on such a system when and if such were to come from the Air Force and the Department of Defense. The current Case II Exercise System by Marquette is upgradable now to 18 leads sampled at 4 kHz by a simple card insert. Up to 32 leads in a portable cart system can be accomplished with only modest engineering effort. The current Hewlett Packard system is a serial 3 channel system, and can take any number of leads in sets of 3 by developing a switching box for the lead array chosen. The ECG R & D section of the company will soon be headed up by Francis Charbonnier, who attended the final peer review session at USAFSAM. He indicates that the company will consider carefully the potential marketability of a larger simultaneous

multi-lead system as this effort progresses. Both vendors have extensive service networks. The specific needs of the USAF for ECG cart service in the field will need to be looked at as this investigation progresses.

#### EDL Laboratories

Roland Wyatt, who worked for years on the engineering aspects of the University of Utah Cardiology Sections multilead mapping system, has recently moved to the Endotech Development Laboratory at the Research Park of the University of Utah and is marketing a 32-channel ECG recording system. Versions of the system can be fabricated in modules of 32-256 channels. A 192-channel sample and hold version with a 1 kHz sampling rate is currently being fabricated. Wyatt indicates that his company would be quite responsive and anxious to bid on a portable ECG cart system when and if the investigative effort of this project identified the software and hardware engineering requirements of such a system. The EDL company has a working relationship for the servicing and repair of its solid state devices with Stortz and Wolf who maintain a worldwide 24 hr solid state and video service. Wyatt states that they have made considerable use of this service and consider it quite responsive and adequate to the customer needs. He considers the servicing of a multilead ECG portable cart exercise system to be of similar complexity to their existing devices, and believes the servicing of the proposed system to pose no special problems.

#### University-Affiliated Multilead ECG Systems Development

Robert Guardo of the Biomedical Engineering Department of the University of Montreal has developed a highly buffered system in multiples of 64 channels that can be selected for frequencies from DC at the low end to 4 kHz at the high end of the spectrum. His section has produced a limited number of these units for other investigators, but is not planning to go into a high level production mode. They would be interested in a development relationship with one of the commercial vendors, however, in the event that a specific need for a large number of portable carts evolves from the present USAFSAM/Rancho-USC modelling project. The University of Utah/Lux mapping system currently undergoing evaluation in the resting subject prior to coronary angiography at the USAFSAM is also adaptable to exercise mapping. Neither this system nor the University of Montreal one currently contains software logic for interpretation of the records, and this might be the major mutual benefit of either of these groups developing a collaborative arrangement with industry.

APPENDIX

ECG FORWARD MODEL TREATISE  
PHYSIOLOGIC RESEARCH AND  
MATHEMATICAL THEORY

J.C. SOLOMON

and

R.H. SELVESTER

## TABLE OF CONTENTS

	<u>page</u>
INTRODUCTION . . . . .	79
DESCRIPTION . . . . .	79
BASIC PHYSIOLOGICAL DEVELOPMENT . . . . .	80
Activation Sequence . . . . .	80
Experimental Observations . . . . .	81
Mathematical Analysis . . . . .	86
Example Analysis . . . . .	87
Animal Model and Data Collection . . . . .	90
WAVE PROPAGATION MODEL . . . . .	98
Heart Geometry . . . . .	98
Propagation Model . . . . .	98
Computer Program . . . . .	101
Program Testing . . . . .	103
Normal Activation . . . . .	105
EQUIVALENT CARDIAC GENERATOR . . . . .	106
Discussion . . . . .	106
Bipolar Model . . . . .	110
Action Potential Profile . . . . .	114
TRANSFER IMPEDANCES . . . . .	116
Boundary Value Problem . . . . .	116
Gelernter-Swihart Method . . . . .	118
Gelernter-Swihart Algorithm . . . . .	119
Transfer Impedances for QRS and T Wave Simulation . . . . .	121
ECG Lead Systems . . . . .	122
REFERENCES . . . . .	126

## INTRODUCTION

The forward model in electrocardiography, presented in this report, is a mathematical-physical description of the genesis of the electrocardiogram transformed into algorithms and coded into a computer program capable of simulating a voltage distribution on the chest produced by electrical activity in the heart. Basic laws in physics yield algorithms for determining how the chest voltages are related to the underlying electrical events in the heart. The computer program is the mechanism for expressing the algorithms; executing the program applies the algorithms to specific input data. Electrical events in the heart and the influence of the inhomogeneous volume conductor are represented as numbers and symbols in the computer program. When the program is executed on this input data, the numbers and symbols are processed in a manner specified by the basic laws of physics, as expressed by the algorithms. Such a computer program allows the genesis of the electrocardiogram to be deduced from basic principles.

Simulating the electrocardiogram with a computer program is similar to performing a controlled experiment; input conditions are specified to the program that correspond to the desired experimental subject and the program computes the resulting ECG. Unlike an actual experiment, where the control conditions are difficult or impossible to establish, the numbers and symbols in the program are not restricted by experimental procedures. Instead the computer program permits any input conditions that are consistent with the algorithms and program design. A forward model for simulating the ECG of humans extends the cardiologist's understanding of how the voltage distribution on the chest is related to normal and abnormal electrical activity in the heart as well as the influence of complicated torso volume conductors. Simulation by a computer may be the only method available to predict complicated ECGs, develop hypotheses about their origin, and establish diagnostic criteria, especially in those cases where the abnormal processes cannot be identified apriori because of insufficient information on how they are manifested in the ECG. Probably the most useful aspect of the forward simulation program is in its ability to generate hypotheses, in the form of ECGs, about such abnormal processes that can subsequently be tested on a human population.

## DESCRIPTION

Ohm's law for current conduction in an extended medium is an uncomplicated way to perceive the heart current source imbedded in the inhomogeneous thorax and the forward model. Stated as a matrix equation, a concise way to represent a large system of equations, Ohm's law becomes:

$$V = A \times D \quad (A-1)$$

where  $V$  is the matrix of body surface voltage distributions,  $A$  is a matrix of impedances for the inhomogeneous volume conductor (commonly known as transfer coefficients), and  $D$  is a matrix of current sources within the heart. ECGs are contained as elements in  $V$ , whereas the elements of  $A$  account for the effects of right and left lung fields, blood masses, and the torso-air interface. Elements of  $D$  correspond to the currents developed during depolarization and repolarization of myocardial cells. Algorithms in the

simulation programs contain numbers and symbols which yield the elements of these matrices when executed. The forward model programs separate naturally into three groups: the first group of programs compute the elements of D, secondly, a group of programs to compute the elements of A, and third a group to combine A and D to yield the body surface voltages V. Computing the elements of D is unrelated to the solution of the boundary value problem to obtain A. The only restrictions on D is that of a current source obeying the conservation of current law with a specified location. Part 1 below discusses the theory and observations about D leading to the algorithms embodied in the forward model. Part 2 discusses the theory and approximate solution to the inhomogeneous boundary value problem in electrocardiography. Part 3 brings together the solutions for A and D in a manner useful to the cardiologist, i.e., in the form of conventional 12 lead ECG, VCGs, body surface maps, and graphic displays of ventricular activation.

Programs for computing the elements of D are written mostly in Fortran with a few assembly language subroutines linked through Fortran calls. These programs require a considerable amount of RAM memory to hold the heart geometry, thereby avoiding an I/O bound leading to excessive CPU overhead. Example: a normal-adult, male human heart requires 125K bytes of storage added to a program of 130K bytes. All of the programs for the boundary value solution are written in Fortran. These programs fit easily into a 64K byte partition. Since the transfer impedances are an iterative solution to a set of 2500 simultaneous equations, the programs are computationally intensive. Depending on the volume conductor specifications and stopping criteria, a set of solutions corresponding to various current source locations will require many hours of CPU time.

## BASIC PHYSIOLOGICAL DEVELOPMENT

### Activation Sequence

One of the major factors influencing the potential distribution on the torso surface is the myocardial activation sequence. Genesis of QRS can be inferred directly from detailed activation maps reconstructed from measurements taken with multi-point intramyocardial bipolar electrodes. Discussions of the many temporal and spatial aspects of the activation sequence in the dog and human can be found in the reports of Scher and Young (A-1) and Durrer (A-2). It is clear that much of what is seen in surface ECGs and VCGs is directly proportional to the area, direction, and timing of the activation front.

Experimental evidence for the existence of the spread of activation in the human heart is documented by studies of epicardial and intramural excitation. Detailed information about human epicardial excitation was obtained from two sources: revived normal hearts and isochronous time relations during surgery. Small multi-point intramural electrodes were used to explore the excitation process from the endocardium to the epicardium. These studies indicate minimal intramural Purkinje fiber penetration into the myocardium.

Numerous intramural and epicardial electrogram recording methods have been developed and the electrical activity analyzed in a manner suitable for

mathematical modeling, especially the methods of Vander Ark and Reynolds (A-3) that observe the excitation front as uniform and closed at a macroscopic level of observation. Micro-electrode recordings, both in vitro and in vivo at the epicardium, reveal information on cellular potentials and nonuniform phase velocity. However, no unifying derivation exists for expressing the macroscopic current-voltage relationships in terms of micro-electrode phenomena. Looked at from the perspective of a forward ECG simulation, only the macroscopic characterization of the electrical events within the heart is useful. It would not be an efficient use of computer resources to include detailed information on the electrical activity that is not manifested in the torso-surface potential distribution. The objective of the forward ECG model is to produce an accurate approximation to the biophysical process rather than realism through inclusion of minutiae. Therefore, in vivo macroscopic observations of the electrical activity in the heart must be recorded at a level commensurate with the resolution of the simulation. It is our choice to take a spatial resolution of 1 mm for the intramural-epicardial recordings and the myocardial geometry in the simulation program. Given that the most useful recording methods will be those employing bipolar electrodes having a separation of 1 mm, a series of experiments were performed on baboons to characterize the electrical events in the heart and used as design input for the forward model.

Activation sequence mapping with bipolar electrodes is a procedure that records the passing of electrical excitation (depolarization) between the bipolar electrodes. Measuring time at which the electrical activity passes over the electrodes and combining it with the electrode's position in the heart defines the propagation of the depolarization within the myocardium. It is the observed propagation within the myocardium that serves as a basis for the design of the wave propagation model to simulate QRS excitation. Because the design and validation of a propagation model require accurate and extensive mapping of intramural and epicardial activation sequences, it became necessary to design and build reliable and efficient electrode arrays capable of rapid and accurate mapping of the entire heart. Two types of electrode arrays were fabricated: a 13-point intramural needle and a 24-point epicardial array. The geometrical arrangement of the bipolar electrodes was chosen to accommodate the equations used to analyze the recordings. Figure A-1 contains photographs of the two types of arrays: top panel is the intramural array and the lower panel is the epicardial clock array.

### Experimental Observations

Intramural multipoint electrodes were designed to insure a strong and reliable intramural bipolar needle electrode configuration; a 20-gauge stainless steel tube was used as a cylindrical support for the wire electrodes. This 20-gauge tube had an .008-inch slot cut the length of the tube which was approximately 3 cm long. Opposite the slot in the tubing, 13 holes were drilled through the wall of the tubing. Each hole was .008 inch in diameter and spaced at 1-mm increments. Stainless steel wire (304 type) having a diameter of .005 inches and coated with Teflon to a diameter of .007 inches, was threaded into the holes drilled through the tubing. The needle assembly is sharpened and coated with epoxy compound. The top panel of Figure A-1 is an enlarged view of a complete needle electrode.

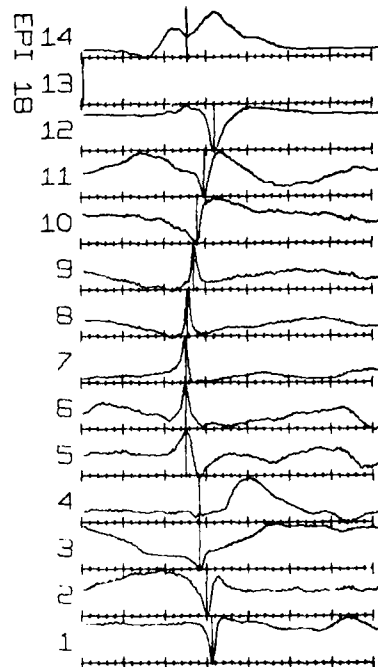
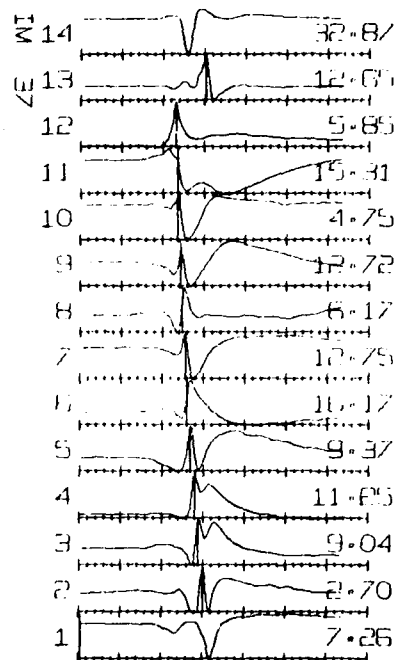
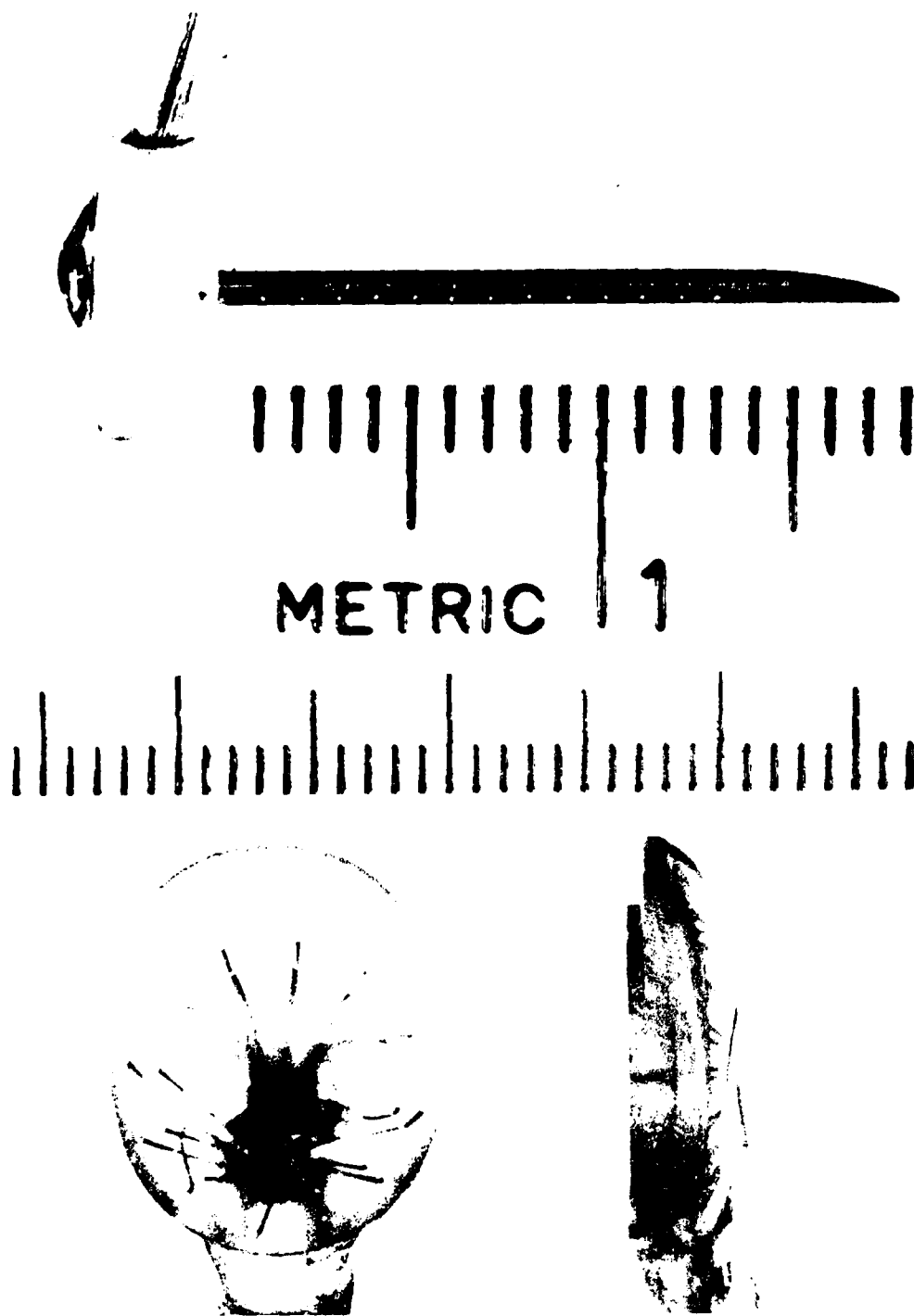


Figure A-1. (Above) Intramural bipolar needle electrode.  
(Below) Clock electrode.



Myocardial activation sequences were reconstructed from the time of occurrence of the peak voltage occurring between the adjacent (1 mm) electrodes and the location of the needle in the myocardium. Activation sequence data consists of 50 sites on the heart surface where the 13-point intramural needles are inserted. A long intramural needle (20 cm) was used to map the septal regions of the heart and to obtain a limited amount of intramural activation data prior to opening the animal's chest by percutaneously advancing the long needle electrode into the myocardium.

The clock electrode consists of 12 bipolar electrodes located around the circumference of a 1-cm-diameter circle. Figure A-2 indicates the 12 bipolar configuration and the labeling convention used to designate the orientation of the array and position of each bipolar pair. Each recording pair consists of .2-mm-diameter, Teflon-coated type 304 stainless steel wire. The exposed ends of the wires are separated a distance of 1 mm symmetrically across the face of a 1-cm-diameter circle. A pair of wires are positioned every 30 degrees around the circle. Epoxy is used to encase the wires in place and support a handle made of a soft metal tube such as copper or aluminum. The 24 wires are placed inside the tube for protection. A typical clock electrode designed for free-hand epicardial mapping is shown in the bottom panel of Figure A-1. A 12 o'clock position is marked on the epoxy support to indicate the orientation of the array. Electrode pairs are numbered as the hours on a clock face, looking down onto the array in its normal resting position on the epicardial surface, as depicted in Figure A-2.

A convention was selected which assigns the positive or upright voltage deflection to activation propagating outward along a radius from the center of the circle containing the bipolar electrodes. Electronic amplifiers measure the voltage at the outside electrode wire with respect to the inside wire.

Figure A-3 is a recording of the electrograms generated across the face of the clock electrode on the epicardial surface of a normal baboon heart. This recording is from a site on the left ventricle near the apex. For the purpose of describing the basis underlying the propagation model of cardiac activation, the baboon is presented as a representative application rather than a study of the activation sequence in the baboon.

In addition to the 12 bipolar recordings, two reference signals were recorded from sites selected on the free wall of the right ventricle near the pulmonary outflow tract. Some form of reference signal is required to time-align the electrograms recorded from various sites on the epicardial surface. Various reference recording sites were tested, such as torso surface ECG, intramural bipolar and intramural unipolar leads. Our experience shows that unipolar and bipolar leads placed at the outflow tract of the right ventricle provided the most stable and trouble-free sites for recording reference electrograms. This region of the heart produced repeatable complexes while the physical position of the heart was altered slightly during the mapping process. In addition, this location minimized the accidental dislocation of the reference electrodes. Separation on the bipolar reference electrode was held at 1 mm.

At each bipolar lead of the clock electrode the arrival time of the activation front at the center of the bipolar pair was chosen at the peak

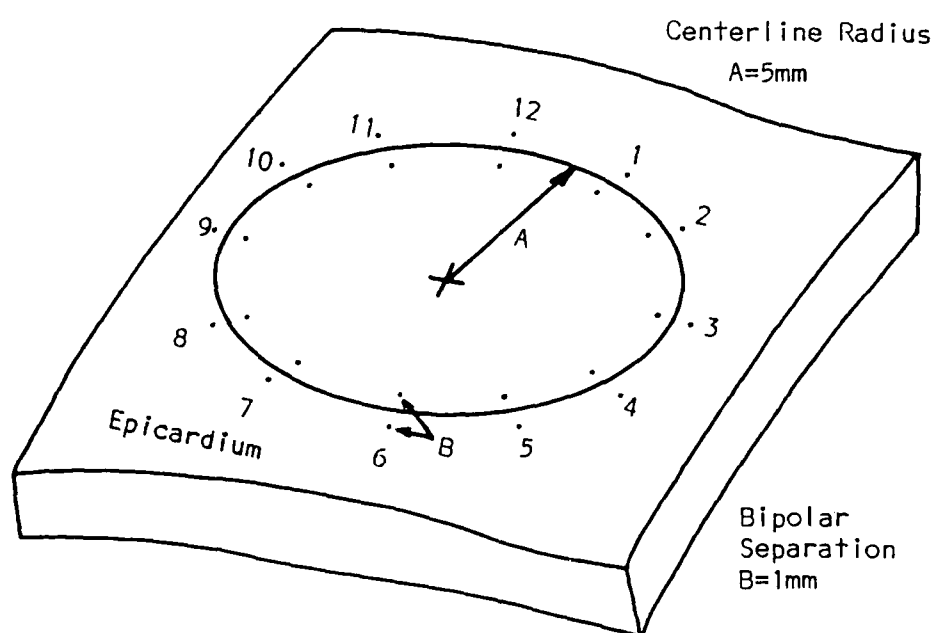


Figure A-2. Twelve bipolar electrode configuration of the clock array as positioned on the epicardium.

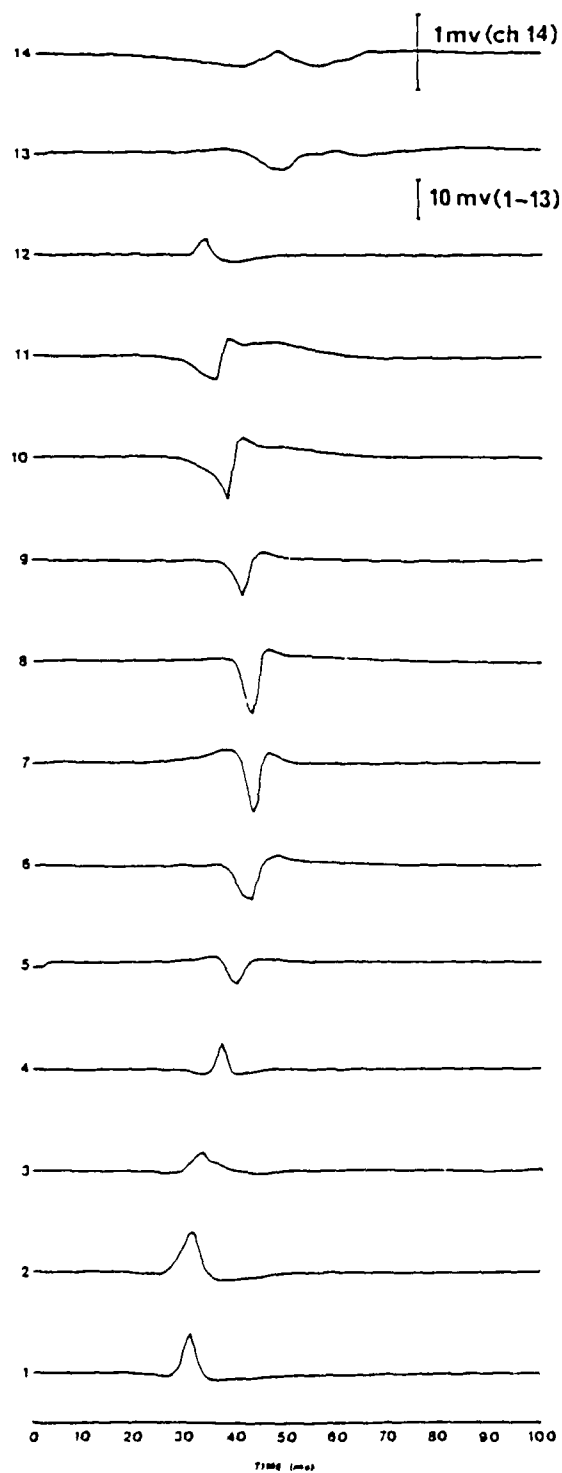


Figure A-3. Recording of the electrograms generated across the face of the clock electrode.

value of the electrogram. For each of the 12 pairs, there is a time  $t_n$ , where  $n = 1, 2, \dots, 12$  corresponding to the arrival of the activation front at the electrode pair. This time  $t_n$  is calculated from a characteristic point on either the unipolar or bipolar reference electrogram recorded from the right ventricular epicardium and referred to the onset of QRS. A characteristic point on a reference electrogram is defined as a distinct peak, notch, or other easily identified mark that remains unchanged over the entire duration required to collect electrograms everywhere on the epicardium. The time assigned to the characteristic point on the reference electrogram is measured from the onset of QRS, usually determined from the onset of the unipolar epicardial lead or from the earliest activation recorded from intramural needle electrodes inserted into the septum. The time at which the peak potential occurs for electrograms 1 through 12 (Figure A-3) is measured with respect to a characteristic point on the reference lead and is assigned a negative sign if it occurs before the characteristic point and a positive sign if it occurs after. This time increment is added algebraically to the characteristic time yielding values of  $t_n$  measured from QRS onset.

### Mathematical Analysis

The principal advantage gained by arranging the electrogram recording wires into a geometric array is that a mathematical analysis of the electrogram timing will yield indirect information on the wavefront properties. Information about the epicardial breakthrough time of ventricular excitation and the direction of propagation over the epicardium can be extracted from computations performed on 12 electrograms. Local knowledge of the time and direction of the excitatory process on the epicardium is calculated for each placement of the clock array. Roving the clock array over the entire epicardial surface, maintaining a constant reference electrogram, produces a global picture of the excitatory process from which the ventricular excitation can be inferred.

The relationship between the electrogram time and position around the clock can be expressed as a parametric equation over the surface of the clock array. A mathematical procedure is invoked to determine the best estimate of the parameters. Estimated values of the parameters are then used in the original equation to calculate the residuals to determine the validity of a single wavefront model having uniform velocity. When the residual error is small compared to the experimental sources of error, the parametric approximation provides a convincing estimate of the epicardial breakthrough time and direction of movement.

Epicardial mapping is essentially constructed from the position of the clock electrode and the times  $t_n$  contained in Figure A-3. On some portions of the epicardial surface, such as where two fronts are approaching from different directions, the best way to construct the activation sequence is to draw isochronous lines over the clock surface. However, for the major portions of the epicardial surface where there is a single activation front, one would like to analyze the activation sequence in a manner that minimizes the influence of variability in the local times  $t_n$  at each electrode. The variability in the time  $t_n$  makes it difficult to construct a smooth epicardial activation sequence by interpolating for isochronous locations and connecting them with straight lines. The object in epicardial mapping is to obtain a

macroscopic estimate for modeling the activation over a finite region of the epicardium rather than activity which is localized to a point on the surface. For this reason, we chose to analyze the times,  $t_n$ , in a manner that utilizes an algorithm in which the parameters are estimated in a least squares sense. It is the average time and direction over the surface of the clock electrode that is being sought to construct the activation sequence.

If the ventricular activation front propagates with a uniform conduction velocity under the surface of the clock electrode array, then the times  $t_n$  will bear a sinusoidal relationship across the face of the clock electrode. A general equation for the time  $t_n$  is given in the following parametric form:

$$t_n = T \sin(\omega_n + \Phi) + B \quad (A-2)$$

where  $T$  is the peak time measured from the baseline time  $B$ .  $\omega_n$  is the angle or the electrode pair measured from the 12 o'clock position.  $\omega_n = 30^\circ \times n$ , where  $n = 1, 2, \dots, 12$ .  $\Phi$  is the azimuth or phase angle which defines the direction of motion across the clock surface. This angle  $\Phi$  is referenced to the 12 o'clock position.  $B$  is the baseline or mean time at the center of the clock electrode. Once the times  $t_n$  are recorded from the clock electrode, the parameters  $T$ ,  $\Phi$ , and  $B$  are estimated by non-linear least squares. Residuals are obtained from initial estimates of the parameters given by the equation:

$$r_i = t_n - T_i \sin(\omega_n + \Phi_i) - B_i \quad (A-3)$$

Improved values of the parameters  $T$ ,  $\Phi$ , and  $B$  are obtained from the data pairs  $(t_n, \omega_n)$ , and the initial estimates  $T_i$ ,  $\Phi_i$ ,  $B_i$ , by minimizing the residuals  $r_i$ . The improvements are accomplished by a differential correction technique based on least squares to minimize the values of  $r_i$ . This technique requires the initial estimates of the parameters to be sufficiently close to the actual values to insure rapid convergence. The differential-correction technique obtains updated estimates from a linear-Taylor series expansion of function (A-2) around the parameters  $T$ ,  $\Phi$ , and  $B$ .

### Example Analysis

As an example of the application, consider the electrogram recordings contained in Figure A-3. These recordings were taken from the left ventricular wall near the apex of a normal baboon heart. Each epicardial electrogram in Figure A-3 corresponds to a clock pair of recording electrodes. The number associated with each clock pair is listed in column one of Table A-1. Column 2 contains the corresponding time for which the electrogram attains a maximum voltage. This time is measured from QRS onset determined from the unipolar reference electrogram identified in Figure A-3 as channel 14. Arrival times at the clock array range from the earliest of 19 ms for pairs 7 and 8. This lapsed time of 12 ms across the 1 cm diameter of the array characterizes the phase relationship for the ventricular activation front intersecting the epicardial surface in the direction between 1:30 and 7:30 of the clock orientation. These raw time points, listed in column 2, appear as circles marking the vertical axis of the graph in Figure A-4.

TABLE A-1. SOLUTION OF EQUATION (A-2) FOR THE ESTIMATED ACTIVATION TIMES FROM A SET OF ELECTROGRAM TIMING  $t_n$ .

Column 1	2	3	4
Bipolar Electrogram	Electrogram Timing $t_n$ , ms	Estimated Activation Time, ms	Residual
1	19	19.2	-0.2
2	19	19.4	-0.4
3	21	21.2	-0.2
4	25	14.2	+0.8
5	28	27.3	+0.7
6	31	29.9	+1.1
7	31	31.3	-0.3
8	31	31.1	-0.1
9	29	29.3	-0.3
10	26	26.4	-0.4
11	24	23.2	+0.8
12	22	20.6	+1.4

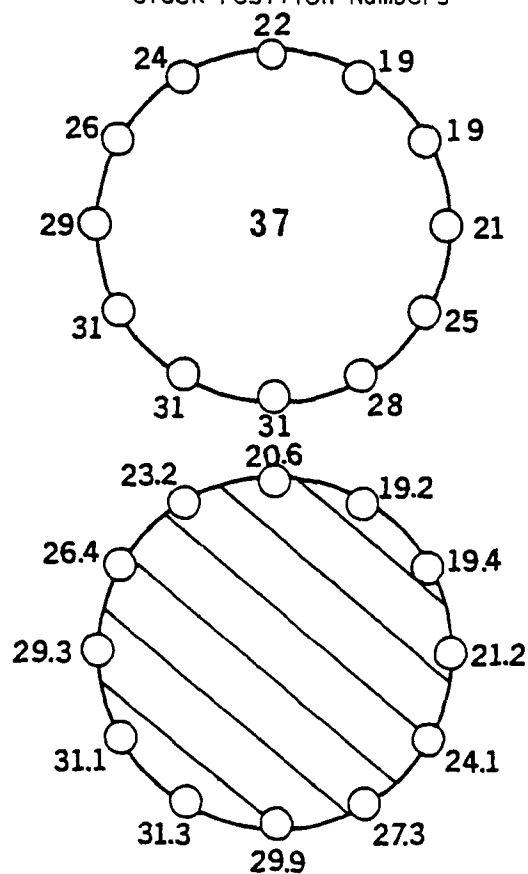
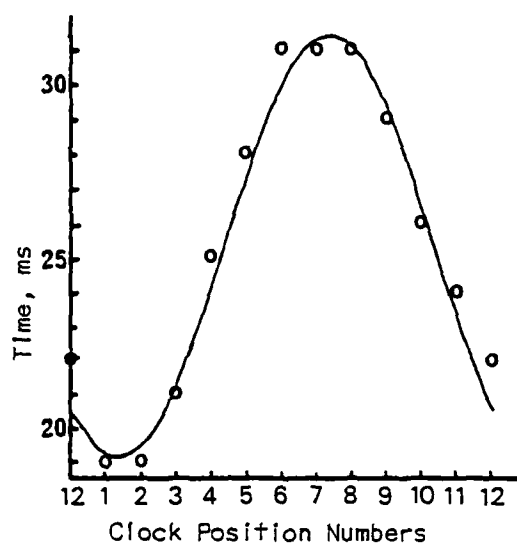


Figure A-4. Output data.

(Above) Activation front across the epicardial surface under the clock electrode.

(Below) Lower curve shows visually the agreement between the reconstructed curve and the original data.

Initial estimates  $T_i$ ,  $\phi_i$ , and  $B_i$  are calculated from the times  $t_n$  given in Table A-1.

$$B_i = 1/2 \sum_{n=1}^{12} t_n \quad ; \text{the average of all 12 values}$$

$T_i = 1/2 (t_{\max} - t_{\min})$  ; 1/2 the time between the earliest and latest times on the clock surface.

$\phi_i = 30^\circ \times n_{\max}$  ;  $n_{\max}$  is the number designating the electrode pair which has the latest time.

Figure A-4 contains two forms of the output data. The upper drawing indicates the activation front across the epicardial surface under the clock electrode. The direction is given by the convergent value. The 2 ms isochronous lines are calculated as  $T_f \sin(\omega + \phi_f) + B_f$ , where the subscript f refers to the final convergent values. The lower curve shows visually the agreement between the reconstructed curve and the original data.

Following initialization with the above values, the parameter estimation procedure produced convergent values of:

$$B_f = 25.2 \text{ msec}$$

$$T_f = 6.1 \text{ msec}$$

$$\phi_f = 222 \text{ degrees}$$

Inserting these convergent values of  $B_f$ ,  $T_f$ , and  $\phi_f$  into equation (A-2) produced the fitted or smoothed values of  $t_n$  listed in column 3 of Table A-1. The residuals for the fitting process are listed in column 4 for each electrode arrival time.

A standard deviation of  $S_y = .7 \text{ msec}$  is obtained from the list of residuals. This value of  $S_y$  is small compared to the time required for transit across the electrode array, i.e., 12.1 msec for transit via the fitted values.

A relative error of 6% (.7/12.1) is considered small, when the proposed use for the data is in modeling efforts. Comparing  $S_y$  to the transit time is a reasonable measure of whether the activation is a single wavefront of uniform velocity.

From the analysis of these 12 electrograms it can be concluded that the epicardial surface at the point where this array was positioned, is a single wavefront centered about  $B_f = 25.2 \text{ msec}$  from QRS onset and is propagating with a phase angle of  $\phi_f = 222 \text{ degrees}$  relative to 12 o'clock and with nearly uniform velocity.

#### Animal Model and Data Collection

Intramural activation in baboons was selected as a basis for examining the use of the intramural and clock electrodes. These animals were normal



adult males of the papio anubus subspecies and weighed 25/30 kg. Animals were anesthetized at 3/4% to 1% halothane during the open-chested recording period which lasted approximately 30 minutes.

Both the intramural needle and clock electrode array data were recorded for later comparison. During both recording sessions the right ventricular reference electrodes were recorded simultaneously with the corresponding clock or intramural needle. These references were obtained from unipolar and bipolar electrodes with a 1-mm separation secured to the right ventricular surface near the outflow tract of the right ventricle. The time of the peaks on the electrograms of both the clock and intramural waveforms was measured from the same peak on one of the reference electrodes. Two reference electrodes were used so there would be a back-up in case one of the reference electrodes was to become dislodged or altered during the course of the entire data collection process. It also provides protection against changes that might be orthogonal to a single electrode. The clock electrode electrograms were collected first from 52 epicardial sites. These sites were pre-selected and located on a pictorial view of the epicardial surface. Approximately 10 cardiac cycles were recorded from each site. The collection process advanced sequentially across the 52 epicardial sites in a continuous recording mode. Lapsed time for the entire epicardial data collection process was 6 minutes. As soon as the epicardial data collection was completed, the intramural collection started. The same 52 epicardial sites were sequentially mapped with the 12-point intramyocardial needle electrodes. An intramural needle electrode was impaled into the ventricle at the same location the epicardial clock had assumed previously. Several moments were allowed for the data to stabilize after the insertion of the intramural electrode before electrograms were recorded on magnetic tape. Electrograms from the septum were recorded from 5 sites with a 20-cm long intramural needle following the completion of the 52 epicardial sites.

#### Intramural sequence

A single cross-section of the intramural activation was chosen to demonstrate the clock array and compare it with the conventional intramural needle construction of the activation sequence. The complete activation sequence would be constructed by repeating the analysis for each cross-section of the heart. This particular cross section (Figure A-5) is perpendicular to a line from the apex to aorta and is at a level 3 cm above the apex. The activation sequence depicted in Figure A-5 was constructed from 12 ventricular and 2 septal insertion sites. Timing was with respect to the onset of QRS which was measured from the reference electrogram. Maximum amplitude of each intramural electrogram marked its position along the electrode and therefore its time relative to the reference electrogram.

#### Phase Velocity

Extrapolating an intramural activation sequence from the clock array requires the approximation of a uniform conduction velocity for the excitatory process within the myocardium. In the case of the baboon, there is no estimated value available for both open and closed chest. An estimated value was obtained by impaling the 20-cm long, intramural needle electrode

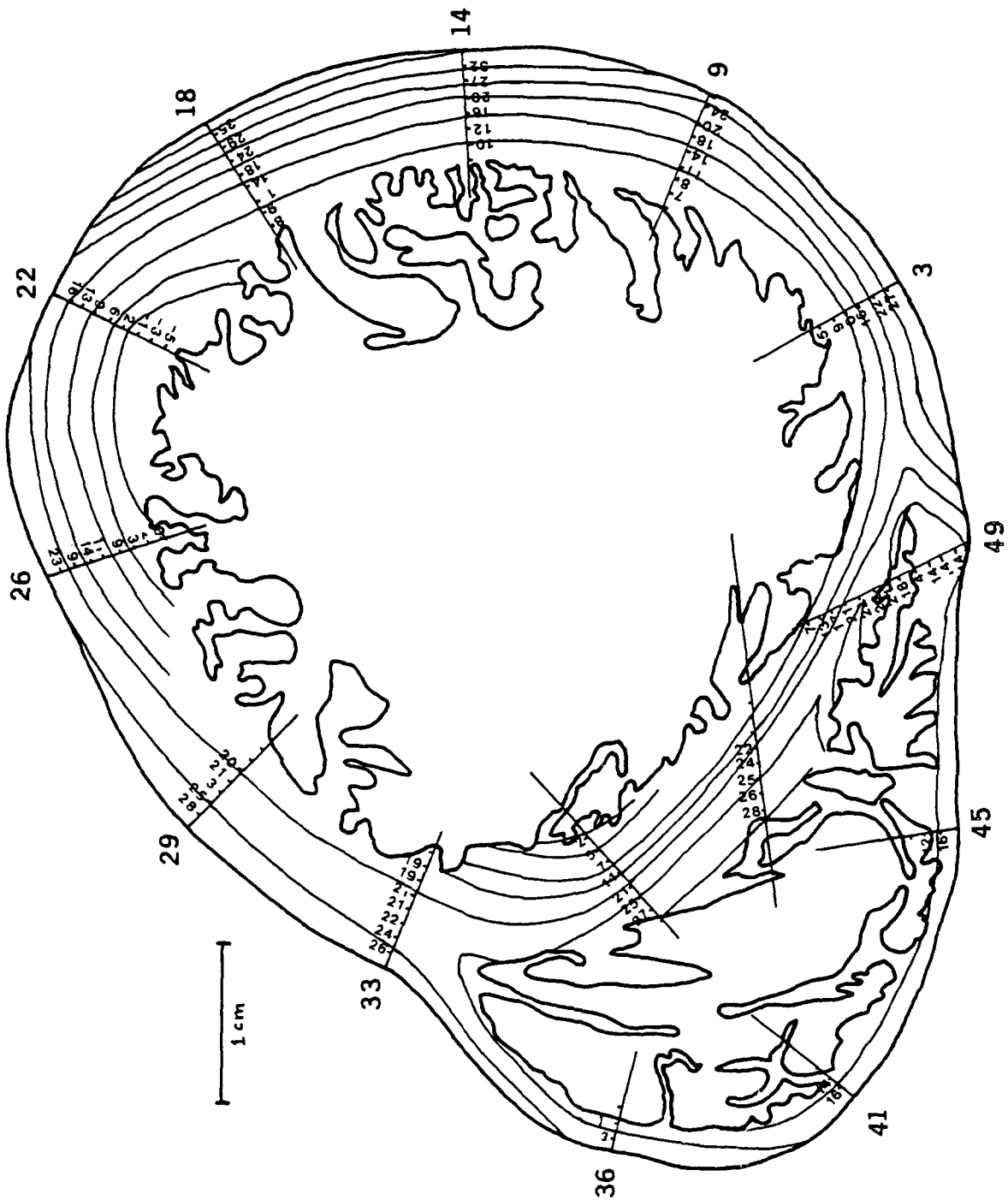


Figure A-5. Cross-section of the heart.

AD-A166 951

OPTIMAL ECG ELECTRODE SITES AND CRITERIA FOR DETECTION  
OF ASYMPTOMATIC CO. (U) UNIVERSITY OF SOUTHERN  
CALIFORNIA DOWNEY R H SELVESTER ET AL. DEC 85

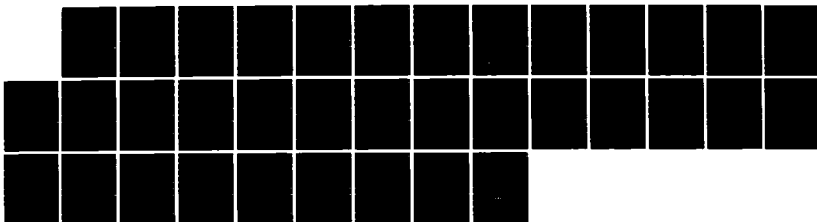
2/2

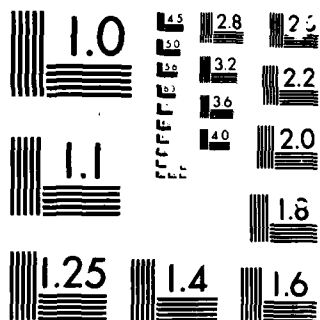
UNCLASSIFIED

F33615-83-D-0603

F/G 14/2

NL





MICROCOPY

CHART

percutaneously into the free wall of the left ventricle just prior to opening the chest. The electrograms were recorded from the intramural needle simultaneously with two conventional limb leads. As soon as the chest was opened, the entrance wound from the intramural needle was located and the needle electrode was re-inserted. Electrograms were recorded again, and the timing information extracted as shown in Figure A-6. Conformity between open and closed chested values of the slope of this line (phase velocity) is within the uncertainty of the measurements and hence no distinction can be made between the apparent differences in the data. Averaging the time data yields a phase velocity of 0.32 mm/ms. At this location in the free wall of the left ventricle, the angle of incidence of the propagating front was estimated from the clock array to be 8 degrees. This small angle of incidence indicates a phase velocity nearly equal to the conduction velocity at this ventricular location. In subsequent calculations involving the clock array a value of 0.32 mm/ms is taken as the conduction velocity within the myocardium.

### Extrapolated Sequence

Electrograms recorded with the clock array from the epicardial sites were analyzed numerically by the procedure just outlined. The 12 epicardial sites lying on the same cross-section of the heart illustrated in Figure A-5 for the intramural activation were used to extrapolate a sequence of activation from the clock electrode. This extrapolated sequence appears in Figure A-7 where the value of the uniform conduction velocity was taken as 0.32 mm/ms. Table A-2 lists the information calculated from the clock array which is needed to estimate the ventricular sequence, mean time at the center of the clock array, and the azimuth and polar angles depicted in Figure A-8. The intramural times, although not used in the extrapolation process, are listed for comparison with the mean epicardial clock times.

Projecting the conduction velocity onto the plane of the cross-section determines the phase velocity in this plane. When the cross-section is taken normal to the epicardial surface, the phase velocity calculation becomes  $V_{ph} = u / \cos \phi$ .

Using a time increment of 5 ms between isochronous lines, the displacement increments are calculated as  $dx = 5 u / \cos \phi$  for each electrode site. Figure A-7 depicts the activation at 5-ms increments and is to be compared with the intramural activation of Figure A-5.

Comparing of the mean clock times and the corresponding outer intramural needle times indicates a discrepancy in the two epicardial maps. The time uncertainty between these epicardial lines is not considered large (2-4 ms) and is related to the uncertainty in the location on the epicardium of the needle and clock array. When the polar angle is large, the uncertainty produced by a small displacement in the electrode position is large; i.e., where the propagation velocity across the epicardial surface is slow, the positioning of the electrode becomes crucial. The purpose for comparing these two sequences is to show the sequence determined from two independent methods of construction, one of which makes use of a modeling simplification,

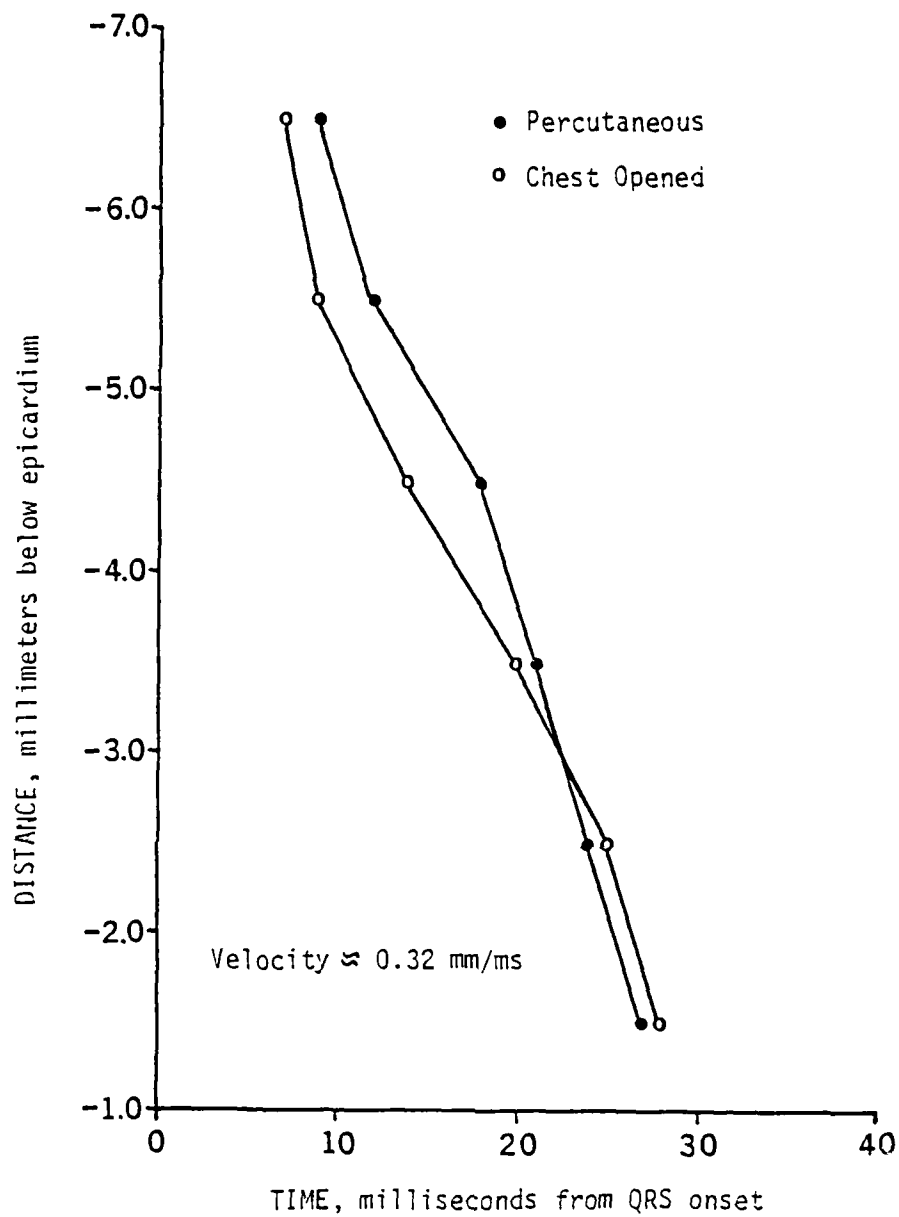


Figure A-6. Phase velocity of ventricular activation in a normal baboon.

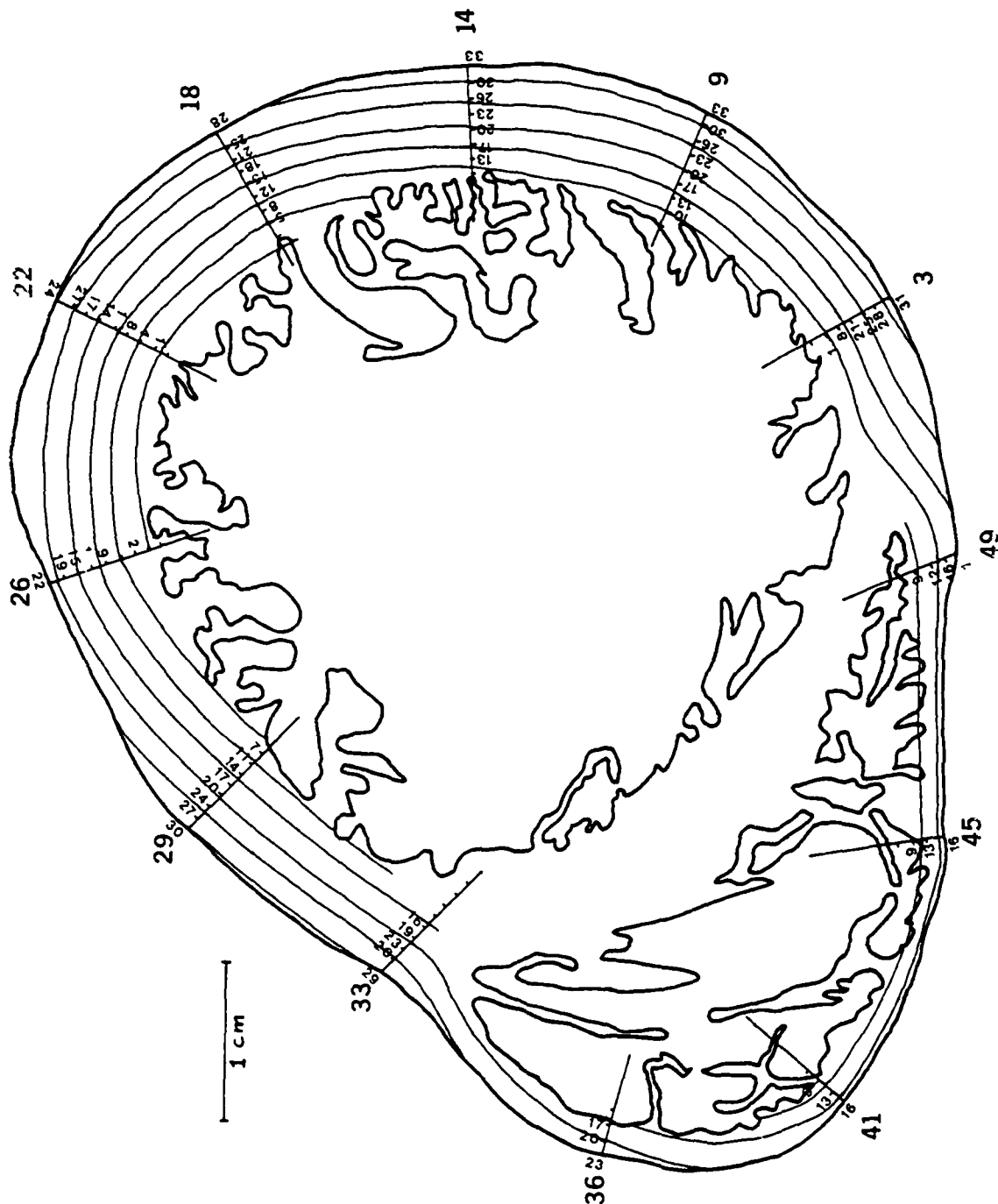


Figure A-7. Extrapolated sequence of activation from the clock electrode.

TABLE A-2. ACTIVATION SEQUENCE EXTRAPOLATED FROM 12 EPICARDIAL SITES USING THE CLOCK ELECTRODE ARRAY

N	B ms	$\theta$ deg	$\varphi$ deg	$U_{ph}$ mm/ms	$\Delta X$ mm	IM ms
3	31-32	8	13.5	.329	1.65	27-31
9	32-33	40	7.5	.323	1.62	24-27
14	33-34	56	7.4	.323	1.62	36-41
18	27-29	216	7.7	.323	1.62	35-39
22	23-24	262	10.3	.325	1.63	16-18
26	21-23	340	1.2	.320	1.60	23-26
29	29-30	79	13.2	.329	1.65	27-29
33	28-29	246	13.8	.330	1.65	26-28
36	23-24	291	17.0	.335	1.68	23-27
41	15-16	147	10.0	.325	1.63	16-18
45	15-17	343	7.5	.323	1.62	16-19
49	17-20	142	10.8	.326	1.63	13-15

N is the electrode site on the epicardium

$$U_{ph} = U / \cos \varphi$$

$$\Delta X = 5 \cdot U_{ph}$$

Columns B and IM are time ranges



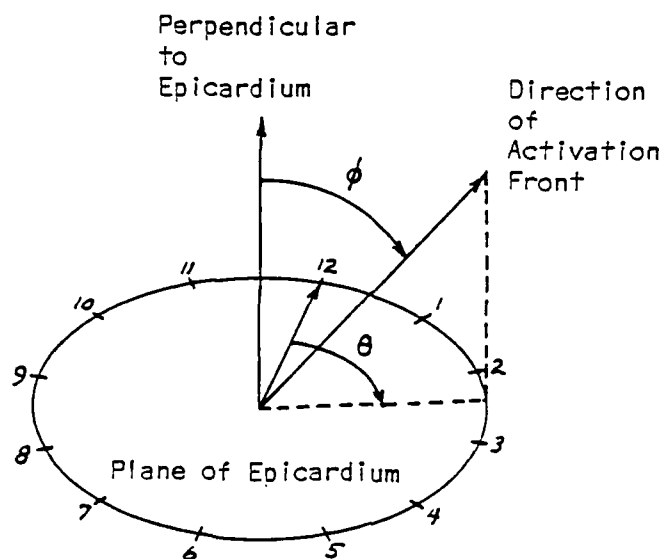


Figure A-8. Definitions of the polar ( $\phi$ ) and azimuth ( $\theta$ ) angles associated with the activation front at the epicardium.

namely uniform conduction velocity. On a macroscopic level of observation, events occurring in the myocardial activation sequence could be expected to manifest themselves in body surface ECGs. Modeling the ECGs of a normal baboon with a propagation program utilizing a uniform conduction velocity would not produce a significant difference in ECGs generated by considering microscopic variations in conduction velocity. The extrapolated ventricular sequence of Figure A-7 is sufficiently similar to the intramural needle method for a depth of 10 mm to be a useful approximation of the wavefront for a forward simulation of ECGs.

## WAVE PROPAGATION MODEL

### Heart Geometry

Since those electrical events that are simulated by the forward model are confined to the cardiac muscle, some consideration must be given to the shape of the myocardial mass. The human heart, specifically the right and left ventricles, is asymmetric in shape and therefore models such as spheres and ellipsoids are unsatisfactory representations for a rigorous simulation of cardiac electrical events. A necessary first step in putting together a forward model was to obtain an accurate human ventricular geometry, representative of normal adult males. Such a ventricular geometry was obtained from a 42-year-old, white, male, auto-accident victim.

Heart fixing and sectioning was performed by first filling the left, and then the right, ventricular cavities with warm formalin agar-agar at the respective normal mean diastolic volumes. The heart was suspended from the root in a square container of warm formalin agar-agar (see Figure A-9) with the A-V groove as near to the transverse as possible. The entire mass was allowed to cool and fix over night. When cooled to near 4°C, the block of solid gelatin containing the heart was placed in a rotary blade macrotome for cutting the heart breadloaf fashion at 2-mm intervals from apex to base (see Figure A-10). Total heart cross-sections were photographed.

Drawings with the estimated normal wall boundaries are made from the photographs of each 2-mm cross-section. A gross anatomical shape of the intact myocardium was constructed for use in simulating the cell-to-cell activation pathway. An on-line digitizing table was used to transform the anatomical shape into a suitable digital format. After digitization, the 2-mm cross-sections parallel to the A-V groove are interpolated to 1 mm and this becomes the anatomical shape and resolution of the ventricles incorporated into the forward model.

### Propagation Model

The propagation model is a computer program that simulates the myocardial activation sequence. This simulation includes the anatomical and physiological factors directly. Parameters such as intramural conduction velocity and rate of Purkinje activation are entered as first-order approximations. Resolution and accuracy of the simulation is sufficient to produce a representative sequence of activation for a particular set of input conditions, such as

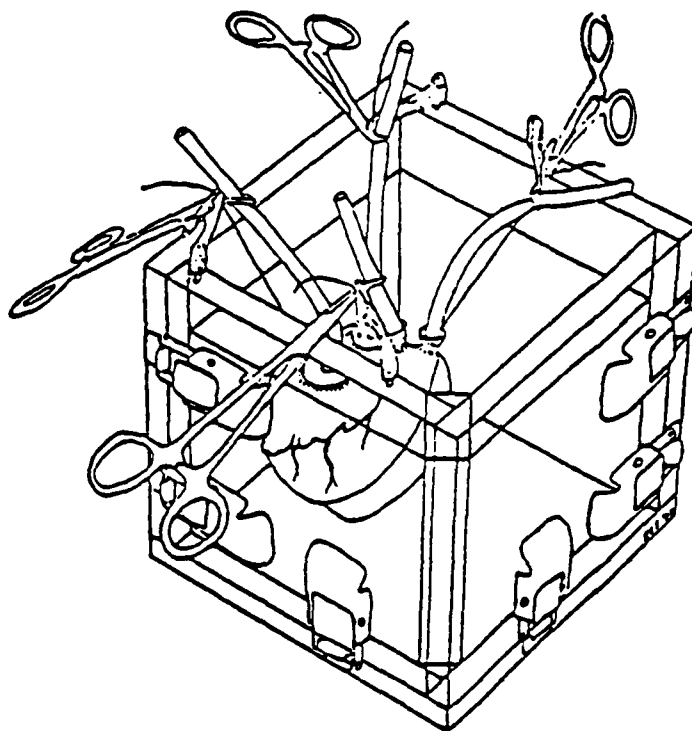


Figure A-9. Square container of warm formalin agar-agar.

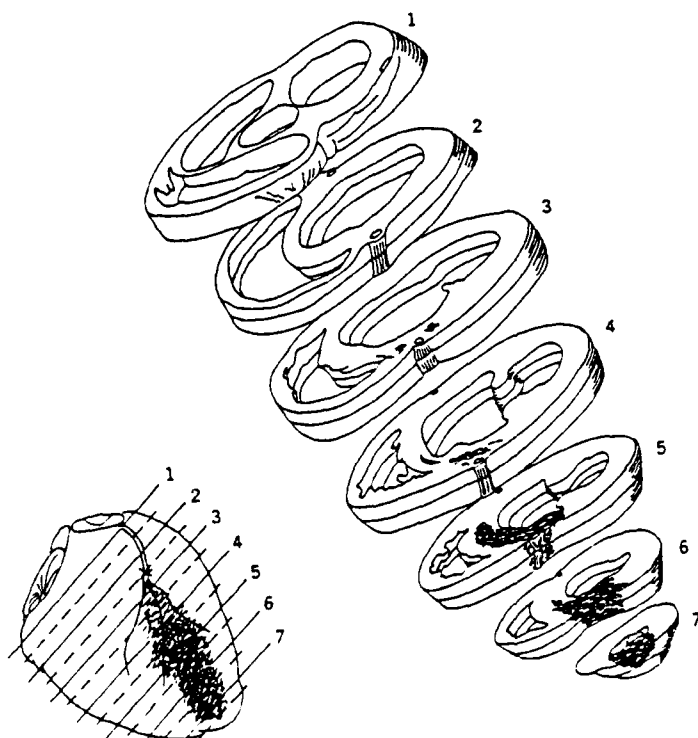
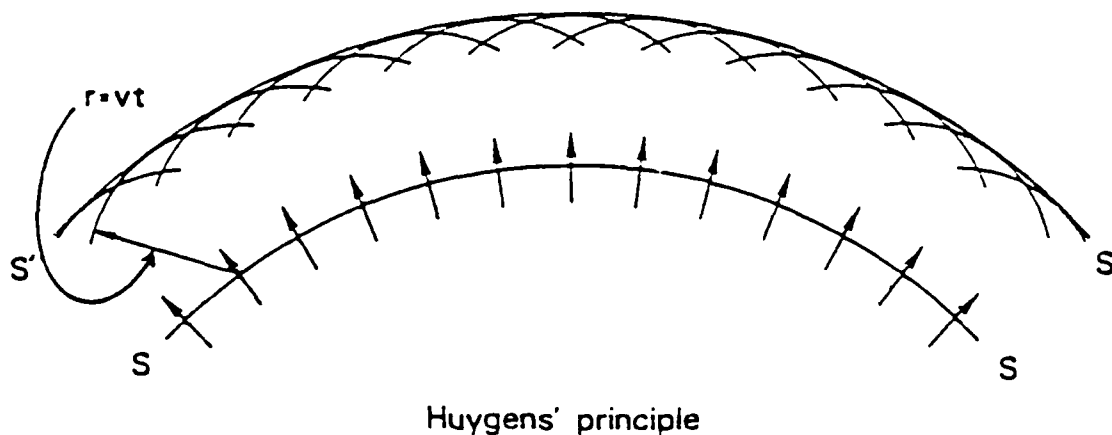


Figure A-10. Heart cross sections.

heart geometry and conduction mechanism. When employed as a mathematical model of the heart generator, the simulation yields data on the area, direction, and locations of points on the activation front at each instant of time.

Our approach to the problem of simulating the pathway of ventricular depolarization was to develop a numerical method analogous to Huygen's geometrical method of wavefront construction in a three-dimensional region. Anticipating a vast amount of data and calculations, the numerical method had to conform to the restrictions of present computer configurations, namely, memory capacity and cycle time. Briefly, Huygen's method consists of approximating the propagating wavefront by a large number of spherical wavelets (see Figure A-11).

The area of the wavefront is taken to be the tangent planes connecting the spherical wavelets. Wavelets for each successive time increment are determined by the product of the velocity of propagation and time increment. This distance is the radius of the spherical wavelets whose centers lie on the previous wavefront. To simulate a method such as this with a resolution that is physiologically meaningful requires a computer with a large memory capacity, since the location, area, and direction of some portion of each wavelet must be computed and preserved as future output data. The digital computer program which we are currently running is essentially a replication of Huygen's method with isotropic and homogeneous propagation velocity. The only limitation on the resolution of the simulation is imposed by the core capacity of the computer. This comes about by the method used to define the



Huygens' principle

Figure A-11. Spherical wavelets.

regions in which the wavefront propagates. We define these regions by their external boundary measurements on a three-dimensional Cartesian coordinate system. The present 65K RAM machine places an upper limit to the resolution of 1 mm on the coordinate system. With a 1-mm coordinate system the wavelets have a radius of 1/2 mm and the velocity-time increment is 1 mm. We confine the ventricular mass to lie within a cube which is 100 mm on a side. To resolve the pathway of ventricular excitation to within 1 mm requires the storage of 1 million coordinate locations in memory.

All of the intersections, of coordinate axes, contained within the external boundaries of an active region are represented by "on" bits in memory. Regions where no activation front is to be generated are represented by "off" bits. As the activation front propagates radially outward through the active region, the "on" bits are switched to the "off" condition until the completion of all activation.

Wavefront generation is initialized by specifying the coordinates of an arbitrary set of points. At any time during the generation of the wavefront, any number of new points can be introduced as additional sites from which wavefront is generated. The logic employed in generating the propagating front across a Cartesian coordinate system is based on finding the "on" bits enclosed on the surface of a sphere of radius 1, 2, or 3 mm. After each three time increments the process is started over using the last "on" bits as the center for the next three spheres. This scheme produces a maximum propagation time error along the diagonals to the principal planes of  $(2\sqrt{2})/3$  or less than 5%.

As the front moves out across the intersections of the coordinate system in a radial manner, the wavelets are constructed at each intersection for which the corresponding bit is in the "on" configuration. Rather than compute each tangent plane connecting each spherical wavelet, some portion of the surface area of each wavelet is used to approximate the tangent plane. This approximation is taken to be the projection of the wavelet's surface area onto one of the principal equatorial planes. The resolution of the wavefront is the minimum increment of area contributed by a single wavefront. This minimum increment is the surface area of one octant of a sphere having a radius of 1/2 mm that is  $\pi/8$  mm. From the unit vectors lying in the coordinate planes and located at the center of the wavelet, the resultant direction of the wavelet is computed by taking the vector sums of the unit vectors which terminate on the boundary of the wavelet. At the present time we have chosen as output the total area of the wavefront and the resultant direction of all wavelets. This output data is presented in the form of vector projections onto the principal planes of the coordinate system. Locations of the wavelets at each instant of time are preserved so that the pathway of the activation front can be displayed.

#### Computer Program

The program requires, including the system support routines, approximately 65,000 locations of memory. The execution time varies depending on the initial condition. Both Fortran IV and assembly language are used. A major part of the required memory is used to store the geometry of the object through which the wave will propagate. This array requires 130,000 bytes, and

is dimensioned 100, 100, 13. Using each bit to represent a location, we end up with a cube 100 locations on a side. All references to the geometry are as if there were 100, 100, 100 words in the array. Assuming the indexing to be in the order X, Y, Z, the location (bit) is reached by using the value of X and Y, and dividing Z by 8, if the quotient is zero, then the absolute location is the 8th bit of that byte. If the quotient is not zero, add one to get the byte and the remainder is the bit in that byte, or absolute location.

Initially, the data specifying the geometry is read in the form of cards or tape. All of the bits in the cube not specified by this geometry are turned off or set to zero. This establishes the criteria that the front may move only to those locations containing a one bit. When the bit is zero, movement to that location is prevented. Next comes the input to modify the geometry. Again this can be either on cards or tape. This input allows the reference geometry to remain fixed, while modifying it in the computer from run to run.

Starting points are specified immediately following the geometry section. These points specify the times and locations for starting and turning on points other than those turned on as the front moves through the geometry. At time zero, all points associated with that time are taken as the initial wavefront.

The first step in the simulation is to compute, considering each point on the front individually, each incremental area and direction. The six bounding points are looked at for each point on the front. If fewer than two are on, then there can be no area. If five or more are on, the incremental area and direction are computed and stored. If there are more than two points, but fewer than five, a check is made to insure that the points do not lie in a plane, allowing the front to degenerate to a line. Based on the results of this test, the total area bounded by the front and its direction is computed from the incremental values and the results stored.

The next step is to zero out the points on the old front and compute the coordinates of those points to represent the new front. The procedure here is to assume that each initial point is the center of a sphere. After the first iteration,  $T = 1$ , the sphere will have a radius of 1. All of the points that lie within a radius of 1 and that are "on" will be included as a point on the new front. The points selected are stored and zeroed out and a new point and sphere are considered. This procedure continues until all of the spheres have been scanned. All of the new points are returned to their "on" status. The same procedure is followed after the completion of the second iteration. After the third iteration, the same procedure for selection of the points on the new front is performed, except these new points are stored as initial points on new spheres of radius one for the next iteration. A radius of three is the maximum a sphere can have. This is also necessary, as a radius of three is a minimum to insure that no points are missed as the front moves and so that the front will move in a uniform manner. This, in essence, says that after every three iterations, the simulation is restarted with a new set of initial values.

The final step in the completion of each iteration is to check to see if any additional points are to be turned on. If there are, then the parameters

of these points are read from the input source and added to points considered part of the current front. The simulation program continues to iterate in the above manner until the number of points for the new front goes to zero.

#### Program Testing

Accuracy of the simulation technique was studied by comparison of the results obtained from propagation within an isotropic and homogeneous sphere. The analytical expression for the wavefront within the sphere can be derived readily when the initial point of activation is on the surface of the sphere. For a sphere of diameter 50 mm and the initial activation point on the surface, surface area of the wavefront of radius  $r$  enclosed by the sphere is given by the equation:

$$A = 2\pi r^2 [1 - r/50] \quad (A-4)$$

Figure A-12 shows a plot of equation (A-4) superimposed on an equatorial plane of the sphere. A smooth, unbroken curve is obtained from equation (A-4) and represents the area of the front of radius  $r$  corresponding to the smooth outer circle which defines the exterior of the sphere. The jagged lines bounding the sphere from the outside represent the approximation of the sphere to within 1 mm. This approximation is taken as the geometry for the simulation which also has its initial activation point on the exterior surface. As shown in Figure A-12, the broken line indicates the surface area of the wavefront calculated by the simulation program at integer values of the radius  $r$ .

Comparing the two curves during the early portion of the wavefront development, it is clear that the area computed from the simulation program is larger than the area computed from equation (A-4) for increasing values of  $r$ , partly because the approximation to the sphere is larger than the sphere itself. The error in this approximation is zero at the equatorial plane which is perpendicular to the direction of propagation. From equation (A-4) the value of the radius  $r$  for the wavefront as it passes through this equatorial plane is given as 33-1/3 mm. This occurs at the extremum for the area  $A$  given by equation (A-4). The true area of the wavefront enclosed by the sphere at  $r = 33-1/2$  mm is 2326 mm<sup>2</sup>, whereas the simulation program computes a value of 2238 mm<sup>2</sup>, or approximately 4% error.

Around a radius of 45 mm the disagreement is largest between equation (A-4) and the simulated wavefront area. The major portion of this error is due to the propagation time lag of 5% along the diagonals to the principal planes. This time lag causes the wavefront to be larger than it should be whenever the amount of active region is decreasing with increasing distance from the initial activation point. In general, this error is a property of the geometry and is indeterministic. In addition, some portion is contributed by the oversized approximation to the geometry of the sphere.

Since the diameter of the sphere is 50 mm and the time-velocity increment of the simulation is taken as 1 mm, there were 50 time points at which the wavefront area, position, and direction were specified. No time lag was present in the total propagation interval because the terminal portions to be

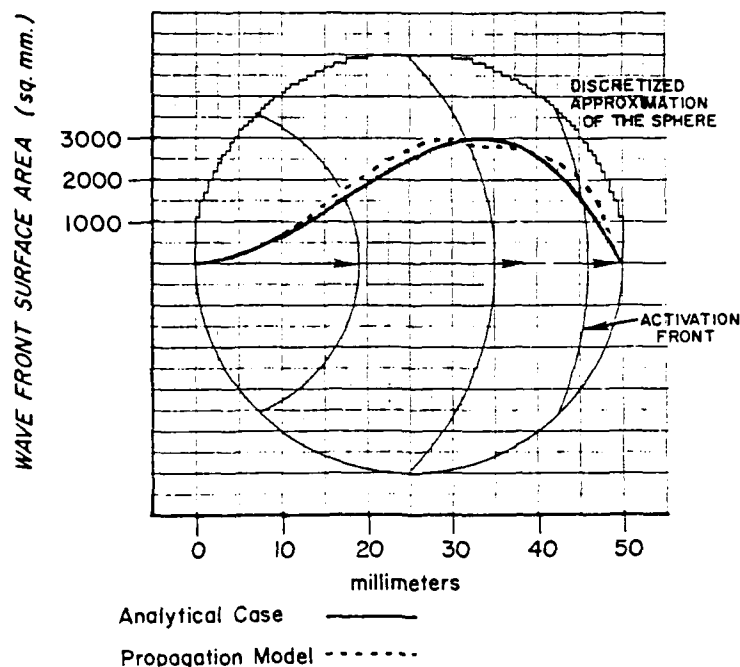


Figure A-12. Plot of equation (A-4) superimposed on an equatorial plane of the sphere.

activated did not lie along the diagonals of the Cartesian coordinate planes. Direction cosine numbers were computed for the resultant wavefront at each of the 50 points. Since the initial activation point was chosen to lie along one of the coordinate axes (viz., the Y axis), it was anticipated that the direction cosine number would be (0,1,0) respectively for the (X,Y,Z) axes. To within three significant figures, the direction cosine numbers were (0.000, 0.999, 0.000) for all 50 time points.

Another analytical case considered was the rectangular parallelepiped. This case was chosen so as to determine how well the simulated wavefront would approximate a plane wave. If the activation is initialized at the center of one face of the parallelepiped and allowed to propagate down, the front is very nearly a plane wave. The dimensions in this case were 11 mm x 50 mm for the rectangular parallelepiped. The activation simulation program required exactly 50 steps to reach the opposite end of the parallelepiped and the direction cosine numbers always remained (0.000, 0.000, 1.000). Near the end of the simulation the area of the wavefront was 113.04 mm which, when compared to the actual 121.00 mm, results in an error of approximately 5%.

Simulation of the Purkinje network is carried out separately from the activation in the ventricular muscle. The computer program is identical in both cases, but the initial points representing the conduction bundles and the points on the endocardial surface representing the Purkinje network are



simulated as a separate phase with a conduction velocity three times larger than the cell-to-cell conduction velocity in the ventricular wall. Results from the first phase of simulation are used as input data to drive the second program which generates the activation sequence throughout the entire cardiac geometry.

#### Normal Activation

The simulation begins by selecting the input parameters to phase one of the computer program. This first phase simulates the Purkinje propagation over the endocardial surface. Only the coordinate locations on the endocardium representing Purkinje are contained in this portion of the program. The effects of the conduction bundles are introduced by initiating Purkinje geometry at three endocardial areas in the left ventricle synchronously, followed by two endocardial areas of the right ventricle and right septal surface. Specifically, the input parameters are five arrays of coordinate points on the endocardial surface from which the propagating wavefront originates. To simulate a normal ventricular activation sequence in the human, we chose input parameters based on the experimental observations of Durrer et al. (A-4). With multi-point, bipolar electrodes, they mapped the time course and instantaneous distribution of the excitatory process on seven isolated human hearts having no history of cardiac disease. We initiated the Purkinje network of this simulation, using their observations that endocardial excitation starts at five sites, three of which are in the left ventricle: high superior paraseptal area, septal anterior, low inferior paraseptal area, and soon followed by the inner wall of the right ventricle and the septal surface of the right ventricle. We assumed the absence of any Purkinje penetration into the myocardium and set the Purkinje conduction velocity at 120 cm per second. The Purkinje network comprised all the points on the endocardial surface except for a region of the base of the left septal surface.

The digital computer program simulation of the activation of the Purkinje network during phase one above, produces a time sequence of points across the endocardial surface. This time sequence of points is used to initiate the simulation of the ventricular depolarization in phase two at the rate of 120 cm per second. Simultaneously the myocardial activation is propagating at a velocity of 40 cm a second isotropically, and homogeneously. This produces activation fronts which are essentially from endocardium to epicardium. The computer program then continues to execute the activation sequence according to Huygen's method until all the points of the cardiac geometry have been traversed.

During each iteration of the computer program, the wavefront propagates a distance of 1 mm, the grid size upon which the cardiac geometry is resolved. At the conclusion of each iteration, the program calculates the total wavefront area and the vectorial area, including the vector location of the numerous spherical wavelets with a radius 0.5 mm, which comprises the excitation wavefront. Selecting the ventricular wavefront velocity of 40 cm per second yields 2.5 ms of time between iterations and therefore isochronous wavefronts separated by 2.5 ms. A discussion of this particular effort to simulate normal human ventricular activation can be found in reference (A-5).

Two views of the activation sequence are presented in Figures A-13 and A-14, a horizontal and a vertical perspective. Isochronous time lines at 5 msec intervals represent the location of the activation front. Conduction velocity of 40 cm/sec yields a time increment of 2.5 msec for each 1-mm iteration step in the activation program. Therefore, the isochronous lines correspond to every other iteration of output data from the program.

Only the gross initializing effects of the right and left conduction bundles are reported in these results. Figures A-13 and A-14 show the gross effects of the bundles. The mid-left septal surface and right septal surface near the apex are activated over areas approximating the regions shown in the activation sequence map in humans reported by Durrer. Also, the effects of the 3 to 1 ratio between Purkinje and ventricular wall velocities can be seen as a rapid movement along the endocardial surface from apex to base and from septum to left free wall. Subendocardial Purkinje penetration was not included in this preliminary simulation.

Qualitatively at least, the simulated activation sequence map corresponds to observed activation in normal humans. General features such as the septal cancellation, movement from apex to base, from inside outward are visible in Figures A-13 and A-14.

## EQUIVALENT CARDIAC GENERATOR

### Discussion

Associated with the excitatory pathway in the ventricles is the myocardial cell membrane action potential. The currents responsible for the ECG on the torso surface arise from the EMFs generated by the cellular action potentials. Figure A-15 is an example of a myocardial action potential, obtained from Burgess. Figure A-16 is a plot of a mathematical model of the action potential (A-P) from a continuous function of time. Specific details of the mathematical model will be discussed later under the subject of equivalent generators. Equivalent cardiac generators depend on the shape of A-Ps and are important to the simulation studies conducted with the forward model. Varying the shape of the A-Ps within regions of the ventricles will result in body surface ECGs via the simulation that reflects these changes.

A convention exists in the literature for discussing the various phases of an action potential. As will become clear in the discussion of the A-P equation, the model parameters are directly related to the phases of the A-P, hence the definitions used in the forward model will be stated at this time. In reference to Figure A-16, the upstroke of the cardiac A-P is labeled phase 0 and is the sudden depolarization of the cell following a stimulus that raises the cell-membrane potential to threshold, by way of the gap junctions of the intercalated discs separating the interiors of adjacent cells. Phase 1 is a brief phase of rapid repolarization that occurs within a few milliseconds following depolarization. The prolonged duration of phase 2 is characterized by a plateau of nearly stabilized membrane potential. Phase 3 marks the final repolarization process of the cell membrane. Following repolarization, the cell remains in its phase 4 resting state. Equivalent

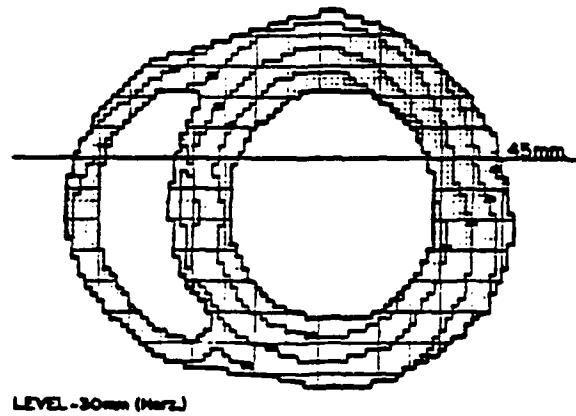


Figure A-13. Horizontal view of the activation sequence.

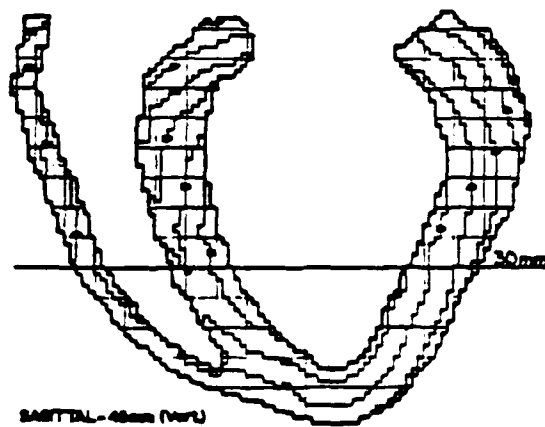


Figure A-14. Vertical view of the activation sequence.

RECOVERY TIMES  
550  
16-JAN-80 12:45:27



Figure A-15. An example of a myocardial action potential, obtained from Burgess.

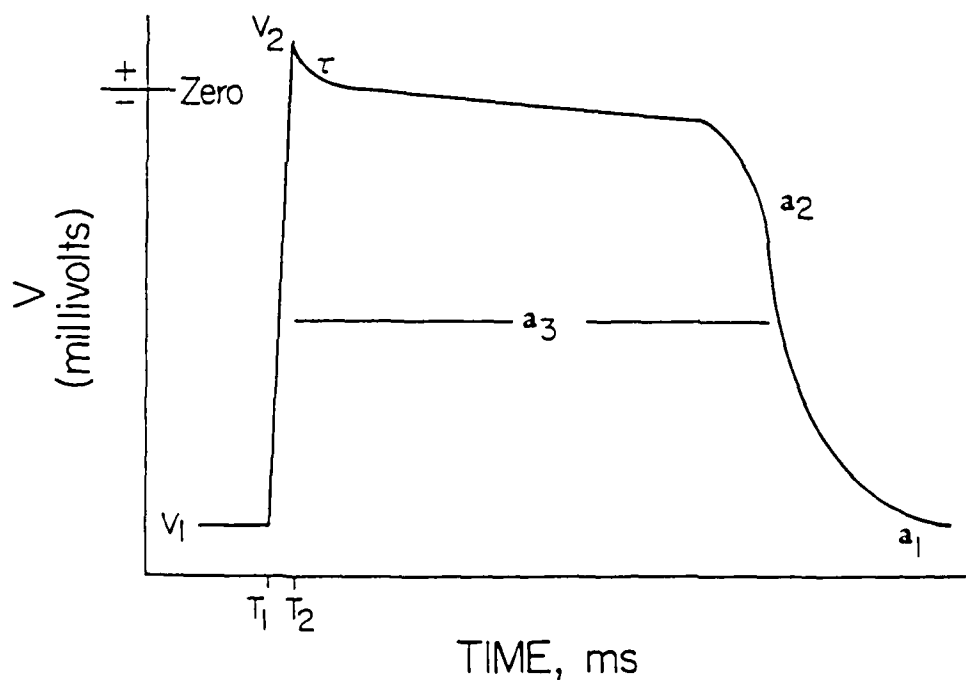


Figure A-16. Plot of a mathematical model of the action potential from a continuous function of time.

generators for the recovery current are obtained from equations of the A-P, the parameters in these equations determine the shapes of the various phases.

The stimulus that invokes a large increase in membrane permeability to sodium (A-6,A-7) in one region of the heart initiates activity that spreads in all directions at a velocity depending on the cable and excitable properties of the cells. Activity spreads through cardiac muscle from cell-to-cell and the tissue acts electrically as a single unit, hence the term "functional syncytium" is used to characterize the pathway of depolarization. In syncytial tissue, depolarization spreads out from the originating point as a wavefront in three-dimensional space. The propagation program, one of the programs comprising the forward model, is a simulation of this functional syncytium and the three-dimensional wavefront of depolarization.

An equivalent cardiac source (ECS), for the purpose of the forward model, is a mathematical expression for the cardiac EMF which replaces the significant physical properties of the actual cardiac source. Since the forward model is essentially a numerical process, the description of the source impressing current into the torso volume conductor must eventually be reduced to a numerical process likewise.

Selecting an ECS is guided by three principal considerations: (1) EQUIVALENCE--the mathematical-physical equation serving to replicate the current source must be equivalent in the sense that the equation of continuity of current density is not violated; (2) REPRESENTATION--the time varying spatial distribution of the actual current source must be approximated to some specified order that establishes how well the equivalent source represents the actual current source; (3) MATHEMATICAL FORM--the mathematical equation for the ECS should lend itself to physical interpretation, i.e., the coefficients and variables should relate to physical phenomena and be quantitatively determined by experimentation. Many trade-offs and approximations are required that compromise the above objectives and result in ECSs that must be evaluated with respect to a set of objectives for the forward simulation.

One of the simplest ECS models that has been considered for a suitable description of the electrical source in the heart is the single dipole. The single dipole is the algebraic sum of all the elemental bipolar current sources in the heart at any one instant. A fixed position dipole with three time-varying orthogonal components is the source model employed in vectorcardiography. A major problem with the fixed position dipole model is the lack of information on the spatial distribution of the elemental bipolar sources. Spatial dimensions within the heart are not small when compared to the distances to the chest surface. Although the single fixed dipole model is equivalent and has a tractable mathematical form, the representation of the actual source produces a poor approximation. A single moving dipole model is less objectionable but still not a sufficiently good approximation.

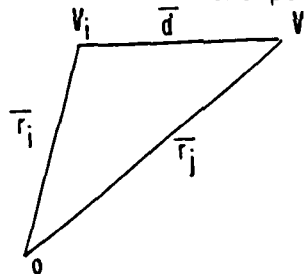
Equivalence and representation of the ECS is well defined for the multipole expansion model. Since the multipole model is attained from a series expansion of the Coulomb potential equation in a Taylor series, equivalence is possible by eliminating the monopole term and the ECS representation by the series is complete in a mathematical sense. Only the number of terms in the expansion determines the order of approximation, which can be determined analytically, and compared to the measurement system errors. The difficulty

with a multipole expansion model is the mathematical form is undesirable since there is no anatomical or electrophysiological correlates to the coefficients in the Taylor series expansion, which are the multipole moments. A model such as this replaces empirical body surface ECG methods with empirical heart multipole methods.

More recently, forward and inverse model studies have been performed with the multiple dipole model as the equivalent cardiac source. As the name implies, multiple (finite number) dipoles are distributed strategically at significant sites within the myocardium. In this manner of approximation, each dipole represents a region of myocardium that has small dimensions when compared to the distance to the chest surface. A multiple dipole model obeys the equivalence criteria and has a mathematical form that is tractable from a numerical analysis perspective. Representation by the multiple dipole source depends on numerous heart-torso variables, but is essentially determined by the number of dipoles and their respective locations. There are no significant constraints on the number of dipoles that can be programmed into the forward model.

### Bipolar Model

Since the propagation model has a spatial resolution of 1 mm, the mathematical model of choice for the ECS will be a bipolar source of EMF with a 1-mm separation. Given two points  $\bar{r}_i$  and  $\bar{r}_j$  in the myocardium separated by 1 mm, the mathematical form of the bipolar source is derived from the potential at these two points. Consider the potential at point  $\bar{r}_i$  as  $V_i$  and similarly for  $\bar{r}_j$ .



A bipolar source vector  $\bar{b}$  is defined for a finite separation of  $\bar{d}$ , taken as 1 mm in the propagation model. Vector  $\bar{b}$  has the following form:

$$\bar{b}_{ij} = [V_j(r_j) - V_i(r_i)] \bar{d}$$

where the direction of  $\bar{b}_{ij}$  is from  $r_i$  to  $r_j$  and is given by

$$\bar{d} = \frac{\bar{r}_j - \bar{r}_i}{|\bar{r}_i - \bar{r}_j|}$$

An equivalent dipole source for a segment of the myocardium is constructed from the vector sum of the bipolar sources within the  $n^{\text{th}}$  segment, i.e.,

$$\bar{p}_n(\bar{r}_n) = \frac{1}{2} \sum_{ij} \bar{b}_{ij}(r_j, r_i)$$

where the point  $r_i$  is summed over six adjacent points, repeated for all  $M$  points in the segment. In the forward model simulation, the number of points  $M$  in each segment varies with the size and shape of each segment, which in

turn depends on the arbitrary subdivision of the myocardium. With more segments in the heart and fewer points in each segment, an increase in resolution is achievable (hence improved representation of cardiac electrical events) at the expense of computer resources and effort to specify the initial conditions to the simulation program. Each composite dipole moment  $P_n$  of the  $n^{\text{th}}$  segment serves as both depolarization and repolarization equivalent cardiac source, since no distinction has been made between depolarization and repolarization potentials. The vector position  $r_n$  of the equivalent dipole is the mean value of the  $m$  triplets  $(x_i, y_i, z_i)$  of coordinate points within the  $n^{\text{th}}$  segment. It is this value,  $r_n$ , for which the boundary value problem of a unit source computes the transfer impedances to the torso surface electrode sites.

Depolarization and repolarization of the cardiac cells produces a system of charges and currents. A simply connected surface can be specified that completely surrounds the cardiac cells. The fixed volume  $\Omega$  bounded by the surface  $\Gamma$  contains all the charges and currents comprising the cardiac source as a function of time. It can be shown that the distributed cardiac system of charges and currents can be represented by a time-varying dipole. In addition, the volume  $\Omega$  can be subdivided into a set of smaller volume elements and a time-varying dipole can be defined for the charges and currents inside each element. Since the equivalent cardiac sources in the forward model are taken as dipole moments, it is essential that the cardiac system of charges and currents be rigorously represented as time-varying vector quantities.

The dipole moment of the charge-current distribution is defined by

$$\bar{P} = \int_{\Omega} \bar{r} \rho \, d\Omega \quad (\text{A-5})$$

where  $\bar{r}$  is the position vector from a fixed origin and  $\rho$  is the volume charge density inside the fixed volume  $\Omega$ . Consider  $\bar{J}$  to be the current density inside  $\Omega$ . Then as an application of Green's theorem on the fields  $\bar{J}$  and  $\bar{r}$ , the following identity results:

$$\int_{\Omega} \bar{J} \, d\Omega = \oint_{\Gamma} \bar{r} (\bar{J} \cdot \hat{n}) \, d\Gamma - \int_{\Omega} \bar{r} \text{DIV } \bar{J} \, d\Omega \quad (\text{A-6})$$

$\bar{J}$  vanishes on the surface  $\Gamma$  because it is contained completely inside  $\Omega$ . Equation (A-6) reduces to

$$\int_{\Omega} \bar{J} \, d\Omega = - \int_{\Omega} \bar{r} \text{DIV } \bar{J} \, d\Omega \quad (\text{A-7})$$

The right-hand side of equation (A-7) can be rewritten, using the equation of continuity for charges

$$\frac{\partial \rho}{\partial t} + \text{DIV } \bar{J} = 0$$

and substituting  $-\frac{\partial \rho}{\partial t}$  for  $\text{Div } \bar{J}$ .

$$\int_{\Omega} \bar{J} d\Omega = \int_{\Omega} \bar{r} \frac{\partial \rho}{\partial t} d\Omega \quad (\text{A-8})$$

The partial derivative of  $\rho$  with respect to time becomes the ordinary time derivative of the integral when brought outside the integral sign.

$$\int_{\Omega} \bar{J} d\Omega = \frac{d}{dt} \int_{\Omega} \bar{r} \rho d\Omega \quad (\text{A-9})$$

By definition, the right-hand integral is the definition of a dipole moment of a charge-current distribution given by equation (A-5).

$$\int_{\Omega} \bar{J} d\Omega = \frac{d\bar{P}}{dt} \quad (\text{A-10})$$

This derivation establishes the validity of using time-varying dipoles as the equivalent cardiac source for the distributed charge-current within the heart. Equation (A-10) is the basis for representing the electrical activity in the heart by an equivalent set of time-varying bipolar sources. Briefly stated, the depolarization and repolarization charge-current distribution  $\bar{J}$  is generated by the cell membrane EMF which is confined to the myocardial volume  $\Omega$ , i.e., the space occupied by ventricular myocardium. Regardless of the spatial distribution or time variation of the cellular EMFs producing the charge-current  $\bar{J}$ , the resulting source (the integral of  $\bar{J}$  over  $\Omega$ ) remains equivalent to a time-varying dipole-vector source  $d\bar{P}/dt$ . The vector  $\bar{P}$ , when expressed as a combination of linearly independent vectors, represents the multiple-dipole, equivalent cardiac source.

The forward simulation of ECGs uses an equivalent cardiac source that is a depolarization-repolarization generator defined as a multiple bipolar source (no limiting process invoked as with the dipole) of EMF within the myocardium which is a function of time measured from the onset of depolarization. Equivalent current is expressed by an equation that is a continuous function of time and the shape of the equation is determined by the values of six parameters. A set of six parameters are specified for each coordinate intersection in three dimensions within the myocardium. Given that the heart



geometry is specified on a 1-mm grid system, the smallest unit of bipolar EMF extends over a distance of 1 mm between source and sink. Each coordinate intersection within the myocardial geometry is a potential source or sink of current. Figure A-17 depicts a typical intersection point inside the myocardial geometry. An equivalent bipolar moment is determined by the sign of the EMF at the intersecting point constructed from a consideration of the six intersection points surrounding some arbitrary point  $R_0(i,j,k)$ , where  $R_0$  is the reference point or location for the equivalent bipolar moment positioned at  $x = i$ ,  $y = j$ , and  $z = k$ .

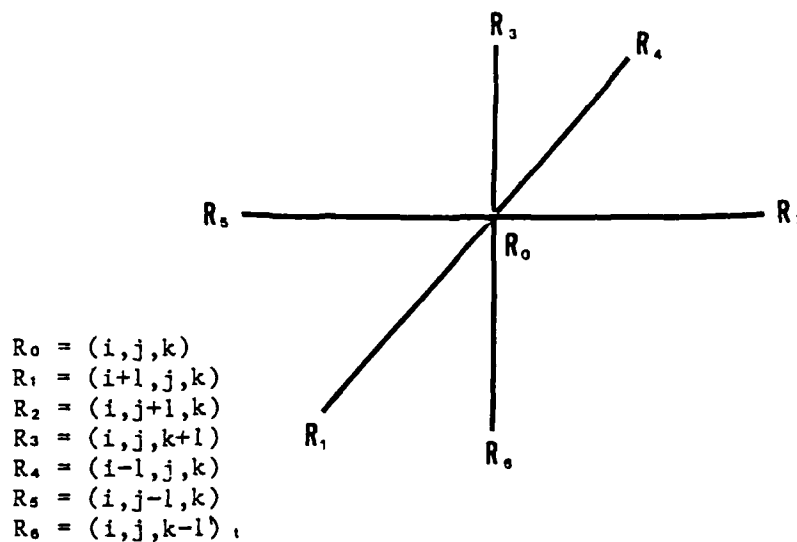


Figure A-17. Typical intersection point inside the myocardial geometry.

The  $x$  component of the bipolar moment is computed as the vector sum of  $\vec{R}_1\vec{R}_0$  and  $\vec{R}_4\vec{R}_0$ . In terms of the voltage at  $R_0$ ,  $R_1$ , and  $R_4$  the expression for the  $x$  component of the bipolar moment becomes:

$$P_x = [V_1 - V_0] d + [V_4 - V_0] d$$

where  $d = 1$  mm.

Similarly for  $P_y$  and  $P_z$

$$P_y = [V_2 - V_0] d + [V_5 - V_0] d$$

$$P_z = [V_3 - V_0] d + [V_6 - V_0] d$$

Hence the vector moment of the equivalent bipolar source formed from  $P_x$ ,  $P_y$ , and  $P_z$  is

$$\bar{P} = P_x \hat{i} + P_y \hat{j} + P_z \hat{k}$$

where  $\hat{i}$ ,  $\hat{j}$ , and  $\hat{k}$  are unit vectors along the x, y, and z axes, respectively. The above expression contains the spatial property for the bipolar source. As a function of time,  $P(i,j,k,t)$  varies implicitly as the voltages  $V_0(t)$ ,  $V_1(t)$ , ...,  $V_6(t)$  vary, while the separation  $d$  is held constant. A mathematical equation expressing the voltage at each coordinate intersection as a continuous function of time is employed to compute each  $V_n$ , and therefore  $P(i,j,k,t)$ .

#### Action Potential Profile

Figure A-18 is a graph of the mathematical equation  $V_n$  for a typical set of parameters.

$$V_n = \begin{cases} V_1 & ; t \leq T_1 \\ V_1 + a_1(t-T_1) & ; T_1 < t < T_2 \\ V_2 e^{-\gamma(t-T_2)} + \cos[.17(t-T_2)] + \frac{10 + V_1 e^{a_2(t-T_2)} - a_3}{1 + e^{a_2(t-T_2)} - a_3} & ; t \geq T_2 \end{cases}$$

Time  $T_1$  is obtained from the propagation simulation program; it is the time relative to an arbitrary reference (usually the onset of QRS) at which the activation front crosses the point (i,j,k).

$$a_1 = (V_2 - V_1)/dt \quad dt = 2.5 \text{ ms, phase 0}$$

$$a_2 = \text{refractory rate, phase 3}$$

$$a_3 = \text{functional refractory time, phase 3}$$

$$V_1 = \text{resting potential difference}$$

$$V_2 = \text{depolarization potential difference}$$

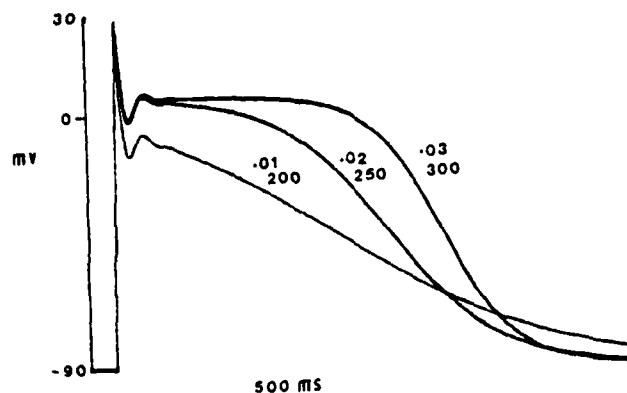
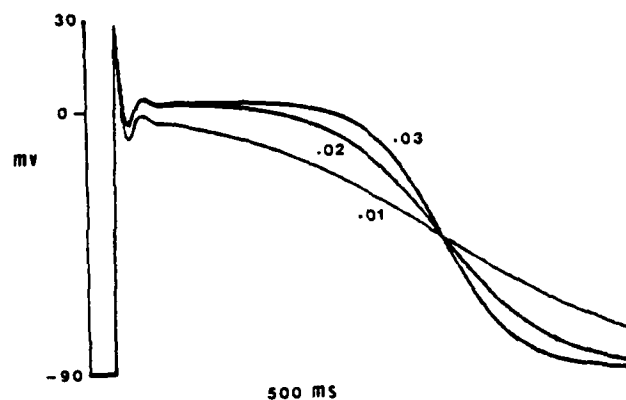
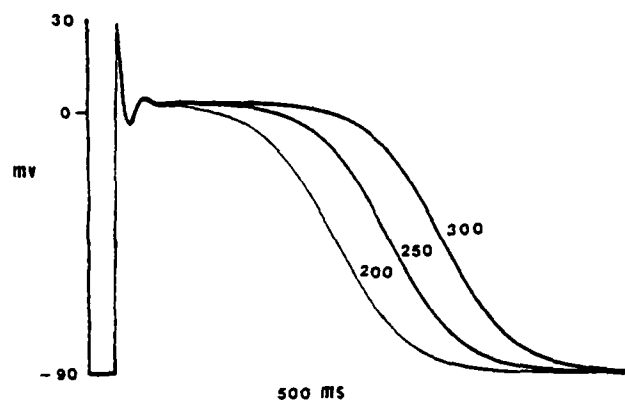


Figure A-18. Action potential waveforms as generated by  $V_n$  on p. 114. In the top set of waveforms, the parameter  $a_3$  (the functional refractory time, phase 3) was changed. In the middle set of waveforms  $a_2$ , the slope of phase 3, was varied. In the bottom panel both were varied as shown.

Each distinct region of the myocardial geometry is characterized by a set of the above parameters. An equivalent depolarization-repolarization source representation of the entire myocardial mass is a matter of practical choice between too few segments to resolve the spatial distribution of EMF and as many as all coordinate intersections, of which there are approximately 250,000. Initially, the equivalent cardiac source consists of 20 segments: 12 for the left ventricle and septum, and 8 for the right ventricle. Each of the 12 segments of the left ventricle and septum is divided into zones. The 4 segments of the apex are divided into 3 zones from endocardium to epicardium. The 4 mid-wall segments are divided likewise into 4 zones, and the base segments divided into 5 zones. In summary, the segment-zone subdivision consists of 56 regions.

## TRANSFER IMPEDANCES

### Boundary Value Problem

The total bioelectric current density  $\bar{J}$  within the volume conductor is contributed by two components given by the following vector equation:

$$\bar{J} = \bar{J}_i + \sigma \bar{E} \quad (A-11)$$

$\bar{J}_i$  is the impressed current density resulting from the nonconservative electric field of depolarization/repolarization such that a path integral, equation (A-12), through the source region yields the imbedded electromotive force.

$$\oint \bar{E}_i \cdot d\bar{L} = \text{EMF} \quad (A-12)$$

The quantity  $\sigma \bar{E}$  is the ohmic current density present in the volume conductor with conductivity  $\sigma$  due to the conservative electric field  $\bar{E}$  produced by  $\bar{J}_i$ .

Applicability of Ohm's law to the electrocardiographic forward problem is based on the nominal values of conductivity and permittivity of volume conductor tissue and the observed maximum rate of change of electrical events within the heart. A full discussion of this area is given by Plonsey (A-8). He points out that nominal values of conductivity and permittivity of tissue yield a sufficiently short time constant to permit the forward problem to be considered quasi-static. This means that volume charge density changes or capacitive effects can be neglected. Forward solutions calculated independently for each time point will not have appreciable time-delay errors caused by the volume conductor.

Setting the volume charge density rate of change  $\partial \rho / \partial t$  equal to zero results in a stationary (non-time-dependent) partial differential equation. The definition of current and the law of conservation of charge leads to the following definition:

$$\frac{dq}{dt} = \frac{d}{dt} \int_{\Psi} \rho d\Psi \quad (A-13)$$

where the current  $dq/dt$  results from the time rate of change of volume current density contained within the volume  $\Psi$ .

Applying Gauss' theorem to equation (A-13) results in the equation of continuity:

$$\nabla \cdot \bar{J} + \frac{\partial \rho}{\partial t} = 0 \quad (A-14)$$

For a stationary problem  $\partial \rho / \partial t = 0$  and equation (A-14) reduces to a divergence equation for the total current density:

$$\nabla \cdot \bar{J} = 0 \quad (A-15)$$

Substituting for the total current density from equation (A-11), a nonhomogeneous partial differential equation appropriate to the forward problem is derived.

$$\nabla \cdot \sigma \bar{E} = - \nabla \cdot \bar{J}_i \quad (A-16)$$

Equation (A-16) can be restated in terms of a potential since the conservative field  $\bar{E}$  is derivable from the gradient of a scalar potential, say  $V$ . Therefore, equation (A-16) becomes

$$\nabla \cdot \sigma \nabla V = \nabla \cdot \bar{J}_i \quad (A-17)$$

For purposes of discussion equation (A-17) will be written in the form of an operator equation:

$$\mathcal{L} V = f \quad (A-18)$$

where the bioelectric current sources impressed by the generator,  $\nabla \cdot \bar{J}_i$ , are replaced by the free term symbol  $f$  and the partial differential operation on the potential function  $V$  is replaced by the operator symbol  $\mathcal{L}$ .

Equation (A-18) leads to a boundary-value problem when the heart-volume conductor is imbedded in an insulating medium. The volume conductor-to-air interface imposes a boundary condition on the normal component of the current

density. For the torso air interface where  $\sigma = 0$ , continuity of the normal component of current density requires it to be zero. That is

$$J_n(\text{torso}) = J_n(\text{air}) = 0$$

where the subscript  $n$  refers to the normal to the surface  $S$ , and from Ohm's law

$$J_n = \sigma E_n = -\sigma \frac{\partial V}{\partial n} = 0$$

This yields the natural boundary condition,

$$\sigma \frac{\partial V}{\partial n} \Big|_S = 0$$

where  $S$  is the surface bounding the volume conductor  $\psi$ . The resulting boundary-value problem can be stated as:

$$\mathcal{L} V = f \text{ in } \psi \quad ; \quad \frac{\partial V}{\partial n} \Big|_S = 0 \quad (\text{A-19})$$

It is well known from operator theory in partial differential equations that a solution to problem (A-19) exists if the operator  $\mathcal{L}$  is positive definite. This existence criteria imposes a restriction on the source term  $f$ , namely,

$$\int_{\psi} f \, d\psi = 0 \quad \int_{\psi} f^2 \, d\psi < \infty \quad (\text{A-20})$$

The equality of sources and sinks of current or non-unipolar nature of the heart current sources insures this physically. The choices of a parametric mathematical model for the forward problem are restricted to equations that satisfy conditions (A-10).

Uniqueness can be established by imposing a reference condition:

$$\int_{\psi} V \, d\psi = 0 \quad (\text{A-21})$$

#### Gelernter-Swihart Method

The Gelernter and Swihart method is a numerical solution to a piece-wise homogeneous Poisson equation for an inhomogeneous volume conductor. It divides the volume conductor into regions of constant conductivity and then

calculates, for an arbitrary source distribution, the potential distribution on an irregularly shaped surface bounded by an insulator. Each homogeneous region R is formulated as a Neumann problem for Poisson's equation:

$$\begin{aligned} -\nabla^2 V &= f & \text{in } R \\ \frac{\partial V}{\partial n} &= g & \text{on } C \end{aligned} \quad (\text{A-22})$$

where R is a bounded connected region with sufficiently smooth boundary C and  $\partial V / \partial n$  denotes the normal derivative taken in the outward direction. It follows from Green's first identity that f and g cannot be chosen independently, but must satisfy the relation

$$\int_R f \, dR = \int_C g \, dC \quad (\text{A-23})$$

The solution to equation (A-23) is only unique up to an additive constant. This constant is usually determined by a normalization process over the surface such that the integral

$$\int_C V \, dC = 0 \quad (\text{A-24})$$

Boundary conditions are of two types; the external boundary requires the normal component of the current density to be zero, whereas the internal interfaces require the normal component to be refracted in proportion to the conductivity on each side of the interface.

#### Gelernter-Swihart Algorithm

The GS procedure for computing the solution to the Neumann problem of Poisson's equation is quite general in scope and is applicable to the forward ECG problem if practical limitations are imposed on the number of internal regions requiring specification of geometry and conductivity, although no such requirements are imposed by the GS method itself. Derivation of the method considers an arbitrary ensemble of generators in a closed, three-dimensional region containing sub-regions that each have a uniform conductivity. The region is required to be embedded in an insulating medium. There are no restrictions other than closure upon the configuration of the sub-regions.

Solving the boundary value problem follows closely the actual events which bring about equilibrium in a charge distribution for a physical process having the same properties that are described numerically in the computer program.

Consider the following as a brief discussion of the Gelernter-Swihart formulation, based on the computer program rather than on their formal treatment (A-9). A dipole of known location and size is contained inside the bounded inhomogeneous volume conductor. Initially, the charge distribution

induced on all surface area elements in an unbounded medium is calculated. Gauss' induction law is employed:

$$E(x_i) \Delta S_i \cos(\phi_i) = q_i$$

where  $E$  is the electric field produced by the dipole at the surface area element  $\Delta S_i$ .  $\phi_i$  is the angle between  $E$  and the unit normal of  $\Delta S_i$ .  $q_i$  is the induced charge on the area element  $\Delta S_i$ .  $Q_0$  is a functional representation for all the  $q_i$ .  $\vec{E}$  for a dipole is given by:

$$\vec{E} = \frac{3(\vec{p} \cdot \vec{x}) \vec{x}}{|\vec{x}|^5} - \frac{\vec{p}}{|\vec{x}|^3}$$

The distribution of charge  $Q_0$  on the boundaries is then redistributed using Coulomb's law for the electric field of point charges and Gauss' induction until the final charge distribution is in equilibrium. This is accomplished numerically by combining Coulomb's and Gauss' laws so that the charge induced on area element  $\Delta S_i$  by a charge at  $x_j$  can be expressed by the solid angle the area  $\Delta S_i$  subtends at  $x_j$ , i.e.,  $\Omega_{ij}$ ,

$$\Delta q_i = \Omega_{ij} q_j$$

For the inhomogeneous regions,  $\Omega_{ij}$  is multiplied by  $(\sigma_1 - \sigma_2)/(\sigma_1 + \sigma_2)$ , the ratio of conductivities at the interfaces. This algorithm is used in an iterative manner until the induced charges go to zero.

Beginning with  $Q_0$  the induced charges on the first iteration become

$$\begin{aligned} \Delta Q_1 &= \Omega Q_0 \\ \Delta Q_2 &= \Omega \Delta Q_1 \end{aligned}$$

second iteration:

$$\begin{aligned} &\cdot \\ &\cdot \\ &\cdot \\ &\cdot \\ \Delta Q_n &= \Omega \Delta Q_{n-1} \end{aligned}$$

as  $n$  becomes large  $\Delta Q_n \rightarrow 0$ . When convergence has been attained, the potential distribution is calculated from the final charge distribution over all subregions and bounding region.

No convergence criteria were provided for the GS method and since no exactly calculated result was available for comparison purposes, they offered the following arbitrary stopping criteria for the charge iteration algorithm:



1. The difference in potential between the maximum and minimum points changes by less than an acceptably small amount from its value at the last iteration.
2. The normal component of the electric field at each surface element has reached an acceptably small percentage of the maximum normal field produced by the uncompensated generator (i.e., the boundary condition at the external surface is acceptably satisfied).
3. The surface potential map has become essentially stable (i.e., the equipotential lines and maximum and minimum points have not changed their position noticeably since the last iteration).

Acceptably small in the above specifications depends upon the order of approximation required of the solutions in a particular application.

Rates of convergence were estimated from solutions of simple problems to solutions of more realistic examples and ranged from 4 to 40 iterations. High conductivity ratios in the vicinity of the generators required the most iterations before the stopping criteria were met.

Analytical solutions can be used to test the program code of the GS formulation; however, the errors attributed to boundary and sub-region discretization, stopping criteria, and source vector position for the arbitrary torso configuration are in doubt without a known solution for comparison. The electrolytic tank with immersed bipolar sources provides a physical situation for which a GS solution can be computed and compared to a measured potential distribution. The torso tank used to test the computer code for mistakes and obtain error estimates in computed solutions is a life-sized Lucite model of a male torso. Bipolar sources are constructed and calibrated with a constant current in a spherical tank before positioning them in the torso tank. A potential distribution on the torso tank surface is measured from 64 uniformly placed electrodes and compared with a corresponding potential distribution calculated by the method of GS. This torso-shaped electrolytic tank test bed is not intended to be a physical replication of the human; its only purpose is to provide a completely and accurately specified problem as input to the GS algorithms, for which a measured solution exists.

#### Transfer Impedances for QRS and T Wave Simulation

Simulation of the T wave requires that the motion of the heart during contraction be taken into consideration. Shortly after the ventricles depolarize and begin repolarizing, the ventricles begin contracting and changing position in the chest. Since the equivalent cardiac generators representing the repolarization EMF must remain in the ventricular myocardium, their positions must follow that of the ventricular wall. Simulation of the ECG during the T wave requires transfer impedances from the repolarization generators to the body surface. With the heart moving, the repolarization generators have a time-varying position during contraction. The forward model of T waves takes into account time-varying transfer impedances by computing 3 sets of transfer impedances -- one at diastole, mid-systole, and end-systole -- and then interpolates between these 3 sets for intermediate transfer impedances over the entire contracting period of the heart.

Data on the location and motion of the equivalent cardiac generators is available in several publications (A-9-11), where Ingels et al. measured the midwall myocardial dynamics in 24 intact patients by radiographic analysis of surgically implanted markers. They implanted tiny coils of tantalum wire into the left ventricular myocardium in 24 patients at the time of cardiac surgery. Seven coil markers were placed in the myocardium; at the left ventricular apex, and at three equidistant points from apex to base along both the anterolateral and inferior margins of the left ventricle in a pattern outlining the ventricular chamber as seen in a 30-degree right anterior oblique projection. Postoperatively the motions of the myocardial markers were visualized in a resting single-plane (30-degree right anterior oblique) fluoroscopic to video recording at 30 frames per second. The positions of all myocardial markers for each frame of three complete cardiac cycles were used to calculate the positions of midwall left ventricular segments.

Figure A-19 defines the length and radii for which Ingels et al. published quantitative data over the entire cardiac cycle, although this figure illustrates the definitions transformed into the ventricular segments of the heart model utilized by the simulation and shown in Figure A-2. Variations in the radii defined in Figure A-1 were graphed as a function of time for 3 cardiac cycles. The values of the radii at diastole, mid, and end systole are taken from the graphics for each ventricular segment 4 through 9 inclusive. Radii for segments 10 to 12 and 1 to 3 are taken as the average of the two segments at the corresponding positions from apex to base. For example, the radius of segment 11 is the average of the radii for 5 and 8.

Parameters such as changing radii, longitudinal axis shortening, and the rotation of the transverse ventricular diameters, become the elements of a transformation matrix applied to the equivalent cardiac source locations in the simulated heart geometry. After performing the contraction matrix transformation on the cardiac source locations, the results are transformed again into the body orientation by the same matrix used to specify all heart geometry information in the chest. These transformations yield the x,y,z coordinates of the cardiac sources within the inhomogeneous volume conductor. Transfer impedances are computed as the solution to a boundary value problem for the new cardiac source locations. Computing these solutions at diastole, mid and end systole produces three complete sets of transfer impedances. All transfer impedances from QRS onset to the end of the T wave are taken from this set of three or are interpolated from them at the appropriate time increment.

### ECG Lead Systems

ECG tracings and vectorcardiograms are comprised of voltages measured as potential differences on the chest surface. Similarly, the forward model produces simulated ECGs and vectors that are computed as potential differences.

Given a set of computed potentials over the chest surface, a mathematical transformation must be performed on these potentials to produce the appropriate voltages. Transforming chest potentials into ECG and vector voltages requires a consideration of two aspects of ECG recording equipment. First the voltages are determined from a specific assortment of potential

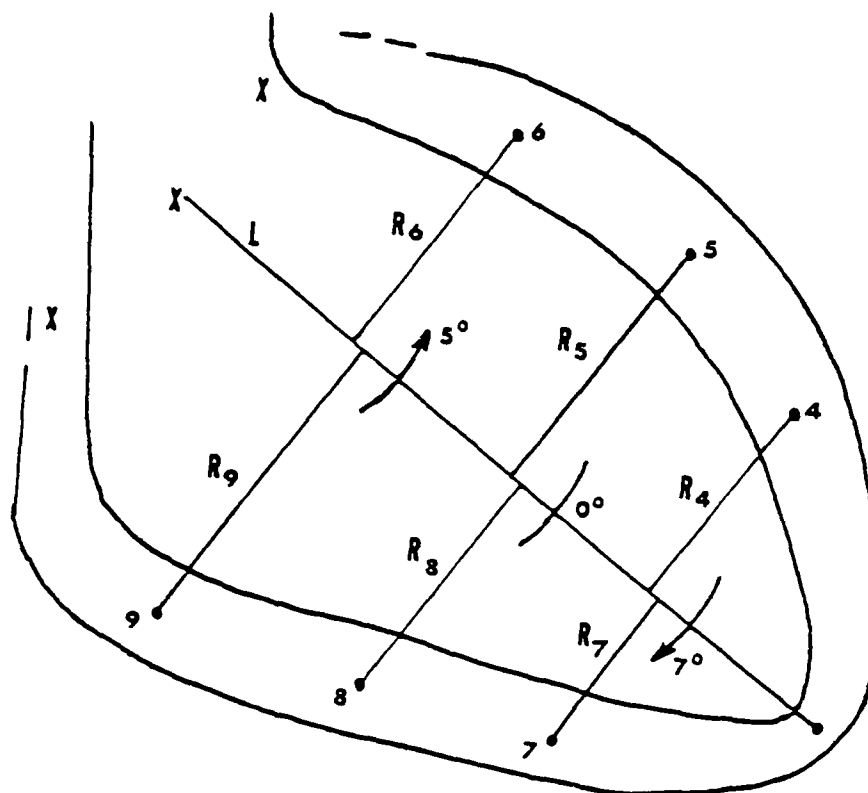


Figure A-19. The radial and length measurements in a typical RAO radiograph are shown as reported by Ingels et al. (A-10). The rotation of the basal segments, on the average, of  $5^\circ$  clockwise around the long axis of the left ventricle as viewed from the apex, is indicated by the upper left arrow. The counterclockwise rotation, on the average, of  $7^\circ$  of the apical segments is shown by the more apically located arrow at the lower right.

differences, and secondly the voltages are combined by weighting factors determined from a set of resistors in the recording equipment. The transformation of chest potentials to ECG and vector leads consists of a matrix array in which the row elements are the weighting factors for each lead and the columns correspond to the various chest potential sites.

Simulating the convention 12-lead ECG, McFee, Frank, Cube, and SVEC III vectors requires 38 potential sites in the chest surface. Potentials from these 38 chest sites are transformed into 24 weighted voltages (12 leads plus 3 for each of the 4 vector systems equals a total of 24). Let the transformation be represented by the following matrix:

$$T_{jk} \quad j = 1, 24 \text{ and } k = 1, 38$$

j	lead	k	site
1	V1	1	41
2	V2	2	47
3	V3	3	103
4	V4	4	322
5	V5	5	362
6	V6	6	494
7	I	7	551
8	II	8	556
9	III	9	589
10	aVF	10	615
11	aVL	11	651
12	aVR	12	661
13	Cx	13	681
14	Cy	14	687
15	Cz	15	692
16	Mx	16	717
17	My	17	744
18	Mz	18	761
19	Fx	19	766
20	Fy	20	770
21	Fz	21	774
22	Sx	22	777
23	Sy	23	792
24	Sz	24	810
		25	825
		26	833
		27	837
		28	845
		29	860
		30	889
		31	902
		32	910
		33	933
		34	955
		35	962
		36	982
		37	1269
		38	1271

Lead voltages for the entire ECG are represented by a matrix  $V(j,n)$ , where  $j$  spans the rows covering the chest electrode sites and  $n$  specifies the column corresponding to each instant in time. The matrix  $V(j,n)$  is defined as the product of the transformation matrix  $T(j,k)$  and the potential distribution matrix  $S(k,n)$ .

$$V(j,n) = T(j,k) * S(k,n)$$

Potential distribution  $S(k,n)$  is a matrix array computed by combining the heart current sources  $P(i,n)$  and the unit potential distributions  $U(k,n,i)$ . Index ( $i$ ) ranges over the bipolar sources  $i = 1$  to 60. Indices ( $k$ ) and ( $n$ ) have the same meaning as above,  $k = 1$  to 38 electrode sites,  $n = 1$  to  $N$  ECG time steps. As a matrix array,  $S(k,n)$  is defined by the following equation:

$$S(k,n) = \sum_i U(k,n,i) * P(i,n)$$

Unit distributions  $U(k,n,i)$  are computed as solutions to the boundary value problem for unit sources imbedded in the volume conductor at locations specified as diastole, mid-systole, and end-systole. From these three solutions, a set of interpolated solutions are computed for each time point between diastole and end-systole. Let any time point during the ECG be represented by the subscript  $n$ . Hence, the ECG lead voltages  $V(j,n)$  become

$$V(j,n) = T(j,k) * \sum_i U(k,n,i) * P(i,n)$$

To summarize:

1.  $V(j,n)$  is the matrix array consisting of the conventional 12-lead electrocardiogram, and the vector cardiograms of McFee, Frank, Cube, and SVEC III positioned in the rows indexed by  $j = 1$  to 38. Each column contains the voltages for a particular time point of which there are a total of  $N$  columns, indexed by  $n = 1$  to  $N$  ECG time divisions.

2.  $T(j,k)$  is the matrix array containing the electrode-lead weighting factors that transform a chest surface potential distribution into ECG lead voltages.

3.  $P(i,n)$  is the matrix array whose row elements are the bipolar source moments produced by the simulation of heart current generators ( $i = 1$  to 60) for each instant of time ( $n$ ), the column index.

4.  $U(k,n,i)$  is the matrix array having row elements corresponding to the unit potential distribution over 38 electrode sites for unit bipolar source ( $i$ ), that are interpolated from diastole to end-systole to provide the column elements corresponding to each instant of time ( $n$ ). The array has a depth ( $i$ ) covering the 60 unit sources.

It is the array  $V(j,n)$  that is displayed on output as the ECGs and vectors for depolarization and repolarization of the ventricles.

#### REFERENCES

- A-1. Scher, A.M. and Young, A.C.: The pathway of ventricular depolarization in the dog. *Circ. Res.*, 4(1956) 461.
- A-2. Durrer, D.: Electrical aspects of human cardiac activity: a clinical-physiological approach to excitation and stimulation. *Cardiovasc. Res.*, (1968) 2, 1-18.
- A-3. Vander Ark, C.R. and Reynolds, E.W.: An experimental study of propagated electrical activity in the canine heart. *Circ. Res.*, 26(1970) 451.
- A-4. Durrer, D., van Dam, R.Th., Freud, G.E., Janse, M.J., Mijler, F.L., and Arzbaecher, R.C.: Total excitation of the isolated human heart. *Circulation*, 41(1970) 899.
- A-5. Solomon, J.C. and Selvester, R.H.: Simulation of measured activation sequence in the human heart. *Am. Heart J.*, Vol 85, No.4(1973) 518-523.
- A-6. Purves, R.D.: Current flow and potential in a three-dimensional syncytium. *J. Theor. Biol.*, 60(1976) 147.
- A-7. Peskoff, A.: Electrical potential in three-dimensional electrically syncytial tissues. *Bull. Math. Biol.*, 41(1979) 163.
- A-8. Plonsey, R: Bioelectric Phenomena. McGraw-Hill Co., 1969.
- A-9. Gelernter, H.L. and Swihart, J.C.: Mathematical-physical model of genesis of electrocardiogram. *Biophys. J.*, 4(1964) 285.
- A-10. Ingels, N.B., Daughters, G.T., Stinson, E.B., and Alderman, E.L.: Measurement of midwall myocardial dynamics in intact man by radiography of surgically implanted markers. *Circulation*, 52(1975) 859.
- A-11. Harrison, D.C., Goldblatt A., Braunwald, E., Glick, G., and Mason, D.T.: Studies on cardiac dimensions in intact, unanesthetized man. *Circ. Res.*, 13(1963) 448.
- A-12. McDonald, I.G.: The shape and movements of the human left ventricle during systole. *Amer. J. Cardiol.*, Vol. 26, No. 3(1970) 221.

END

FILMED

6-86

DTIC